

Group chase and escape in the presence of obstacles

J.R. Šćepanović^a, A. Karač^b, Z.M. Jakšić^a, Lj. Budinski-Petković^c, S.B. Vrhovac^{a,*}

^a Scientific Computing Laboratory, Center for the Study of Complex Systems, Institute of Physics Belgrade, University of Belgrade, Pregrevica 118, Zemun 11080, Belgrade, Serbia

^b Polytechnic faculty, University of Zenica, Bosnia and Herzegovina

^c Faculty of Engineering, Trg D. Obradovića 6, Novi Sad 21000, Serbia

HIGHLIGHTS

- Hunting in the presence of obstacles is studied.
- Dynamics of smart chasing and escape between two species is studied by MC simulations.
- Stretched exponential behavior excellently describes the capture dynamics.
- Characteristic time τ decreases with the initial density of targets as a power law.
- Characteristic timescale τ increases with the density of obstacles.

ARTICLE INFO

Article history:

Received 13 November 2018

Received in revised form 20 February 2019

Available online 14 March 2019

Keywords:

Group chase and escape

Square lattice

Obstacles

Stretched-exponential function

ABSTRACT

We study a stochastic lattice model describing the dynamics of a group chasing and escaping between two species in an environment that contains obstacles. The Monte Carlo simulations are carried out on a two-dimensional square lattice. Obstacles are represented by non-overlapping lattice shapes that are randomly placed on the lattice. The model includes smart pursuit (chasers to targets) and evasion (targets from chasers). Both species can affect their movement by visual perception within their finite sighting range σ .

We concentrate here on the role that density and shape of the obstacles plays in the time evolution of the number of targets, $N_T(t)$. Temporal evolution of the number of targets $N_T(t)$ is found to be stretched-exponential, of the form $N_T(t) = N_T(0) - \delta N_T(\infty) (1 - \exp[-(t/\tau)^\beta])$, regardless of whether the obstacles are present or not. The characteristic timescale τ is found to decrease with the initial density of targets ρ_0^T according to a power-law, i.e., $\tau \propto (\rho_0^T)^{-\gamma}$. Furthermore, temporal dependences of the number of targets $N_T(t)$ are compared for various combinations of chasers and targets with different sighting ranges, $\sigma = 1, 2$, in order to analyze the relationship between the ability of species and the capture dynamics in the presence of obstacles.

© 2019 Elsevier B.V. All rights reserved.

1. Introduction

The collective motion of interacting organisms such as bacteria colonies [1–3], amoeba [4–6], cells [7–9], insects [10,11], fish [12,13], birds [14,15], and humans [16–20] has drawn great attention of researchers from diverse fields in

* Corresponding author.

E-mail address: vrhovac@ipb.ac.rs (S.B. Vrhovac).

URL: <http://www.ipb.ac.rs/~vrhovac/> (S.B. Vrhovac).

the past two decades [21]. Pursuit and evasion problems have a long and interesting history [22]. It is well known that collective motion of individuals with escape and pursuit behavior serve as a protection mechanisms against chasers. The goal for chaser (predator) and target (for example, prey) is to choose an efficient motion strategy that optimizes their respective chances of successful pursuit or evasion. At first, developing computational systems and techniques enabled one to deal with a two-particle system consisting of one chaser and one target, where there existed a challenging mathematical problem for obtaining analytical expressions [22]. Also, a class of pursuit-and-evasion problems involving a single evading prey that is being hunted by $N > 1$ predators has been modeled and analyzed [23–25]. In addition to these modeling efforts, extensive research has been devoted to developing multi-agent models that consider the role of multiple predators and/or preys [26–35].

Kamimura and Ohira [26] have introduced a lattice model to analyze the group spatial chase and escape phenomena. The model assumes that chasers and targets are initially placed randomly on the square lattice as pointlike particles. Both species perform independent nearest-neighbor random walks on a lattice following simple dynamical rules, increasing or decreasing the distance from the nearest particle of the opposite group. Chasers start a direct chase whenever a target appears within their sighting range. Targets try to evade capture by making a distance of one lattice spacing in a direction away from the nearest chaser. Target is caught upon the first encounter with a chaser. In their model, although each chaser independently moves in order to catch one of the nearest targets, some groups of chasers are simultaneously formed. In the simulation, the chasers form flocks and seem to cooperate to catch the flocks of targets [24,26,33,34,36]. In the basic version of the model, chasers can sense the positions of the targets at an arbitrary distance. The authors have considered several extensions to this simplest version of the model, including the search range of chasers and targets, and introduction of a term designed to account for random fluctuations that are usually present in real systems. Despite its simplicity, the model is able to reproduce a lot of interesting behaviors [27].

Based on a concept proposed by Kamimura and Ohira [26] we built up a bio-inspired realistic agent-based approach to model collective chasing and escaping in a discrete space and time with periodic boundary conditions for the case when the lattice is initially covered with obstacles at various concentrations. The depositing objects (obstacles) are formed by a small number of lattice steps on the square lattice. Spatial distribution of the obstacles on the lattice is created using the random sequential adsorption (RSA) method [37,38]. The dominant effect in RSA is the blocking of the available surface area. When the surface is saturated by the adsorbed objects so that no further objects can be placed, the system reaches the jamming limit ρ_j . Thus, an element of stochasticity of environment, which is present in any natural system, is incorporated into the model. It must be emphasized that birth and death processes [39,40] are not considered here, so the results obtained apply only on the time scales short compared to the typical lifetime of single organisms. The role of multiple predators and preys has also been studied by using an off-lattice models [41,42], based on the modeling of the self-propelled organisms by Vicsek et al. and including the chase-escape mechanisms through simple intergroup pairwise interactions [43]. In such models, an analysis of the impact of geometrically complex boundary conditions, such as obstacles, would require taking into account a hard core repulsion term in the interaction. However, the lattice-based models allow easier handling of objects (obstacles) of various shapes and sizes.

For the real life systems, simulation resembles to two animal species fighting for the survival. Obstacles may be trees, rocks, or anything that is big enough for the evader and pursuer to become “invisible” for the other. The chasers and evaders can also be human beings, but with different roles, like police officers and robbers, where buildings, grocery stores and similar objects can be viewed as obstacles.

We study the survival of N_0^T targets (for example, prey) that is captured by N_0^C chasers (predators) in the presence of static obstacles. We have kept the rules governing the dynamics of the processes at the individual level as simple as possible to focus entirely on the effects of obstacles. Each species has its specific sighting range σ in which it can see the other species. In [26], for each target, the distance to each chaser is calculated as the Euclidean distance. Unlike the Kamimura and Ohira model [26], distances as well as sighting ranges in the present study are measured by a L^1 (“Manhattan”) metric. Manhattan distance between sites P_1 and P_2 on a square lattice is equal to the length of all paths connecting P_1 and P_2 along horizontal and vertical segments, without ever going back. Therefore, Manhattan metric more correctly than Euclidean’s determines the length of the path between two sites in the lattice-based models. In our model, there are two types of chasers and targets and each of them has its own sighting range σ , which describes their skills at chasing and escaping, respectively. In reality, chasers search for targets in their vicinities. Similarly, targets can recognize the existence of nearby chasers. Therefore, analysis of the capture dynamics in the present study is limited to species with two different sighting ranges, i.e., $\sigma = 1, 2$. If the value of σ equals zero, the movement is equivalent to the random walkers [26,28,40,44]. It has been confirmed that the idea of animals using blind search strategies does not seem to be usable since it neglects the role of animals’ smartness and experience in guiding them [45]. We investigate the role that the density of obstacles plays in the time evolution of the number of targets, $N_T(t)$. A detailed analysis of the contribution to the capture dynamics coming from the size and the shape of obstacles is carried out. Furthermore, temporal dependences of the number of targets $N_T(t)$ in the presence of obstacles are compared for various combinations of chasers and targets with different chasing and avoidance skills in order to analyze the relationship between the ability of species and the capture dynamics. In particular, we try to find a universal functional type that describes the decrease in the number of targets $N_T(t)$ in the best way.

We organized the paper as follows. Section 2 describes the details of the model and simulations. In Section 3 results of numerical simulation are presented and discussed. Finally, Section 4 contains some additional comments and final remarks.

2. Definition of the model and the simulation method

The environment where two interacting species coexist is represented by the two-dimensional square lattice of linear size L with periodic boundary conditions. In our model the lattice is initially occupied by obstacles of various shapes and sizes at the effective density ρ_0 . This density is defined as a fraction of sites of the lattice that are occupied by the obstacles. Linear obstacles are k -mers of length $\ell = k - 1 = 0, 1, \dots, 6$, shown in Table 1 as objects (A_1) – (A_7) . Extended shapes that we have used as obstacles are the crosses of two different sizes, shown in Table 2 as objects (C_1) and (C_2) .

Obstacles cannot overlap and their spatial distribution at density ρ_0 is generated using the random sequential adsorption (RSA) method [37,38]. In the case of mixtures of obstacles, at each deposition attempt, one of the objects that makes the mixture is selected at random and deposition of the selected object is tried in a randomly chosen lattice site. In this way we are able to prepare the environment in disordered initial state with a statistically reproducible density ρ_0 of obstacles. To initialize the model, N_0^C chasers and N_0^T targets are randomly distributed as monomers in the lattice. Each site can be either empty or occupied by one particle: by a chaser or escapee (target) or by a particle that belongs to an obstacle.

After placing the chasers and the targets up to the chosen densities $\rho_0^C = N_0^C/L^2$ and $\rho_0^T = N_0^T/L^2$, we switch the species deposition events off and initiate a random diffusive dynamics in the system. At this stage, apart from the hard core interaction between the species, and between the species and the obstacles, there are simple rules governing the dynamic processes at the individual level. Movement within the lattice and the population dynamics are modeled as discrete time processes. At each Monte Carlo step a lattice site is selected at random. If the selected site is unoccupied or occupied by an obstacle, the configuration remains unchanged and a new site is selected at random. If the selected site is occupied by a chaser or an escapee, each species follow the hopping rules described below.

Chaser has a certain pursuit region within which it can locate targets; simultaneously, target has an escape zone inside which it can detect chasers. In other words, each species has its specific sighting range σ in which it can see the other species. By definition, the metric is L^1 , so e.g. the site (x, y) is at distance $|x| + |y|$ from the origin, with lattice spacing equal to unity. Two types of chasers and targets are used in our model depending on the sighting range σ : Chasers-I and Targets-I have sighting range $\sigma = 1$, while for Chasers-II and Targets-II, $\sigma = 2$.

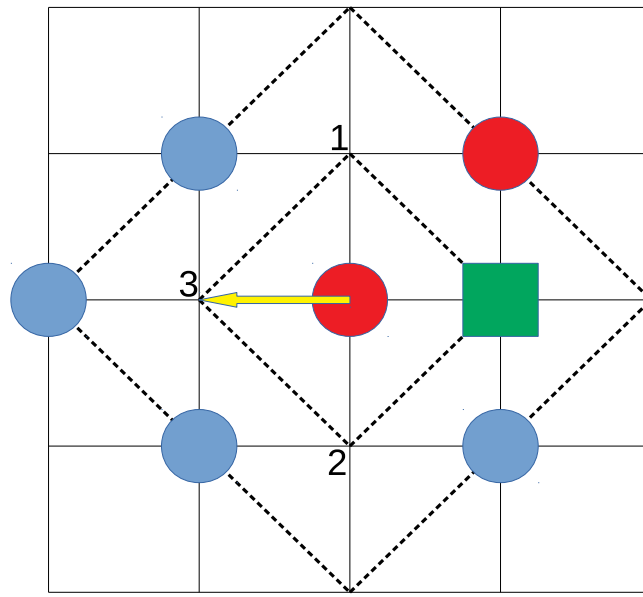
Suppose that Chaser-I is placed in a randomly selected site of the lattice. If the first neighbors of the selected site are entirely occupied with obstacles and chasers, the chosen chaser stays at its original position. Then, the time t is updated, $t \rightarrow t + 1/L^2$ and the process continues by choosing a new lattice site at random. Suppose that some of the first neighbors of the selected site are occupied with targets. Then we randomly select a target among them, remove the selected target from the grid, and move the chosen chaser to this empty place. However, if the first neighbors of the chosen chaser are not occupied with targets, the chaser executes a jump as long as there is at least one empty nearest neighbor site. In this case, the chaser is moved to the randomly selected empty adjacent site.

Now, suppose that Target-I is placed in a randomly selected site of the lattice. If there are no empty nearest neighbors of the selected site, the chosen target does not change its position, and the time increases by $1/L^2$. If the selected site has empty adjacent sites, the chosen target moves into one of them randomly.

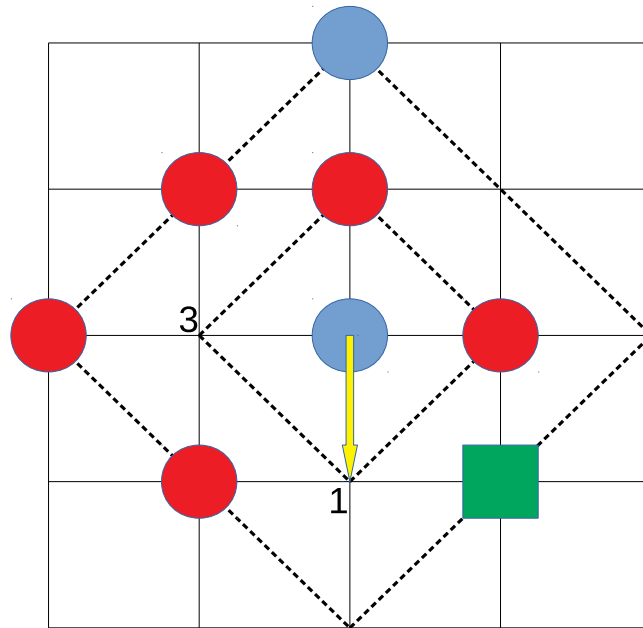
In our model we introduce chasers and targets with different chasing and avoidance skills, respectively, depending on the sighting range σ . Accordingly, decision for every step both of the Chaser-II and Target-II depends on the species that are found at the places of second neighbors. Algorithms for movement of species I and II are different only in the method of selection of the empty neighboring sites for a jump. Species I randomly chooses an empty nearest neighbor site for a jump. However, Chaser-II moves to the empty adjacent site that is surrounded by the highest number of targets, $n_T^{(\max)}$, as its first neighbors (see, Fig. 1(a)). On the contrary, Target-II jumps to the empty nearest neighbor site that is surrounded by the lowest number of chasers, $n_C^{(\min)}$, as its first neighbors (see, Fig. 1(b)). If two or more empty nearest neighbor sites correspond to the same highest/lowest number of targets $n_T^{(\max)}$ /chasers $n_C^{(\min)}$, one of them is selected at random. It must be emphasized that Target-II moves to the selected site only if $n_C^{(\min)}$ is less than or equal to the number of chasers surrounding it in its original position. In both cases when the sighting range σ is one or two, pursuer and evader can move only to a neighboring site. Neither chasers nor evaders can see through the obstacles and they make their decision about the movement without the knowledge of the situation behind the obstacle.

The time t is counted by the number of attempts to select a lattice site and scaled by the total number of lattice sites $N = L^2$. Since in one Monte Carlo time step each lattice site is randomly checked once on the average, it can be considered that all chasers and targets are active at all times and that none of the species have a priority in the number of attempts to make a move. The simulation data are averaged over 100 independent runs for each coverage of obstacles and each initial chasers and targets concentrations.

The simulations have been performed for a wide range of obstacle densities, $\rho_0 < 0.45$, below the corresponding percolation thresholds [46,47]. Considering the underlying percolation problem on the lattice, a geometric transition occurs at the percolation threshold p_c^* , above which the void space falls completely apart into finite clusters. As density of obstacles is increased above a certain critical value p_c^* , the initial large cluster of empty lattice space breaks into tiny non-communicating components and connectivity between both sides of the lattice disappears. In this case, spatially separated groups of chasers and targets can be formed on the lattice during the initialization process. Such artificial situations will not be considered in this paper.



(a)



(b)

Fig. 1. Hopping rules for (a) chasers and (b) targets. Diamonds represent their respective sighting ranges, $\sigma = 1, 2$. The green squares show the obstacles. Chasers (red circles) look for the nearest target and move to one of the nearest sites in order to catch the target. Targets (blue circles) try to escape from the nearest chaser. When a target is in a site nearest to a chaser, the chaser catches the target by hopping to the site, and then the target is removed from the system. Panel (a): Yellow arrow from the chaser to the adjacent site indicates that the Chaser-II hops to the empty site that is surrounded by the highest number of targets ($n_t^{(\max)} = 3$). Chaser-I has three choices. Panel (b): Yellow arrow from the target to the adjacent site indicates that Target-II hops to the empty site that is surrounded by the lowest number of chasers ($n_c^{(\min)} = 1$). Target-I has two choices. Values of the number of the nearest targets and chasers are given for the empty adjacent sites.

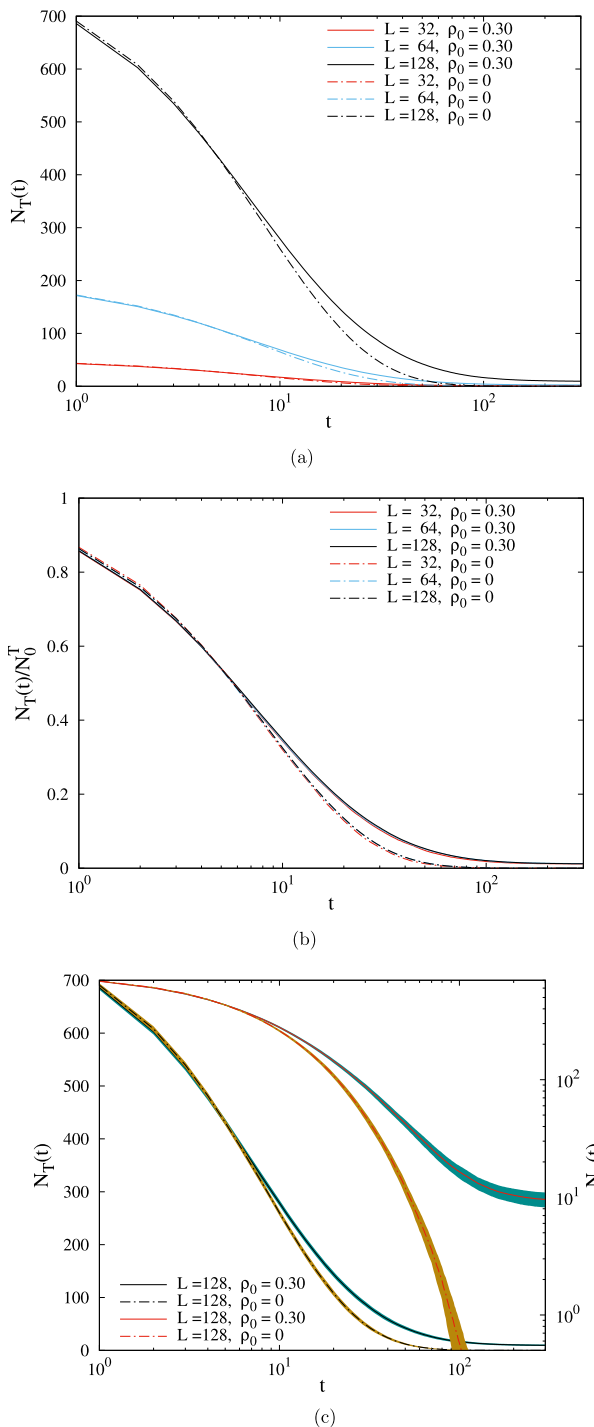


Fig. 2. Time dependences of the number of targets $N_T(t)$ (panel (a)) and of the normalized number of targets $N_T(t)/N_0^T$ (panel (b)) on the lattices of size $L = 32, 64,$ and $128,$ as indicated in legend. The full curves represent the results obtained when obstacles are the binary mixtures of trimers (A_3) and crosses (C_1) of density $\rho_0 = 0.30$ (see, Tables 1 and 2). The dashed curves represent the results obtained in the absence of obstacles. Panel (c): Shown here are the temporal dependences of the number of targets $N_T(t)$ on the lattice of size $L = 128,$ obtained for the same conditions as in panel (a) (see legend). The black (red) lines are plotted against the left-hand (right-hand) axis. The shaded region represents the standard deviation. Results shown in panels (a), (b), and (c) are obtained for the same initial densities $\rho_0^C = 0.0439$ and $\rho_0^T = 0.0488,$ for all lattices. Initial values for the number of chasers/targets are $N_0^C/N_0^T = 45/50, 180/200, 720/800$ for $L = 32, 64, 128,$ respectively.

3. Results and discussion

While the number of chasers, $N_C(t)$, remains constant N_0^C , the number of targets, $N_T(t)$, monotonically decreases along with the catches. Here we focus on the model that includes species with sighting range $\sigma = 2$ (Chasers-II + Target-II), and study the effects of obstacles on the time evolution of the number of targets, $N_T(t)$. In addition, we will compare the results for all four combinations of previously defined species I and II, as shown in Table 3.

In our model, lattice size L is an arbitrary parameter. In Fig. 2(a) we show the temporal dependence of the number of targets $N_T(t)$ on the lattices of size $L = 32, 64,$ and 128 , when obstacles are the binary mixtures of trimers (A_3) and crosses (C_1) of density $\rho_0 = 0.30$ (see, Tables 1 and 2). For comparison, we also plot the temporal dependences of the number of targets $N_T(t)$ in the absence of obstacles for these three lattices. It is important to note that the initial densities of chasers ρ_0^C and targets ρ_0^T have not changed with the lattice size L . Numerical results for $N_T(t)$ in Fig. 2(a) are given for the initial densities $\rho_0^C = 0.0439$ and $\rho_0^T = 0.0488$, with the same ratio $\rho_0^C/\rho_0^T = N_0^C/N_0^T = 0.9$ for all the lattices. In Fig. 2(b), the values of the normalized number of targets $N_T(t)/N_0^T$ versus the time t are presented for the simulation results shown in Fig. 2(a). It is evident that for the given density of the obstacles ρ_0 , the time evolution of the normalized number of targets $N_T(t)/N_0^T$ does not depend on the lattice size L . However, for the lattice of fixed size L , time evolution of $N_T(t)/N_0^T$ depends on the initial number of chasers N_0^C and targets N_0^T . We shall return to this point later on in connection with the relationship between the densities of species and dynamics of the model.

In Fig. 2(c) we show the temporal dependence of the number of targets $N_T(t)$ on the lattice of size $L = 128$ obtained for the same conditions as in Fig. 2(a). The shaded strips in Fig. 2(c) indicate an interval of one standard deviation above and below the estimated mean value. In addition, the double logarithmic plots of the same results are also shown in the same panel. In this way, a better insight into the values of the standard deviation during the entire process is enabled. Standard deviations from the average value of $N_T(t)$ are of the order $\pm 1\%$ throughout the whole process of interest. In very late times, when the number of targets disappears, the standard deviation is less than 10%. As it can be seen, the statistical error bars slightly exceed the line thickness.

It must be stressed that all simulations have been performed in the conditions of sufficiently low densities of agents. In this way, we have tried to avoid the effects of the self volume [34,48,49]. In reality, chasers and targets are impenetrable bodies. For example, in an abundant population of prey, the prey species may obstruct each other while trying to escape. Moreover, at sufficiently large densities of targets, target can be temporarily trapped in “cages” formed by their neighbors of the same species. Then the motion of target is restricted by a shell of nearest neighbors, and its movement is influenced by the effect of trapping. However, in our model, agents can be temporarily caged by a dense network of obstacles. In order to make the analysis of the results simpler, it is necessary that these two effects are not present in simulations at the same time. Consequently, all simulations are carried out in the conditions of sufficiently low densities of agents.

In the absence of obstacles, simulations are carried out until all targets have been caught by chasers, i.e. $N_T(t) = 0$. However, in the presence of obstacles, there may be targets that cannot be eliminated by the chasers. Such targets are located within clusters of empty sites (“cages”) in which chasers have not been deposited during the initialization process. The number of inaccessible targets increases with the density of obstacles ρ_0 . Fig. 3 shows two typical snapshot configurations obtained in the case of the binary mixture of obstacles (trimers (A_3) and crosses (C_1)) of density $\rho_0 = 0.30$. The snapshots are taken at the beginning of the process ($t = 1$), and after a long enough time ($t = 300$) when only a few targets ($N_T(300) = 6$) are left in the “cages” formed by obstacles.

Now, we present and discuss the numerical results regarding the time evolution of the number of targets $N_T(t)$ in the absence of obstacles, for several initial densities of chasers ρ_0^C and targets ρ_0^T on the lattice of the fixed size $L = 128$. The initial numbers of species (N_0^C, N_0^T) were chosen as (20, 25), (40, 50), (80, 100), (160, 200), (320, 400), and (640, 800), so that we have the same ratio $N_0^C/N_0^T = 0.8$ in all simulation runs. Temporal evolution of the normalized number of targets $N_T(t)/N_0^T$ for various initial densities $\rho_0^C = N_0^C/L^2$ and $\rho_0^T = N_0^T/L^2$ (provided that $\rho_0^C/\rho_0^T = 0.8$) are presented in Fig. 4. We observe that the decrease of $N_T(t)/N_0^T$ with time gets drastically slower when the initial densities ρ_0^C and ρ_0^T decrease. Analyzing the curves in Fig. 4 we find that the decrease of $N_T(t)/N_0^T$ is slower than exponential in time. In addition, the curves for different values of the initial density of species are very similar in form. In order to provide the best analytical approximation for the temporal behavior of the number of targets $N_T(t)$, we have probed a wide set of phenomenological fitting functions for relaxation processes in many complex disordered systems [50]. The best agreement with our simulation data was obtained by the Kohlrausch–Williams–Watts (KWW) or stretched exponential function. The fitting function we have used is of the form:

$$\frac{N_T(t)}{N_0^T} = 1 + \left(\frac{N_T(\infty)}{N_0^T} - 1 \right) \left(1 - \exp \left[- \left(\frac{t}{\tau} \right)^\beta \right] \right), \quad (1)$$

where β is the parameter measuring the deviation from the single exponential form ($0 < \beta \leq 1$) and τ is the characteristic time. Fits of this stretched exponential form to the simulation data are shown as dashed lines in Fig. 4. Since the asymptotic number of targets $N_T(t) \rightarrow N_T(\infty)$, $t \gg \tau$, in the absence of the obstacles is equal to zero for all initial densities of species, the characteristic time τ can be defined as the time it takes for the simulation curves of $N_T(t)/N_0^T$ to fall to the level of $1/e$, i.e., $N_T(\tau)/N_0^T = 1/e$. In the absence of obstacles, the fitting parameter τ is given in Fig. 5 as a function of the initial density of targets ρ_0^T , for two values of the ratio $N_0^C/N_0^T = 0.8, 1.0$. In numerical simulations with the ratio $N_0^C/N_0^T = 1.0$, the

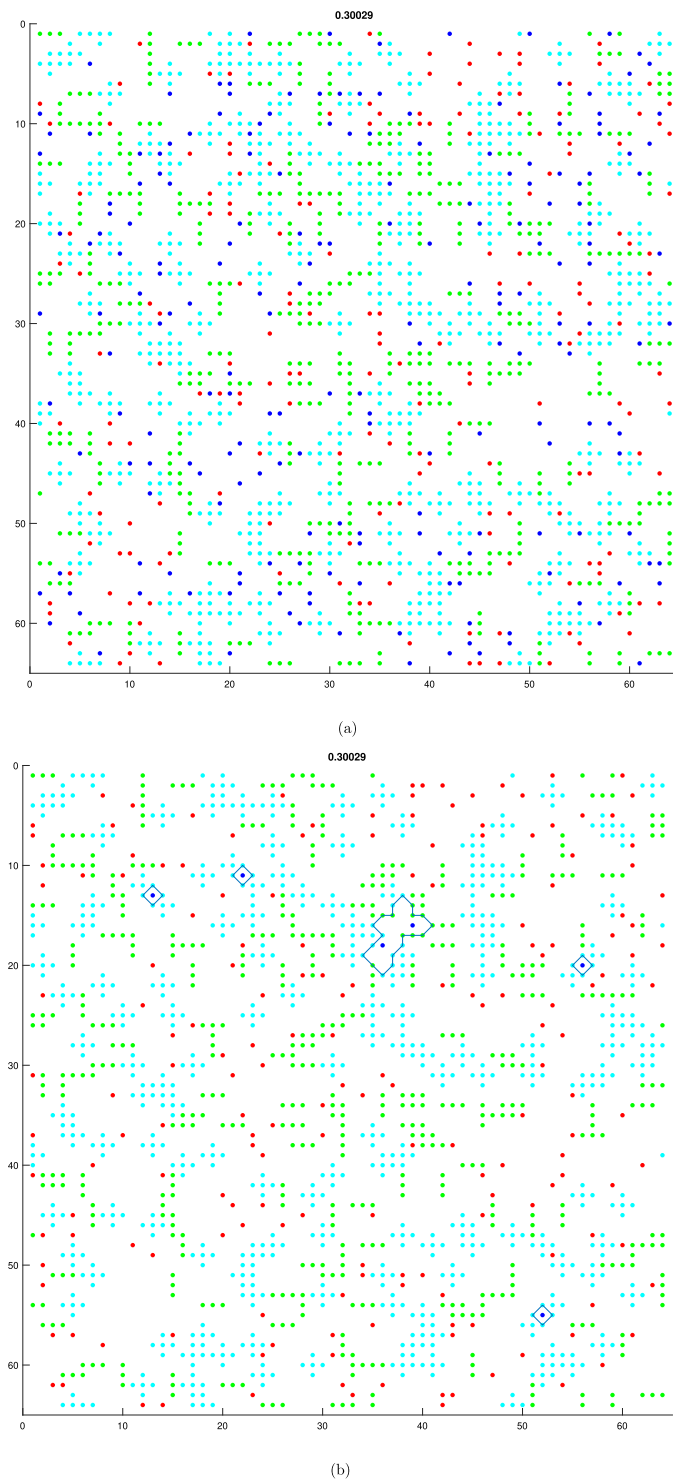


Fig. 3. Typical configurations of chasers (red dots) and targets (blue dots) at lattice of size $L = 64$ in the case of the binary mixture of obstacles (trimers (A_3) and crosses (C_1)) of density $\rho_0 = 0.30$. The snapshots are taken at the beginning of the process ($t = 1$, panel (a)), and after long enough times ($t = 300$, panel (b)) when only six targets are left on the lattice. Five cages with the remaining targets are marked on the panel (b) with thin blue lines. Initial number of chasers/targets is $N_0^C/N_0^T = 180/200$.

initial numbers of species were chosen to be $N_0^C = N_0^T = 25, 50, 100, 200, 400$, and 800 . It is obvious that the parameter τ seems to be a simple power law of the initial density of targets ρ_0^T :

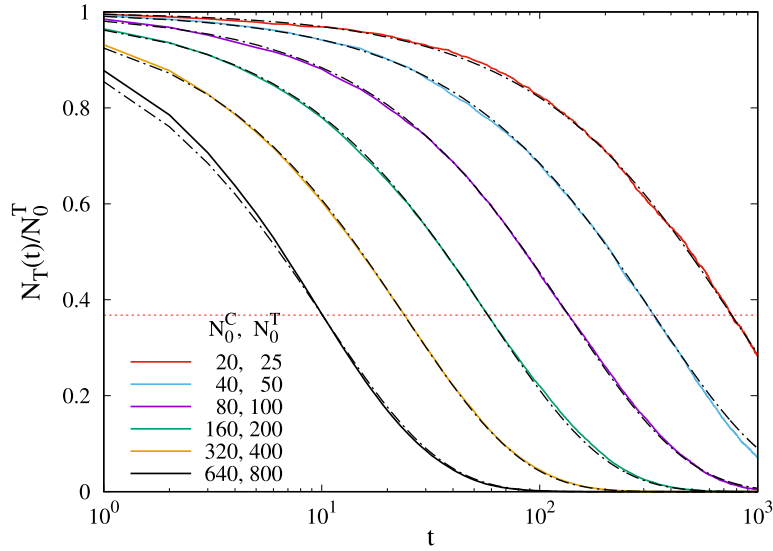


Fig. 4. Temporal evolution of the normalized number of targets $N_T(t)/N_0^T$ obtained in the absence of obstacles on the lattice of the size $L = 128$, and for various initial numbers of species (N_0^C, N_0^T), as indicated in the legend. The dashed curves are the stretched exponential fits of Eq. (1), with the parameter τ given in Fig. 5 and $\beta = 0.802$. Here, the ratio $N_0^C/N_0^T = \rho_0^C/\rho_0^T = 0.8$ is the same in all simulation runs. The horizontal dashed line indicates the $1/e$ value.

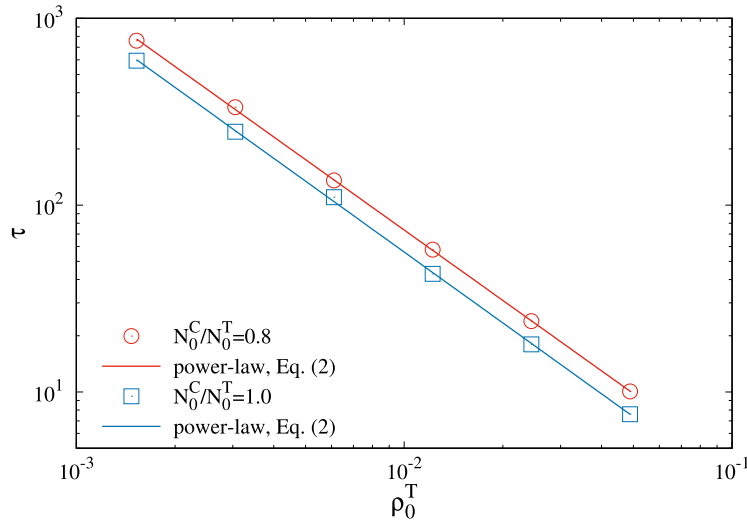


Fig. 5. Fitting parameter τ of the fit (1), as a function of the initial density of targets ρ_0^T in the case of the absence of obstacles, for two values of the initial ratio of chasers to targets $N_0^C/N_0^T = 0.8, 1.0$. The straight lines are the fits using Eq. (2). Dependence of τ on ρ_0^T seems to be well described by the simple power law (2). The values of fitting parameters are $A = 0.230, \gamma = 1.252, \beta = 0.802$ for $N_0^C/N_0^T = 0.8$; for $N_0^C/N_0^T = 1.0$, the fitting parameters are $A = 0.169, \gamma = 1.261, \beta = 0.805$.

$$\tau = A (\rho_0^T)^{-\gamma}. \tag{2}$$

Exponent γ is approximately equal to $\gamma = 1.256 \pm 0.006$ for all examined ratios N_0^C/N_0^T . On the other hand, the stretching exponent β has the values below one, which confirms the nonexponential functional dependence of $N_T(t)/N_0^T$. Furthermore, for the fixed value of ratio N_0^C/N_0^T the exponent β is rather weakly dependent on the initial density of targets ρ_0^T . This provides the collapse of $N_T(t)/N_0^T$ vs. t curves onto a single curve when the time is scaled as t/τ . Fig. 6 shows the time-density superposition of the $N_T(t)/N_0^T$ curves in the case of the ratio $N_0^C/N_0^T = 0.8$, for all initial densities of species investigated. This figure clearly demonstrates the existence of a single universal master function.

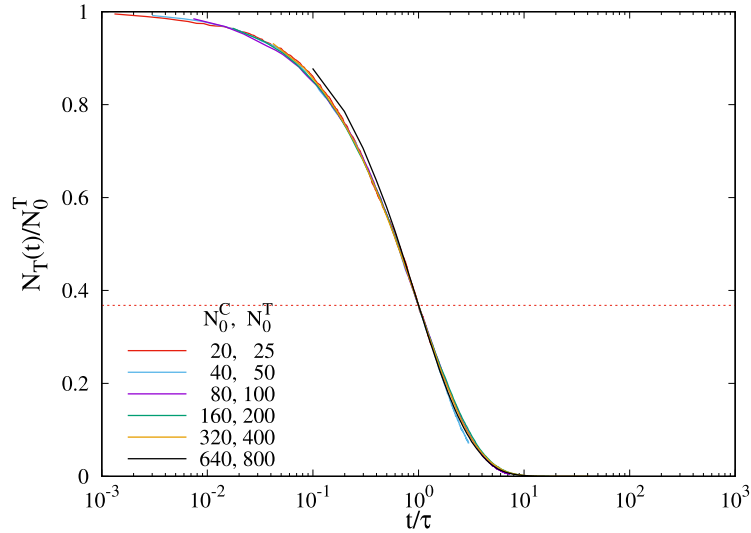


Fig. 6. Normalized number of targets $N_T(t)/N_0^T$ obtained in the absence of obstacles and rescaled to t/τ , for various initial numbers of species (N_0^C, N_0^T), as indicated in the legend. Here, the ratio $N_0^C/N_0^T = \rho_0^C/\rho_0^T = 0.8$ is the same in all simulation runs. The horizontal dashed line indicates the $1/e$ value.

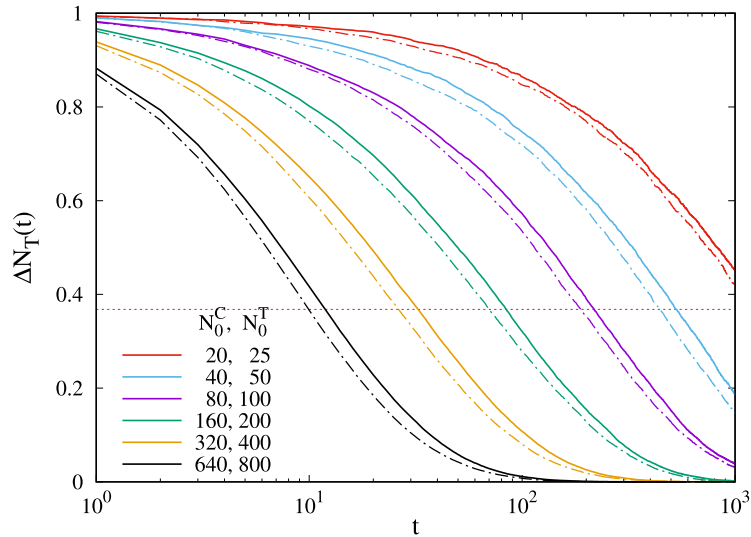


Fig. 7. Temporal evolution of the normalized deviation $\Delta N_T(t)$ (Eq. (3)) of the number of targets $N_T(t)$ obtained in the presence of obstacles (A_1) (solid lines) and (C_1) (dashed lines) on the lattice of size $L = 128$, and for various initial numbers of species (N_0^C, N_0^T), as indicated in the legend. Here, the ratio $N_0^C/N_0^T = \rho_0^C/\rho_0^T = 0.8$ is the same in all simulation runs. The horizontal dashed line indicates the $1/e$ value.

In the following, we analyze the time evolution of the number of targets $N_T(t)$ in the presence of obstacles, for various initial densities of chasers ρ_0^C and targets ρ_0^T on the lattice of the fixed size, $L = 128$. In order to gain a better insight into the effect of obstacles on the capture dynamics, simulations are performed both for point-like obstacles (A_1) and for obstacles of cruciform shape (C_1) covering five lattice sites (see, Tables 1 and 2). Furthermore, the results are obtained for the various values of density of the obstacles, $\rho_0 = 0.15, 0.20, 0.25$, and 0.30 . Let us first focus our attention on the representative results given in Fig. 7 for the case of density $\rho_0 = 0.25$. Fig. 7 shows the time evolution of the normalized deviation $\Delta N_T(t)$ of the number of targets $N_T(t)$ from the asymptotic value $N_T(\infty)$ for various initial densities ρ_0^C and ρ_0^T , provided that $N_0^C/N_0^T = \rho_0^C/\rho_0^T = 0.8$. The quantity $\Delta N_T(t)$ is defined as

$$\Delta N_T(t) = \frac{N_T(t) - N_T(\infty)}{N_0^T - N_T(\infty)}. \quad (3)$$

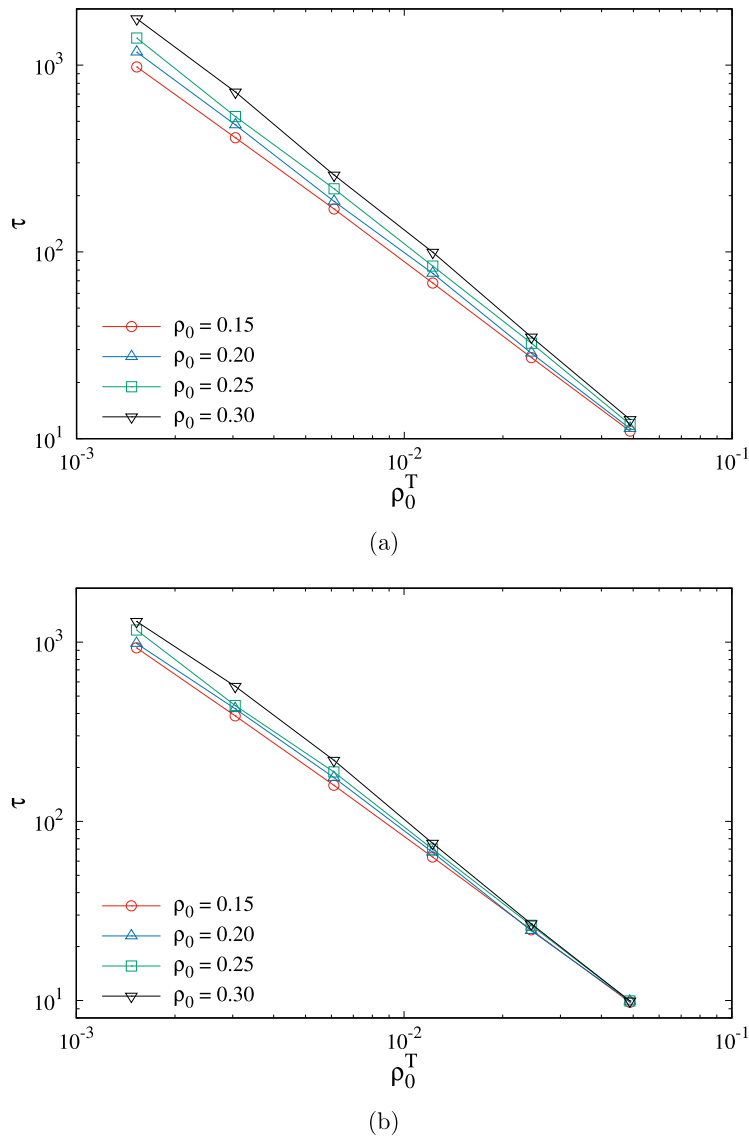


Fig. 8. Fitting parameter τ of the fit (1), as a function of the initial density of targets ρ_0^T in the case of the presence of (a) obstacles (A_1), and (b) obstacles (C_1). The curves in each graph correspond to various values of the density of obstacles $\rho_0 = 0.15, 0.20, 0.25, 0.30$, as indicated in the legend. All the results are for $N_0^C/N_0^T = 0.8$.

As in the case of the absence of obstacles, we observe that the decrease of $N_T(t)/N_0^T$ with time gets slower with the decrease in the initial densities ρ_0^C and ρ_0^T . Comparing the results from Fig. 7 for different obstacles at the same density $\rho_0 = 0.25$, one can see that the number of targets $N_T(t)$ in the case of point-like obstacles (A_1) decreases more slowly in time than for the case of obstacles of cruciform shape (C_1). This change in the capture dynamics is the result of a different structure of empty space that is formed after the deposition of obstacles of different size up to the chosen coverage fraction ρ_0 . Actually, the mesh structure of the open spaces look very different for the adsorbing point-like obstacles (A_1) in comparison with the extended obstacles (C_1) [38,51]. Deposition of the extended obstacles (C_1) is characterized by domains of large islands of unoccupied sites. On the other hand, small obstacles such as monomers (A_1) cover the surface more uniformly, so that the empty space on the lattice is broken into small areas. Such a different free space view is the cause of the enhanced mobility of species in the case of cruciform shapes (C_1) as compared to those in the case of point-like shapes (A_1), resulting in a faster decrease of the number of targets $N_T(t)$ in the former case.

It must be stressed that the stretched-exponential fit (Eq. (1)) also accurately describes the temporal dependence of the number of targets $N_T(t)$ in the presence of obstacles (not shown here). Dependences of the nonlinear fitting parameter τ on the initial density of targets ρ_0^T are shown in Fig. 8 on a double logarithmic scale for various densities of obstacles (A_1) and (C_1), $\rho_0 = 0.15 - 0.30$. For all examined densities and obstacle shapes these plots are nearly straight lines, indicating

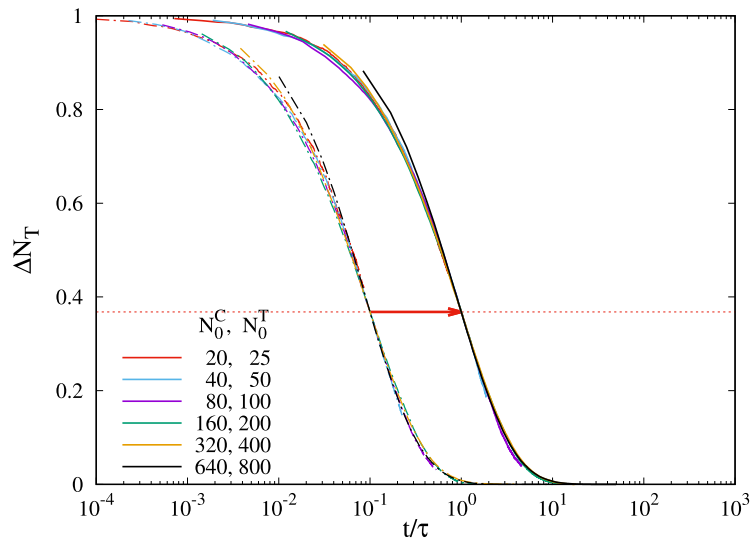


Fig. 9. Normalized deviation $\Delta N_T(t)$ (Eq. (3)) of the number of targets $N_T(t)$ obtained in the presence of obstacles (A_1) (solid lines) and (C_1) (dashed lines) and rescaled to t/τ , for various initial numbers of species (N_0^C, N_0^T), as indicated in the legend. For clarity, the data for obstacle (C_1) are shifted to the left ($t \rightarrow t/10$). Here, the lattice size is $L = 128$, density $\rho_0 = 0.25$, and the initial ratio of chasers to targets $N_0^C/N_0^T = \rho_0^C/\rho_0^T = 0.8$ are the same in all simulation runs. The horizontal dashed line indicates the $1/e$ value.

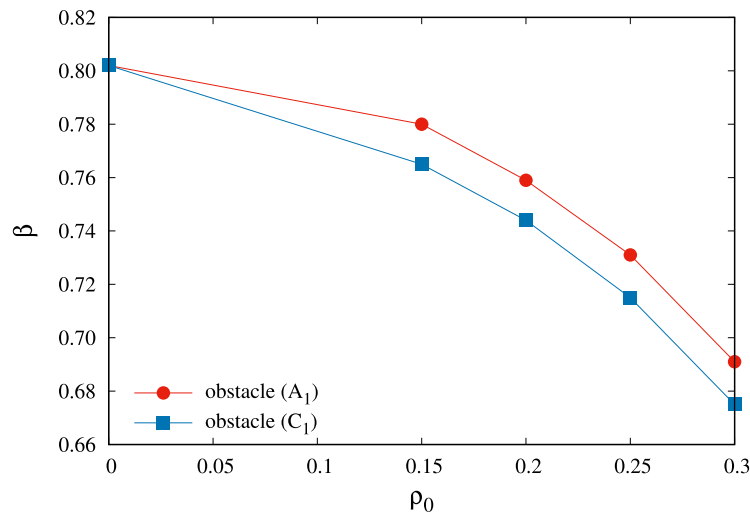


Fig. 10. Parameter β of the fit (1) vs. the density ρ_0 of the obstacles. Circles and squares correspond to obstacles (A_1) and (C_1) in Tables 1 and 2, respectively. Other parameters: $L = 128$, $N_0^C/N_0^T = \rho_0^C/\rho_0^T = 0.8$.

that the fitting parameter τ is a simple power-law of the initial density of targets ρ_0^T (see Eq. (2)). As in the case of the absence of obstacles, we observe that the dynamical behavior of our model is severely slowed down with the decrease of the initial densities ρ_0^C and ρ_0^T . In addition, the characteristic time τ is found to increase with the density of obstacles ρ_0 . As one can see from Figs. 8(a) and 8(b), the increase of τ with ρ_0 is more pronounced for the lower initial densities of targets. Indeed, the efficiency of chasing becomes very high at larger densities of targets and weakly dependent on the presence of obstacles, due to the smaller mean distance between chasers and targets. Then the chasers quickly and efficiently find the neighboring targets, regardless of whether there are obstacles or not. However, for the lower initial concentration of targets the presence of obstacles noticeably slows down the dynamics of the system. We notice, the lower is the concentration of the targets, the longer is the mean distance that a chaser crosses to find a target and catch it. Along the longer path, chaser will interact with a larger number of obstacles. Therefore, obstacles more effectively suppress the chasing for lower densities of targets. Also, at sufficiently low densities of targets, obstruction of chasing is more pronounced at the higher densities of the obstacles.

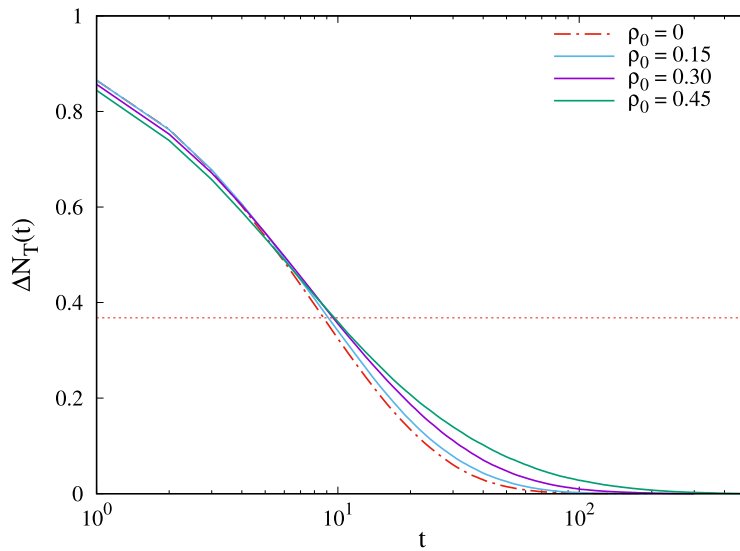


Fig. 11. Temporal evolution of the normalized deviation $\Delta N_T(t)$ (Eq. (3)) of the number of targets $N_T(t)$ obtained in the presence of obstacles (A_3) (solid lines) for various densities ρ_0 , as indicated in the legend. The dashed line represents the temporal behavior of $\Delta N_T(t)$ in the absence of obstacles. Other parameters: $L = 128$, $N_0^C/N_0^T = 720/800 = 0.9$.

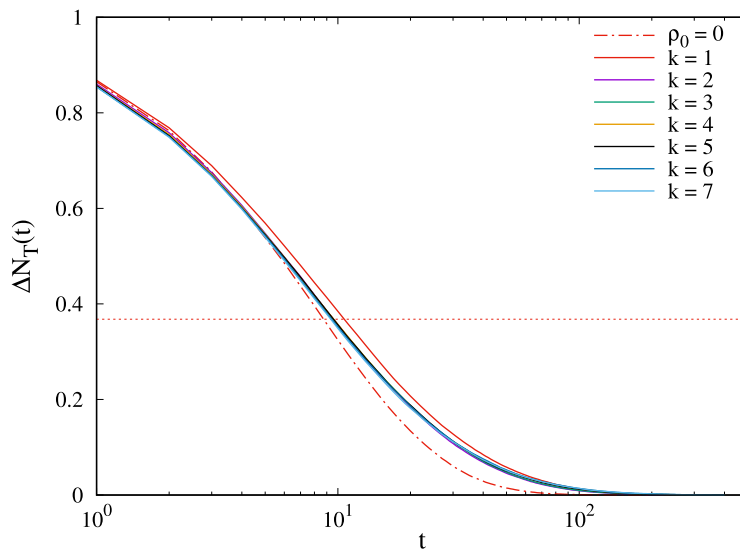


Fig. 12. Temporal evolution of the normalized deviation $\Delta N_T(t)$ (Eq. (3)) of the number of targets $N_T(t)$ obtained in the presence of obstacles (A_1, A_2, \dots, A_7) of density $\rho_0 = 0.30$ (solid lines). The dashed line represents the temporal behavior of $\Delta N_T(t)$ in the absence of obstacles. Other parameters: $L = 128$, $N_0^C/N_0^T = 720/800 = 0.9$.

Fig. 9 illustrates that when the normalized deviations $\Delta N_T(t)$ (see, Eq. (3)) presented in Fig. 7 are plotted as a function of t/τ , the data for the all initial numbers of targets, $N_0^T = 25, 50, 100, 200, 400$ and 800 , collapse onto a single curve. We note that different choices of obstacles give qualitatively similar results. This superposition of ΔN_T vs. t/τ curves is a consequence of the fact that for the fixed values of ratio N_0^C/N_0^T and density of obstacles ρ_0 , the fitting parameter β is rather weakly dependent on the initial density of targets ρ_0^T . However, the stretching exponent β depends on the density ρ_0 of the obstacles. Fig. 10 shows dependence of parameter β on density ρ_0 for the two types of obstacles (A_1) and (C_1). Parameter β measures the rate of the chasing process on the time scale determined by the parameter τ . Consequently, in the late stage of the chasing process the decay rate of the number of targets $N_T(t)$ for the point-like obstacles (A_1) is higher than for the extended obstacles (C_1).

Now we consider in more details the influence of the length ℓ and density ρ_0 of the linear segments that make the obstacles on the temporal behavior of the number of targets $N_T(t)$. The simulations have been performed for linear segments (k -mers) of lengths $\ell = k - 1$, $k = 1, 2, \dots, 7$ (see, Table 1), and for a wide range of obstacle densities,

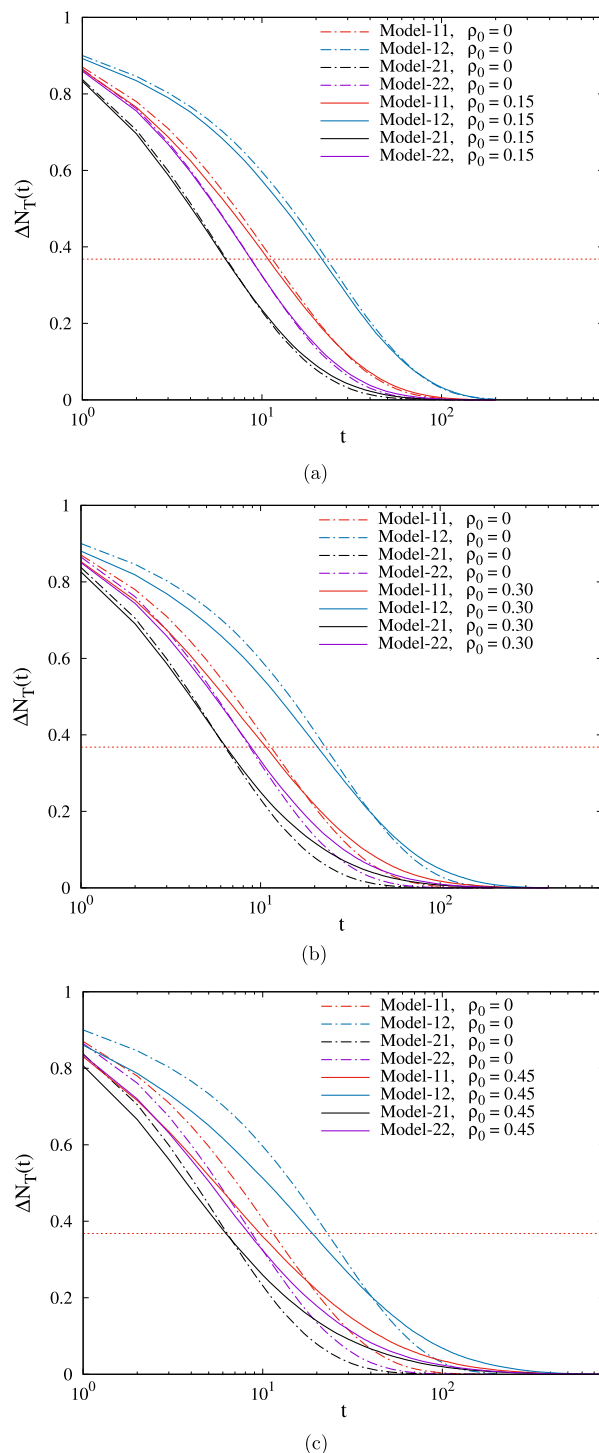


Fig. 13. Temporal behavior of the normalized deviation $\Delta N_T(t)$ (Eq. (3)) for the four models (Model- ij , $i, j = 1, 2$) created by combining the two types of chasers and targets, as shown in Table 3. The solid lines represent the results obtained in the presence of obstacles C_2 (see, Table 2) at densities $\rho_0 = 0.15$ (a), 0.30 (b), 0.45 (c). The dashed lines represent the temporal behavior of $\Delta N_T(t)$ in the absence of obstacles. Other parameters: $L = 128$, $N_0^C/N_0^T = 720/800 = 0.9$.

$\rho_0 = 0 - 0.45$. At first, we present the results of simulations for one representative linear segment, i.e., for the trimer (A_3) at densities $\rho_0 = 0.15, 0.30, 0.45$. The corresponding time dependences of the normalized deviation $\Delta N_T(t)$ (see,

Table 1

Jamming coverages $\rho_j^{(x)}$ for various k -mers (x) of length $\ell^{(x)}$ on a square lattice. The estimated statistical errors are on the last given digits.

(x)	k -mer	$\ell^{(x)}$	$\rho_j^{(x)}$
(A_1)	•	0	1.0
(A_2)	—	1	0.9067
(A_3)	— —	2	0.8465
(A_4)	— — —	3	0.8102
(A_5)	— — — —	4	0.7867
(A_6)	— — — — —	5	0.7699
(A_7)	— — — — — —	6	0.7578

Table 2

Jamming coverages $\rho_j^{(x)}$ for extended shapes (x) of size $s^{(x)}$ on a square lattice. The estimated statistical errors are on the last given digits.


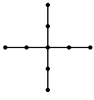
(x)	Shape	$s^{(x)}$	$\rho_j^{(x)}$
(C_1)		2	0.6988
(C_2)		4	0.5691

Table 3

Four models created by combining the two types of chasers and targets. Depending on the sighting range σ , chasers and targets with different chasing and avoidance skills, respectively, can be distinguished.

Model	Chaser	Target
Model-11	Chaser-I ($\sigma = 1$)	Target-I ($\sigma = 1$)
Model-12	Chaser-I ($\sigma = 1$)	Target-II ($\sigma = 2$)
Model-21	Chaser-II ($\sigma = 2$)	Target-I ($\sigma = 1$)
Model-22	Chaser-II ($\sigma = 2$)	Target-II ($\sigma = 2$)

Eq. (3)) for the aforementioned densities ρ_0 are given in Fig. 11 together with the result obtained in the absence of the obstacles. It can be seen that the capture dynamics gets slower, and the evolution of the number of targets $N_T(t)$ toward the asymptotic value $N_T(\infty)$ takes place on much wider time scale when the density of trimers ρ_0 increases. We note that different choices of the linear segments give qualitatively similar results.

In Fig. 12 we compare the temporal evolution of the normalized deviation $\Delta N_T(t)$ (see, Eq. (3)) for the linear segments (k -mers) covering $k = 1, 2, \dots, 7$ lattice sites. Time dependences of $\Delta N_T(t)$ are displayed both for the density $\rho_0 = 0.30$ of obstacles, and for the case of lattice without obstacles. In the presence of k -mers, reduction in the number of targets $N_T(t)$ takes place on the approximately equal time scale for all k -mers. As expected, the decrease of the number of targets $N_T(t)$ with time is significantly faster in the absence of obstacles. It is interesting that $\Delta N_T(t)$ vs. t curves have similar shapes for all finite-size k -mers ($k > 1$). As can be seen, for the point-like obstacles ($k = 1$) the capture dynamics gets slower, especially in the intermediate time regime. There is an important difference between the deposition of point-like and elongated obstacles on a square lattice. Deposition of elongated objects is characterized with domains of parallel objects and large areas of unoccupied sites. Blocking of the lattice area is enhanced with the growth of the obstacle length, making the surface more porous (unoccupied sites can form open and large pores). On the other hand, the point-like objects (monomers) cover the surface more uniformly and efficiently. Lower porosity of the surface is responsible for the reduced mobility of species, and therefore for slower dynamics in the case of the point-like obstacles.

In Section 2 we have introduced the chasers and the targets with different chasing and avoidance skills, respectively. Depending on the sighting range σ , less ($\sigma = 1$) and more ($\sigma = 2$) capable chasers or targets can be distinguished (see, Table 3). It is now useful to explore the relationship between the ability of species and the capture dynamics. In Fig. 13 we compare the temporal evolution of the normalized deviation $\Delta N_T(t)$ (see, Eq. (3)) for all four combinations of previously defined species, as shown in Table 3. The results are given for the obstacle C_2 (see, Table 2) at densities $\rho_0 = 0.15, 0.30, 0.45$, as well as for the lattice without obstacles. By comparing the results for the Model-12 with those for the Model-22 and Model-11, it can be observed that the less capable chasers or the more capable targets cause a significantly slower decrease in the number of targets $N_T(t)$ to the asymptotic value $N_T(\infty)$. On the contrary, by comparing results for the Model-21 with those for the Model-22 and Model-11, it is obvious that the less capable targets or the more capable chasers hasten the dynamics of the chasing process.

As can be seen from Fig. 13 the decrease in the number of targets in the presence of obstacles at sufficiently small times is faster than in the absence of obstacles, and this effect is more pronounced for the larger densities of obstacles.

At the beginning of the process, the density of targets is high, so that the mean distance between them is small. As a consequence, a chaser quickly and efficiently find targets in its own vicinity. At the same time, the obstacles make it difficult for the targets to escape from the nearest chaser. Therefore, the presence of obstacles increases the efficiency of chasers in the initial phase of the evolution of the number of targets.

However, in the late chasing stage inversion occurs, i.e., the presence of obstacles slows down the dynamics of the system (see, Fig. 13). Indeed, the lower is the concentration of the targets, the longer is the time necessary for the chaser to find a target and catch it. Thus, the mean distance that a chaser crosses between two consecutive catches increases over time. Along the longer path, chaser will interact with a larger number of obstacles. Therefore, obstacles more effectively hinder the chasers when the density of the targets becomes small enough.

In models with more capable chasers (Model-22 and Model-21), the presence of obstacles induces larger changes in the dynamics of the system in the late chasing stage than in the initial phase of the process. At the beginning of the process, more capable chasers quickly and efficiently find the neighboring targets, regardless of whether there are obstacles or not. However, less capable chasers interact with a larger number of obstacles between two consecutive catches. Consequently, in the cases of less capable chasers (Model-11 and Model-12), the differences in the dynamics of the system with and without obstacles are pronounced even in the initial phase of the evolution of the number of targets.

4. Summary

We have numerically studied a stochastic lattice model describing a group chase and escape with sight-limited chasers and targets. We take into account the spatial structure of the environment where the species coexist in an explicit way. The environment heterogeneities are built by randomly selecting a fraction of the sites of the square lattice that are considered forbidden for the species. Specifically, the obstacles are represented by non-overlapping lattice shapes that are randomly placed and fixed on the lattice. Our focus in this paper was to investigate the role that density and shape of obstacles plays in the time evolution of the number of targets, $N_T(t)$. Basic mechanisms responsible for the studied phenomenon were investigated and for this reason we ignored the birth/death processes. Such processes will be considered in the future work.

It was shown that the stretched exponential behavior (Eq. (1)) excellently describes the temporal dependence of the number of targets $N_T(t)$ regardless of whether the obstacles are present or not. The characteristic timescale τ was found to decrease with the initial density of targets ρ_0^T according to a power-law (2), $\tau \propto (\rho_0^T)^{-\gamma}$. Furthermore, it was obtained that the characteristic time τ increases with the density of obstacles ρ_0 . This effect was much more pronounced at the lower densities ρ_0 investigated.

We have considered the behavior of the stretched exponent β (Eq. (1)) as a function of the initial density of targets ρ_0^T and the density of obstacles ρ_0 . At the given density of obstacles ρ_0 , the exponent β is weakly dependent on the initial density of targets ρ_0^T , provided the initial ratio of chasers to targets $N_0^C/N_0^T = \rho_0^C/\rho_0^T$ is constant. However, the stretching exponent β , which measures the rate of the chasing process, decreases with the density of the obstacles ρ_0 . At the fixed density ρ_0 , parameter β depends on the shape and size of the obstacles.

The simulations have shown that the time dependences of $\Delta N_T(t)$ (Eq. (3)), at the fixed density ρ_0 , are very similar for all finite-size k -mers ($k > 1$). However, slowing down in the capture dynamics was observed in the case of the point-like obstacles ($k = 1$). Indeed, randomly deposited monomers cover the lattice more uniformly and therefore efficiently reduce the mobility of species.

We have discussed the significance of the sighting range σ of species for governing the capture dynamics in the presence of obstacles. It was shown that the less capable chasers/targets ($\sigma = 1$) or the more capable targets/chasers ($\sigma = 2$) slow-down/hasten the dynamics of the chasing process. It was observed that the decrease in the number of targets in the presence of obstacles at sufficiently small/large times is faster/slower than in the absence of obstacles, and this effect is more pronounced for larger densities of obstacles. In the case of more capable chasers ($\sigma = 2$), the presence of obstacles induces larger changes in the dynamics of the system in the late chasing stage than in the initial phase of the process. In the case of the less capable chasers ($\sigma = 1$), differences in the dynamics of the system with and without obstacles are pronounced in the initial phase of the evolution of the number of targets.

This model can easily be generalized using obstacles of various shapes, describing the system of interest. Features of the chasers and escapees as well as their capabilities can also be modified according to the system of interest. Our simulation can describe in a simple manner some real life systems or tools that are still in development, and becoming more important. Application can be seen even in robotics, especially in unmanned vehicles, designed to avoid obstacles (something that could be developed in new versions of our simulation) and win certain targets that are fixed or in motion, depending on its goal. For instance, one can observe a security robot trying to capture and eliminate malicious evader that is trying to escape. Robot can be instructed not to capture but to follow and monitor the evader (something that could also be developed in other versions of the simulation) and report its behavior. Just visual monitoring can be greatly useful in the home caring situations, for example following elderly people and report if there is an emergency.

Acknowledgments

This work was supported by the Ministry of Education, Science, and Technological Development of the Republic of Serbia under projects ON171017, III45016, and by the European Commission under H2020 project VI-SEEM, Grant No. 675121. Numerical simulations were run on the PARADOX supercomputing facility at the Scientific Computing Laboratory of the Institute of Physics Belgrade.

References

- [1] A. Czirók, E. Ben-Jacob, I. Cohen, T. Vicsek, Formation of complex bacterial colonies via self-generated vortices, *Phys. Rev. E* 54 (1996) 1791–1801.
- [2] A. Czirók, M. Matsushita, T. Vicsek, Theory of periodic swarming of bacteria: Application to proteus mirabilis, *Phys. Rev. E* 63 (2001) 031915.
- [3] A. Sokolov, I.S. Aranson, J.O. Kessler, R.E. Goldstein, Concentration dependence of the collective dynamics of swimming bacteria, *Phys. Rev. Lett.* 98 (2007) 158102.
- [4] D.A. Kessler, H. Levine, Pattern formation in dictyostelium via the dynamics of cooperative biological entities, *Phys. Rev. E* 48 (1993) 4801–4804.
- [5] S. Nagano, Diffusion-assisted aggregation and synchronization in dictyostelium discoideum, *Phys. Rev. Lett.* 80 (1998) 4826–4829.
- [6] W.-J. Rappel, A. Nicol, A. Sarkissian, H. Levine, W.F. Loomis, Self-organized vortex state in two-dimensional dictyostelium dynamics, *Phys. Rev. Lett.* 83 (1999) 1247–1250.
- [7] B. Szabó, G.J. Szöllösi, B. Gönci, Z. Jurányi, D. Selmeczi, T. Vicsek, Phase transition in the collective migration of tissue cells: Experiment and model, *Phys. Rev. E* 74 (2006) 061908.
- [8] P. Friedl, D. Gilmour, Collective cell migration in morphogenesis, regeneration and cancer, *Nat. Rev. Mol. Cell Biol.* 10 (2009) 445457.
- [9] J.M. Belmonte, G.L. Thomas, L.G. Brunnet, R.M.C. de Almeida, H. Chaté, Selfpropelled particle model for cell-sorting phenomena, *Phys. Rev. Lett.* 100 (2008) 248702.
- [10] J. Buhl, D.J.T. Sumpter, I.D. Couzin, J.J. Hale, E. Despland, E.R. Miller, S.J. Simpson, From disorder to order in marching locusts, *Science* 312 (2006) 1402–1406.
- [11] B. Collignon, J.L. Deneubourg, C. Detrain, Leader-based and self-organized communication: Modelling group-mass recruitment in ants, *J. Theoret. Biol.* 313 (2012) 79–86.
- [12] C. Becco, N. Vandewalle, J. Delcourt, P. Poncin, Experimental evidences of a structural and dynamical transition in fish school, *Physica A* 367 (2006) 487–493.
- [13] M. Zheng, Y. Kashimori, O. Hoshino, K. Fujita, T. Kambara, Behavior pattern (innate action) of individuals in fish schools generating efficient collective evasion from predation, *J. Theoret. Biol.* 235 (2005) 153–167.
- [14] I.L. Bajec, F.H. Heppner, Organized flight in birds, *Anim. Behav.* 78 (2009) 777–789.
- [15] C.K. Hemelrijk, H. Hildenbrandt, Some causes of the variable shape of flocks of birds, *PLoS One* 6 (2011) e22479.
- [16] D. Helbing, F. Schweitzer, J. Keltsch, P. Molnár, Active walker model for the formation of human and animal trail systems, *Phys. Rev. E* 56 (1997) 2527–2539.
- [17] D. Helbing, I. Farkas, T. Vicsek, Simulating dynamical features of escape panic, *Nature* 407 (2000) 487–490.
- [18] M. Moussaïd, D. Helbing, G. Theraulaz, How simple rules determine pedestrian behavior and crowd disasters, *Proc. Natl. Acad. Sci.* 108 (2011) 6884–6888.
- [19] J. Kwak, H.-H. Jo, T. Luttinen, I. Kosonen, Collective dynamics of pedestrians interacting with attractions, *Phys. Rev. E* 88 (2013) 062810.
- [20] M. Gutiérrez-Roig, O. Sagarra, A. Oltra, J.R.B. Palmer, F. Bartumeus, A. Díaz-Guilera, J. Perelló, Active and reactive behaviour in human mobility: The influence of attraction points on pedestrians, *Open Sci.* 3 (2016).
- [21] T. Vicsek, A. Zafeiris, Collective motion, *Phys. Rep.* 517 (2012) 71–140.
- [22] P.J. Nahin, *Chases and Escapes: The Mathematics of Pursuit and Evasion*, Princeton University Press, Princeton, NJ, 2007.
- [23] P.L. Krapivsky, S. Redner, Kinetics of a diffusive capture process: Lamb besieged by a pride of lions, *J. Phys. A: Math. Gen.* 29 (1996) 5347.
- [24] G. Oshanin, O. Vasilyev, P.L. Krapivsky, J. Klafter, Survival of an evasive prey, *Proc. Natl. Acad. Sci.* 106 (2009) 13696–13701.
- [25] R. Escobedo, C. Muro, L. Spector, R.P. Coppinger, Group size, individual role differentiation and effectiveness of cooperation in a homogeneous group of hunters, *J. R. Soc. Interface* 11 (2014) <http://dx.doi.org/10.1098/rsif.2014.0204>.
- [26] A. Kamimura, T. Ohira, Group chase and escape, *New J. Phys.* 12 (2010) 053013.
- [27] T. Vicsek, *Nature* 466 (2010) 43.
- [28] R. Nishi, A. Kamimura, K. Nishinari, T. Ohira, Group chase and escape with conversion from targets to chasers, *Physica A* 391 (2012) 337–342.
- [29] P. Romanczuk, I.D. Couzin, L. Schimansky-Geier, Collective motion due to individual escape and pursuit response, *Phys. Rev. Lett.* 102 (2009) 010602.
- [30] V. Zhdankin, J.C. Sprott, Simple predator-prey swarming model, *Phys. Rev. E* 82 (2010) 056209.
- [31] X.-P. Han, T. Zhou, B.-H. Wang, Scaling mobility patterns and collective movements: Deterministic walks in lattices, *Phys. Rev. E* 83 (2011) 056108.
- [32] T.H. Chung, G.A. Hollinger, V. Isler, Search and pursuit-evasion in mobile robotics, *Auton. Robots* 31 (2011) 299.
- [33] T. Iwama, M. Sato, Group chase and escape with some fast chasers, *Phys. Rev. E* 86 (2012) 067102.
- [34] S. Yang, S. Jiang, L. Jiang, G. Li, Z. Han, Aggregation increases prey survival time in group chase and escape, *New J. Phys.* 16 (2014) 083006.
- [35] Y. Chen, T. Kolokolnikov, A minimal model of predators-warm interactions, *J. R. Soc. Interface* 11 (2014) <http://dx.doi.org/10.1098/rsif.2013.1208>.
- [36] A. Kamimura, S. Matsumoto, T. Nogawa, N. Ito, T. Ohira, Stochastic resonance with group chase and escape, in: 2011 21st International Conference on Noise and Fluctuations, 2011, pp. 200–203.
- [37] J.W. Evans, Random and cooperative sequential adsorption, *Rev. Modern Phys.* 65 (1993) 1281–1329.
- [38] Lj Budinski-Petković, I. Lončarević, D. Dujak, A. Karač, J.R. Šćepanović, Z.M. Jakšić, S.B. Vrhovac, Particle morphology effects in random sequential adsorption, *Phys. Rev. E* 95 (2017) 022114.
- [39] N. Boccara, O. Roblin, M. Roger, Automata network predator-prey model with pursuit and evasion, *Phys. Rev. E* 50 (1994) 4531–4541.
- [40] A.F. Rozenfeld, E.V. Albano, Critical and oscillatory behavior of a system of smart preys and predators, *Phys. Rev. E* 63 (2001) 061907.
- [41] H. Chaté, F. Ginelli, G. Grégoire, F. Raynaud, Collective motion of self-propelled particles interacting without cohesion, *Phys. Rev. E* 77 (2008) 046113.
- [42] L. Angelani, Collective predation and escape strategies, *Phys. Rev. Lett.* 109 (2012) 118104.
- [43] T. Vicsek, A. Czirók, E. Ben-Jacob, I. Cohen, O. Shochet, Novel type of phase transition in a system of self-driven particles, *Phys. Rev. Lett.* 75 (1995) 1226–1229.
- [44] H. Wang, W. Han, J. Yang, Group chase and escape with sight-limited chasers, *Physica A* 465 (2017) 34–39.
- [45] J. Travis, Do wandering albatrosses care about math? *Science* 318 (2007) 742–743.
- [46] N. Vandewalle, S. Galam, M. Kramer, A new universality for random sequential deposition of needles, *Eur. Phys. J. B* 14 (2000) 407–410.
- [47] V. Cornette, A.J. Ramirez-Pastor, F. Nieto, Percolation of polyatomic species on a square lattice, *Eur. Phys. J. B* 36 (2003) 391–399.
- [48] M. Bruna, S.J. Chapman, Diffusion of multiple species with excluded-volume effects, *J. Chem. Phys.* 137 (2012) 204116.
- [49] M. Schwarzl, A. Godec, G. Oshanin, R. Metzler, A single predator charging a herd of prey: Effects of self volume and predator-prey decision-making, *J. Phys. A* 49 (2016) 225601.
- [50] R. Hilfer, Analytical representations for relaxation functions of glasses, *J. Non-Cryst. Solids* 305 (2002) 122–126.
- [51] Lj. Budinski-Petković, I. Lončarević, Z.M. Jakšić, S.B. Vrhovac, N.M. Švrakić, Simulation study of anisotropic random sequential adsorption of extended objects on a triangular lattice, *Phys. Rev. E* 84 (2011) 051601.

Random sequential adsorption of lattice animals on a three-dimensional cubic latticeI. Lončarević,¹ Lj. Budinski-Petković,¹ J. R. Šćepanović,² Z. M. Jakšić,² and S. B. Vrhovac^{1,2,*}¹*Faculty of Engineering, Trg D. Obradovića 6, Novi Sad 21000, Serbia*²*Scientific Computing Laboratory, Center for the Study of Complex Systems, Institute of Physics Belgrade, University of Belgrade, Pregrevica 118, Zemun 11080, Belgrade, Serbia*

(Received 15 September 2019; published 14 January 2020)

The properties of the random sequential adsorption of objects of various shapes on simple three-dimensional (3D) cubic lattice are studied numerically by means of Monte Carlo simulations. Depositing objects are “lattice animals,” made of a certain number of nearest-neighbor sites on a lattice. The aim of this work is to investigate the impact of the geometrical properties of the shapes on the jamming density θ_j and on the temporal evolution of the coverage fraction $\theta(t)$. We analyzed all lattice animals of size $n = 1, 2, 3, 4$, and 5 . A significant number of objects of size $n \geq 6$ were also used to confirm our findings. Approach of the coverage $\theta(t)$ to the jamming limit θ_j is found to be exponential, $\theta_j - \theta(t) \sim \exp(-t/\sigma)$, for all lattice animals. It was shown that the relaxation time σ increases with the number of different orientations m that lattice animals can take when placed on a cubic lattice. Orientations of the lattice animal deposited in two randomly chosen places on the lattice are different if one of them cannot be translated into the other. Our simulations performed for large collections of 3D objects confirmed that $\sigma \cong m \in \{1, 3, 4, 6, 8, 12, 24\}$. The presented results suggest that there is no correlation between the number of possible orientations m of the object and the corresponding values of the jamming density θ_j . It was found that for sufficiently large objects, changing of the shape has considerably more influence on the jamming density than increasing of the object size.

DOI: [10.1103/PhysRevE.101.012119](https://doi.org/10.1103/PhysRevE.101.012119)**I. INTRODUCTION**

A broad variety of structures are created of objects packed together, and describing the packing processes are among the most persistent problems in science [1,2]. Understanding of various aspects of packing is of a great scientific and industrial importance, with applications in nanotechnology, material science, biology, agriculture, and ecology [3–7]. Particle packing is still far from well understood. Packing structure is still not able to be predicted by a general model that takes into account various controlling parameters, such as geometric and material properties of objects, gravity, and packing methods.

One common approach to studying the packaging of objects of various shapes is the random sequential adsorption (RSA) method [8] which appears to be the simplest but non-trivial model of random packing. The RSA model considers sequential addition of particles of various shapes at randomly chosen places on the n -dimensional substrate. Overlapping of the particles is not allowed, and there is no diffusion of the deposited objects. The time evolution of the coverage (or the density of the system), $\theta(t)$, i.e., the fraction of the substrate occupied by the deposited objects at time t , describes the kinetic properties of the deposition process. Once an object is placed, it affects the geometry of all later placements, so that the dominant effect in RSA is the blocking of the available substrate space. At sufficiently large times the coverage $\theta(t)$ approaches the jamming value θ_j , where only gaps too small to place new particles are left on the substrate.

Depending on the system of interest, the substrate can be continuum or discrete, and RSA models can differ in substrate dimensionality. Analytical results are available mostly for one-dimensional problems [9–11]. Due to the complexity of deposition of objects of various shapes in higher dimensions, Monte Carlo simulations remain a main tool for describing such systems. The long-term behavior of the coverage fraction $\theta(t)$ is known to be asymptotically algebraic for continuum substrates [11–15] and exponential for lattice models [16–20]. For the discrete case, the approach of the density $\theta(t)$ to the jamming limit θ_j is of the form

$$\theta_j - \theta(t) \sim \exp(-t/\sigma), \quad (1)$$

where jamming density θ_j and the characteristic time σ are the parameters that depend on the details of the model, such as shape and symmetry properties of the depositing objects [17,18,20]. In our model, relaxation time σ is the fitting parameter that will be discussed within the context of the orientational freedom of the shape.

During the past few decades the methods of random sequential deposition of different objects on substrates of various dimensions have developed extensively. Previously, the majority of work has been done for spherical particles [21–23]. To examine the significance of particle anisotropy in formation of the jammed state coverings, RSA of many different object shapes has been studied for both continuum and lattice models. For example, RSA on continuous substrates has been studied for lines and ellipses [24,25], rectangles [26,27], starlike particles [28], superdisks bounded by the Lamé curves [29], spherocylinders and ellipsoids [24,30], cubes [31], cuboids [32], and polymers modeled as chains

*vrhovac@ipb.ac.rs; <http://www.ipb.ac.rs/~vrhovac/>

of identical spheres [33]. It was found that the kinetics of irreversible deposition and morphological characteristics of the packing are strongly dependent on the shape and size of the depositing particles.

Formation of random deposits on discrete substrates has also been extensively studied for various object shapes [16–19,34,35]. Wang and Pandey [36] have studied the RSA kinetics of self-avoiding walk chains on a square lattice and found that the jamming coverage decreases with the chain length according to a power law. Deposition of objects of various sizes and rotational symmetries was studied for a square and triangular lattice [17,18]. It was found that the rapidity of the approach to the jamming coverage depends only on the symmetry order of the shape. The crucial role of the object shape in deposition dynamics was also confirmed in Ref. [20], where the depositing objects were formed by self-avoiding lattice steps, whereby the size of the objects was gradually increased by wrapping the walks in several different ways. Values of the relaxation time σ have been found to depend only on the symmetry properties of the shape, and it can be seen that objects differing in only one lattice step can have significantly different values of the relaxation time. This work provides the link between the decay of probability for the insertion of a new particle onto a lattice and the intrinsic properties of the shapes, such as parameter of nonsphericity of the objects.

Much attention has been paid to the RSA on 1D and 2D lattices, but there are only a few studies of irreversible deposition in 3D. Irreversible deposition on three-dimensional lattices has been studied mostly for k -mers [37–40]. Tarasevich and Cherkasova [38] examined the percolation and jamming properties of dimers on simple 3D cubic lattices. In Ref. [40], the study of Tarasevich and Cherkasova is extended to larger k -mers ($2 \leq k \leq 64$) to determine the dependence of the jamming coverage on the size of the deposited k -mers for 3D cubic lattices. To the best of our knowledge, there are no results for RSA of various shapes formed by connected sites on a 3D lattice. It should be stressed that examining all possible positions of irregular shapes during the RSA process is complex and very time consuming. There is also a number of papers dealing with percolations in 3D [41–45], including some results for more complex systems.

It is obvious that object deposition is not physically realizable in three dimensions since sometimes it requires objects to be placed in locations that are surrounded by objects previously deposited. However, RSA in 3D is useful as the simplest, yet nontrivial model of random packing, which takes into account excluded volume effects. Most research is focused on the random close packings (RCPs) where neighboring particles touch each other [2]. The RCP state is difficult to define because by introducing order, higher packing fractions can be obtained [46]. In other words, the properties of RCPs are very sensitive to a numerical protocol used for packing objects. In contrast to random close packings, for RSA packing, the mean packing density is unambiguously defined, and it is more convenient for studying the influence of object shape on the structure of the packing and its density.

The aim of this work is to study the RSA of large collections of objects made by connected sites on a simple 3D cubic lattice, the so called “lattice animals.” More precisely, a lattice

animal can be viewed as a finite set of lattice sites connected by a network of nearest neighbor bonds. Object size is the number n of nodes that lattice animal covers on the grid. In the physics literature lattice animals are often called clusters, due to their close relationship to percolation problems [47,48]. Series expansions for the percolation probability or the average cluster size can be obtained as weighted sums over the number of lattice animals $g_{n,p}$, enumerated according to their size n and perimeter p [49]. Lattice animals have also been suggested as a model of branched polymers with excluded volume [50,51]. In the present study the deposition kinetics and the jamming limit are analyzed for all lattice animals of size $n = 1, 2, 3, 4$, and 5 (41 different shapes). Our results suggest that the number of different orientations that lattice animals can take when placed on a cubic lattice exerts a decisive influence on the adsorption kinetics near the jamming limit θ_j . To further confirm this finding, we have analyzed some additional lattice animals of size $n = 6$ (8 objects) and $n \geq 7$ (11 objects).













The paper is organized as follows. Section II describes the model and the details of the simulations. The jamming densities and the jamming configurations are analyzed in Sec. III A. The approach of the coverage fraction $\theta(t)$ to the jamming limit θ_j is analyzed in Sec. III B. Finally, Sec. IV contains some additional comments.

II. DEFINITION OF THE MODEL AND THE SIMULATION METHOD

Depositing objects are “lattice animals,” made of a certain number of connected sites. In mathematics, and combinatorics in particular, the term polyominoes and polycubes are frequently used for 3D discrete objects. A polyomino of size n is an edge-connected set of n squares on the square lattice \mathcal{Z}^2 (the set of integers is denoted by \mathcal{Z}). Polycubes are the 3D analogues of the planar polyominoes, i.e., polycube of size n is a face-connected set of n cubes in the simple-cubic lattice \mathcal{Z}^3 . Because the square (cubic) lattice is self-dual, the number of polyominoes (polycubes) with n cells is precisely the number of 2D (3D) site animals with n vertices. Consequently, polyominoes (polycubes) are equivalent to site animals on the dual lattice. In this work we use the term “lattice animal” interchangeably with the other relevant terms such as “polyomino” and “polycube.”

Fixed polycubes are considered distinct if they have different shapes or orientations. In other words, two fixed polycubes are identical if one of them can be translated into the other. The number of fixed d -dimensional polycubes of size n is usually denoted in the literature by $A_d(n)$. In the mathematical literature, fixed polycubes are most discussed in the context of simple combinatorial problem—enumeration. Enumeration deals with determining the number of polycubes corresponding to a certain parameter, usually their size or perimeter. Lunnon [52] has made the first successful enumeration. He computed the number of polyominoes up to size 18 [with a slight error in $A_2(17)$]. It is very interesting that to this day there is no known analytic formula for $A_d(n)$ ($d > 1$). The only known methods for computing $A_d(n)$ are based on explicitly or implicitly enumerating all the polyominoes or polycubes using various numerical algorithms [52–56].

TABLE I. All polycubes (x) of size $n = 1, 2, 3, 4$ and their number of orientations m .

(x)	m	shape	(x)	m	shape
(M)	1		(I4)	3	
(D)	3		(L4)	24	
(I3)	3		(O4)	3	
(V3)	12		(P4)	8	
(A4)	12		(S4)	12	
(B4)	12		(T4)	12	

Free lattice animals, however, are distinguished only by shape, not by orientation. The number of free d -dimensional polycubes of size n with m different orientations is denoted by $A_d^m(n)$. Lunnon [57] analyzed three-dimensional polycubes by considering symmetry groups, and computed (manually!) $A_3(n)$ up to $n = 6$. Most polycubes are asymmetric, but many have more complex symmetry groups. The maximum symmetry for a polycube is the full symmetric group of a cube, with 48 elements—achiral octahedral group O_h . Lunnon found [57] that O_h has 98 subgroups falling into 33 conjugacy sets (polycube symmetry types). A polycube without symmetry has 24 different orientations. This is easy to visualize with a die. A die has 6 faces numbered 1 thru 6. If we place a die on the table with the “1” showing up, then we can rotate it to get 4 different orientations with the “1” still on top. Since there are 6 faces, there are $6 \times 4 = 24$ different orientations. It is evident that a number of orientations that a polycube may take varies with the symmetry of the polycube. Since we solely consider free lattice animals in this work, the term “free” is omitted in the following text.

Table I shows all polycubes of size $n = 1, 2, 3$, and 4. Polycubes of size $n = 1, 2, 3$ are planar with a maximum of 12 different orientations (object V3). There are eight tetracubes

TABLE II. All polycubes (x) of size $n = 5$ and their number of orientations m .
























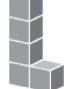













(x)	m	shape	(x)	m	shape	(x)	m	shape	(x)	m	shape
(A5)	24		(L25)	24		(S15)	24		(V25)	12	
(F5)	24		(L35)	24		(S25)	24		(W5)	12	
(I5)	3		(L45)	24		(T5)	12		(X5)	3	
(J15)	12		(N5)	24		(T15)	12		(Y5)	24	
(J25)	24		(N15)	24		(T25)	24		(Z5)	12	
(J45)	24		(N25)	24		(U5)	12				
(L5)	24		(P5)	24		(V5)	12				
(L15)	12		(Q5)	24		(V15)	12				

TABLE III. Some polycubes (x) of size $n = 6$ and their number of orientations m .

(x)	m	shape
(I06)	3	
(Ba6)	4	
(Xb6)	6	
(Tp6)	6	
(Th6)	12	
(Zf6)	12	
(Te6)	24	
(Ti6)	24	

(fourth-order polycubes), five of which are planar [58]. It must be emphasized that polycubes are usually counted with mirror pairs (so-called chiral twins) distinguished, as would be natural for the cubical case in ordinary space. For example, a tetracube A4 and its mirror image B4 are considered distinct because there is no rigid motion that transforms one onto the other.

All polycubes of size $n = 5$ (pentacubes) are shown in Table II. There are 29 distinct three-dimensional pentacubes [58]. As it can be seen, 12 pentacubes are flat and correspond to solid *pentominoes*. Among the nonplanar pentacubes, there are five that have at least one plane of symmetry (A5, L35, Q5, T15, T25) and each of them is its own mirror image. The remaining twelve nonplanar pentacubes form six chiral pairs: {J15, L15}, {J25, L25}, {J45, L45}, {N15, S15}, {N25, S25}, {V15, V25}. Of the 29 pentacubes, for two flats (I5, X5) there are only three possible orientations. Ten pentacubes have twelve orientations and each of the remaining 17 pentacubes has 24 orientations.

Polycubes of size $n \leq 5$ can have 1, 3, 8, 12, or 24 different orientations. However, there are hexacubes (sixth-order polycubes) that have four and six different orientation. There are 166 hexacubes, 35 of which are planar [58]. Some hexacubes are shown in Table III. Hexacube Ba6 is the sole polycube of size $n \leq 6$ with four orientations. It is interesting that among the polycubes of size $n \leq 6$ only one object has eight different orientations (see, tetracube P4 in Table I).

TABLE IV. Shown here is the number of polycubes $A_3^m(n)$ of size n with the specified number of possible orientations m . The results are shown for all polycubes of size $n \leq 6$.

n	A_3^1	A_3^3	A_3^4	A_3^6	A_3^8	A_3^{12}	A_3^{24}	$N = \sum_m A_3^m$
1	1							1
2		1						1
3		1				1		2
4		2			1	4	1	8
5		2				10	17	29
6		1	1	3		34	127	166

Further, three hexacubes have six orientations. Most of the hexacubes have 12 and 24 different orientations (34 and 127 objects, respectively). Table IV shows the number of possible orientations m for polycubes of size $n \leq 6$ and the number of objects $A_3^m(n)$ with the specified number of orientations.

A. Simulation method

In this paper the *primary* lattice animal is a connected set of sites in \mathbb{Z}^3 that contains the origin (0,0,0). We call that point the head of an object. At each Monte Carlo step a lattice site is selected at random. If the selected site is unoccupied, then deposition of the object is tried in one of the 24 orientations which is chosen at random. Then we fix the head of the object at the selected site and search whether all necessary sites are unoccupied. If so, then we occupy these sites and place the object. If the attempt fails, then a new site and a new orientation are selected at random, and so on.

It is crucial to explain how to choose a random object orientation. A basic rotation of the lattice animal is a rotation about one of the axes of a coordinate system. Each rotation is specified by an angle ψ of rotation. The rotation angle ψ is defined to be positive for a rotation that is counterclockwise when viewed by an observer looking along the rotation axis towards the origin. In accordance with the Euler's rotation theorem any arbitrary rotation can be composed of a combination of these three rotations [59]. The rotation matrices that rotate a vector around the x , y , and z axes are given by [59]

$$R_x(\alpha) = \begin{bmatrix} 1 & 0 & 0 \\ 0 & \cos(\psi_1) & -\sin(\psi_1) \\ 0 & \sin(\psi_1) & \cos(\psi_1) \end{bmatrix}$$

(counterclockwise rotation around x axis), (2)

$$R_y(\beta) = \begin{bmatrix} \cos(\psi_2) & 0 & \sin(\psi_2) \\ 0 & 1 & 0 \\ -\sin(\psi_2) & 0 & \cos(\psi_2) \end{bmatrix}$$

(counterclockwise rotation around y axis), (3)

$$R_z(\gamma) = \begin{bmatrix} \cos(\psi_3) & -\sin(\psi_3) & 0 \\ \sin(\psi_3) & \cos(\psi_3) & 0 \\ 0 & 0 & 1 \end{bmatrix}$$

(counterclockwise rotation around z axis). (4)

For example, a vector \mathbf{v} can be rotated in any direction using a composition of three rotations [59]: $\mathbf{v}' = R_a(\psi_1)R_b(\psi_2)R_c(\psi_3)\mathbf{v}$, $a, b, c \in \{x, y, z\}$. In our model, rotation angles can take the following values: $\psi_1, \psi_2, \psi_3 \in \{0, \pi/2, \pi, 3\pi/2\}$.

When choosing a random object orientation, it is essential that the numerical algorithm provides a search of all possible object orientations. If we apply a sequence $R_aR_bR_c$, $a, b, c \in \{x, y, z\}$ of basic 3D rotations to the lattice animal, then it is known that the order in which they are applied affects the final result. In other words, operators of rotation in 3D [Eq. (4)] are noncommutative [59]. Therefore, when we try to deposit an object, one random permutation $(a b c)$ of

a set $\{x, y, z\}$ is selected at first. Random permutation $(a b c)$ defines the order of successive rotations $R_aR_bR_c$ of an object about the axes $a, b, c \in \{x, y, z\}$ of the coordinate system. Further, three random rotation angles ψ_1, ψ_2, ψ_3 of an object around the $a, b, c \in \{x, y, z\}$ axes are chosen from the set $\{0, \pi/2, \pi, 3\pi/2\}$. The primary object is rotated by applying the operator $R_a(\psi_1)R_b(\psi_2)R_c(\psi_3)$, after which its head is moved from the point $(0,0,0)$ to a randomly selected lattice site and checked for any overlap with neighboring lattice animals already placed in the lattice. Let us remark that a different choice of the head of the object does not change the obtained results. We have verified that usage of different heads for all examined objects gives quantitatively the same results

TABLE V. All lattice animals (x) of size $n = 1, 2, 3, 4$ and their number of orientations m .

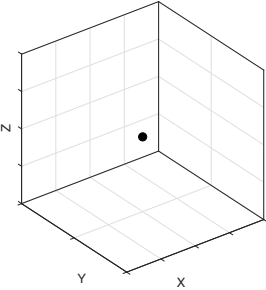
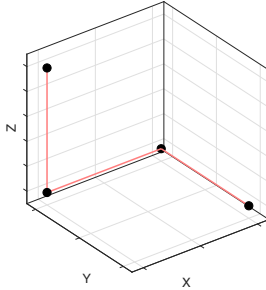
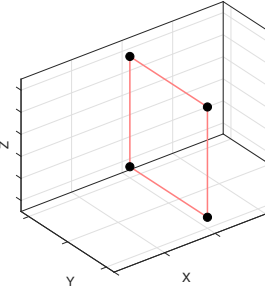
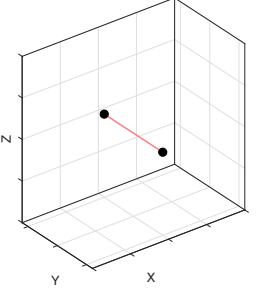
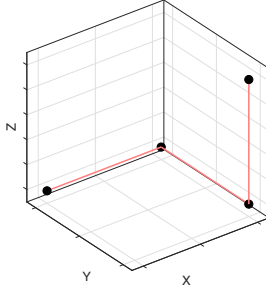
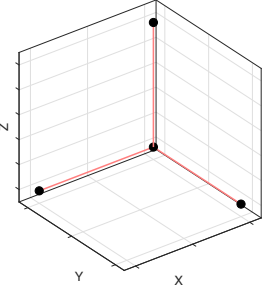
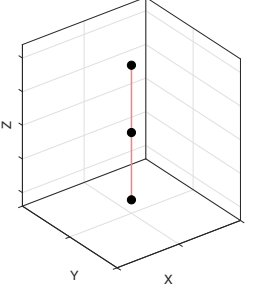
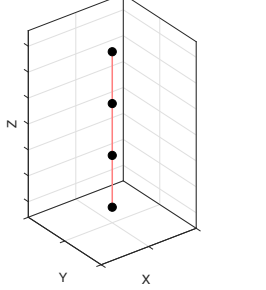
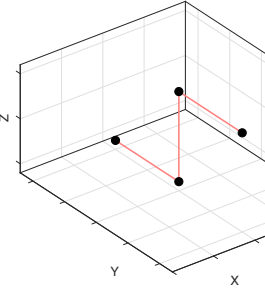
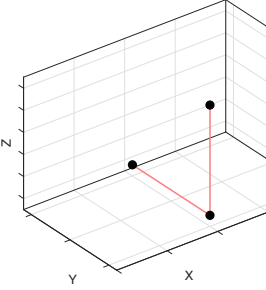
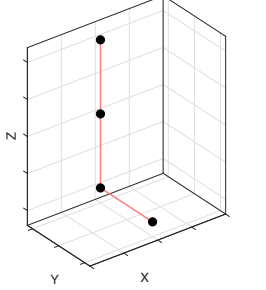
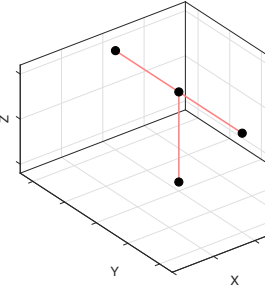
(x), m shape	(x), m shape	(x), m shape
(M),1 	(A4),12 	(O4),3 
(D),3 	(B4),12 	(P4),8 
(I3),3 	(I4),3 	(S4),12 
(V3),12 	(L4),24 	(T4),12 

TABLE VI. All lattice animals (x) of size $n = 5$ and their number of orientations m .

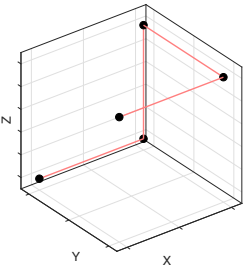
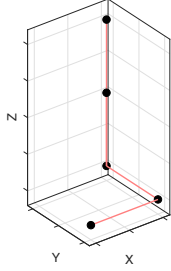
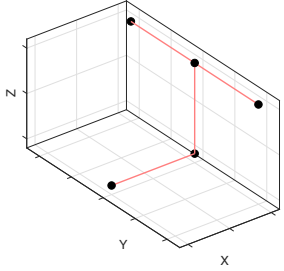
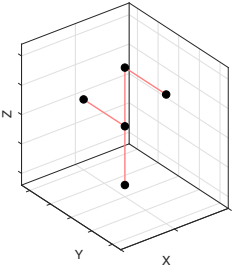
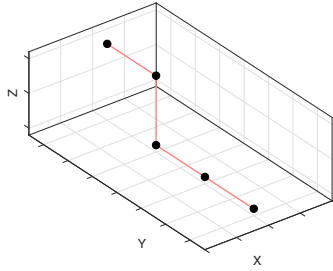
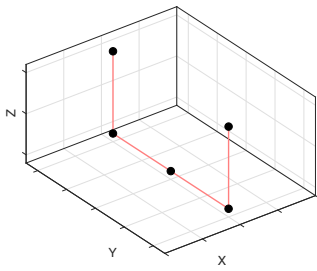
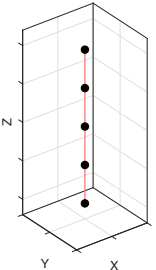
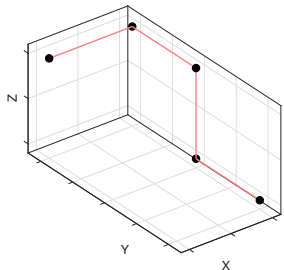
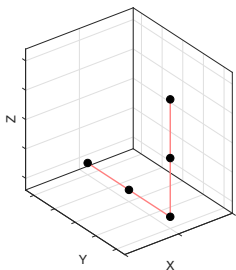
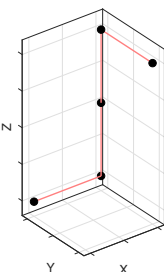
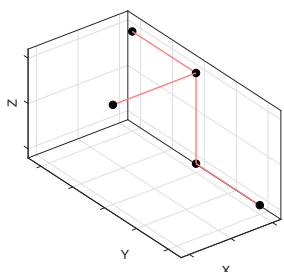
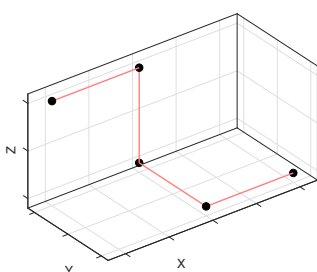
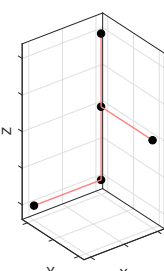
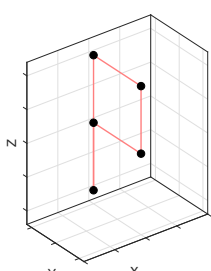
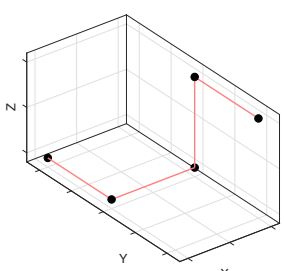
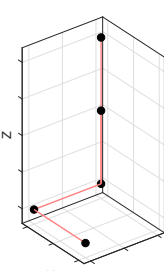
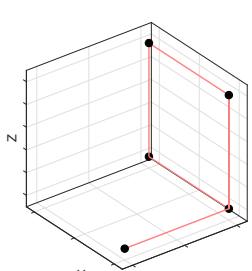
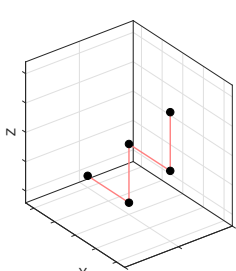
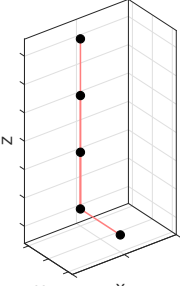
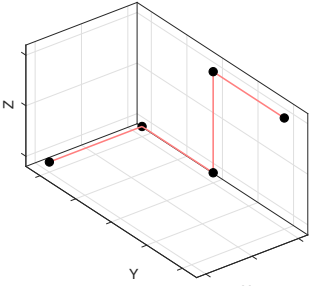
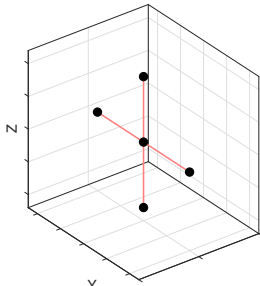
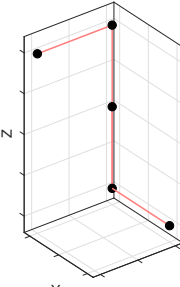
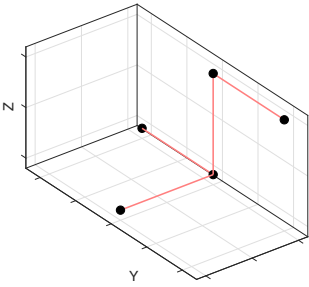
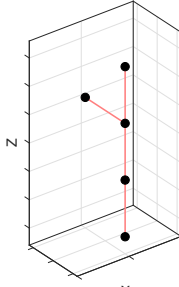
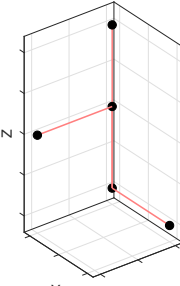
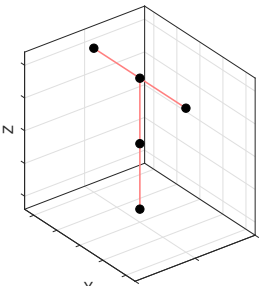
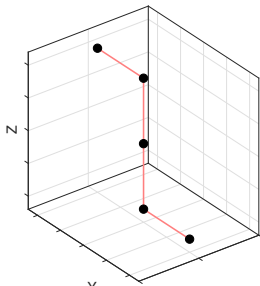
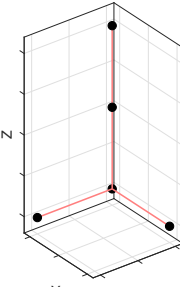
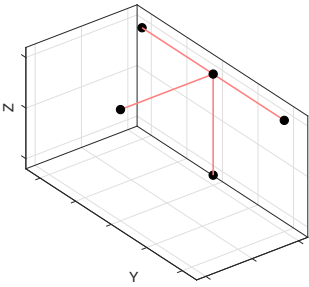
(x), m shape	(x), m shape	(x), m shape
(A5),24 	(L45),24 	(T25),24 
(F5),24 	(N5),24 	(U5),12 
(I5),3 	(N15),24 	(V5),12 
(J15),12 	(N25),24 	(V15),12 
(J25),24 	(P5),24 	(V25),12 
(J45),24 	(Q5),24 	(W5),12 

TABLE VI. (Continued.)

(x), m shape	(x), m shape	(x), m shape
 (L5),24	 (S15),24	 (X5),3
 (L15),12	 (S25),24	 (Y5),24
 (L25),24	 (T5),12	 (Z5),12
 (L35),24	 (T15),12	

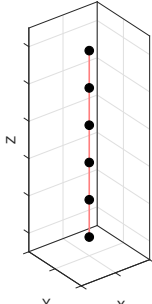
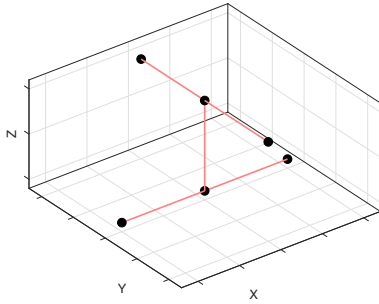
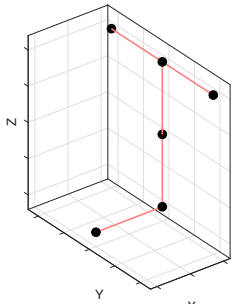
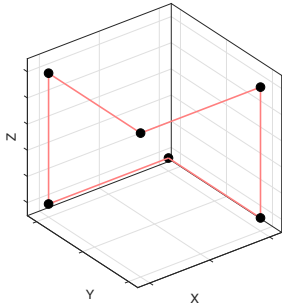
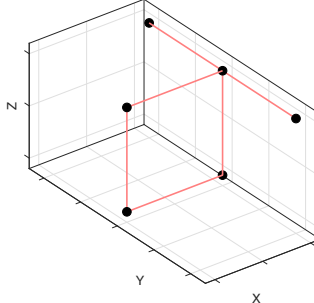
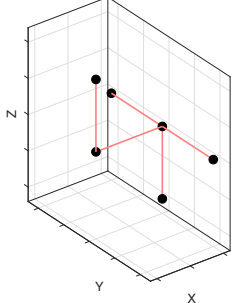
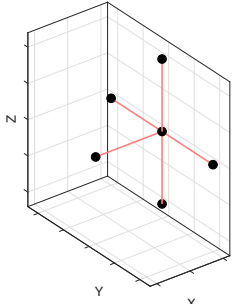
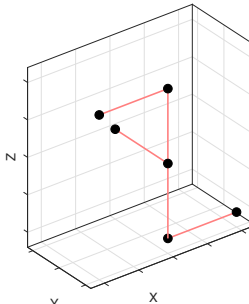
for the temporal evolution of density $\theta(t)$ and the jamming limit θ_j .

During the simulation, we can record the number of all inaccessible sites in the lattice. These include the occupied sites and the sites that are unoccupied but cannot be the head of the object deposited in any of the 24 possible orientations. The jamming limit is reached when the number of inaccessible sites is equal to the total number of sites in the lattice. Checking this condition is performed after every kL^2 attempts to absorb the object, starting at some late time point estimated in the trial simulations on smaller

lattices. Depending on the object size, the values of parameter k are 5, 20, and 50. If the condition is true, then we stop the current run and continue with the next simulation run.

The Monte Carlo simulations are performed on a 3D cubic lattice of size $L = 128$. Periodic boundary conditions are used in all directions. The time is counted by the number of attempts to select a lattice site and scaled by the total number of lattice sites $L^3 \approx 2$ million. The data are averaged over 100 independent runs for each of the investigated lattice animals.

TABLE VII. Some lattice animals (x) of size $n = 6$ and their number of orientations m .

(x), m shape	(x), m shape	(x), m shape
 <p>(I06),3</p>	 <p>(Tp6),6</p>	 <p>(Te6),24</p>
 <p>(Ba6),4</p>	 <p>(Th6),12</p>	 <p>(Ti6),24</p>
 <p>(Xb6),6</p>	 <p>(Zf6),12</p>	

III. RESULTS AND DISCUSSION

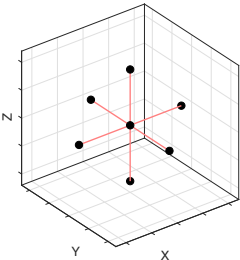
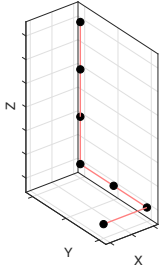
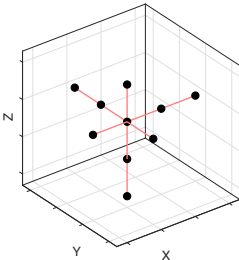
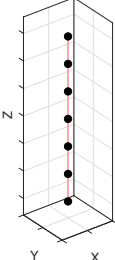
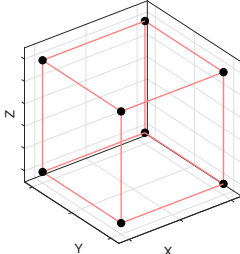
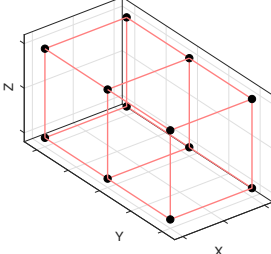
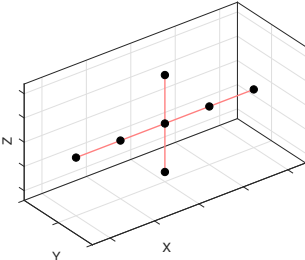
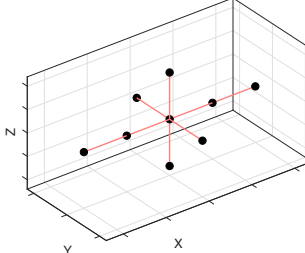
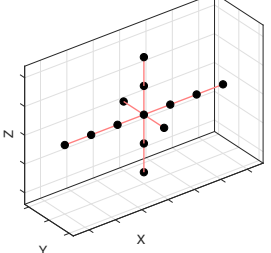
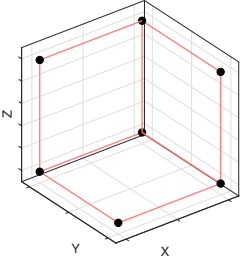
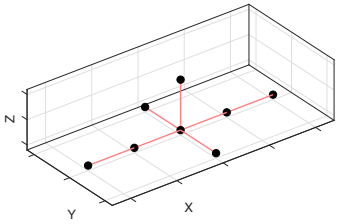
As stated in Sec. II, the structure of a polycube can be represented by means of a lattice animal that has a vertex for each cube and an edge for each two cubes that share a square. Lattice animals that are equivalent to polycubes presented in Tables I–III are shown in Tables V–VII. Some additional lattice animals of size $n \geq 7$ are shown in Table VIII. The number of examined objects represents a good basis for studying the impact of the geometrical properties of the shapes on the packing process in 3D, i.e., on the jamming coverage θ_j and on the temporal evolution of the coverage fraction $\theta(t)$.

A. Jamming densities

The first quantity of interest is the jamming limit θ_j which is reached when no more objects can be placed in any position on the lattice. Numerical values of the obtained jamming limits θ_j are given in Tables IX–XII for all examined shapes. We can see that in each chiral pair, both objects have the identical values of the jamming density. From Tables IX and X it is evident that for small shapes ($n \leq 5$), jamming densities θ_j decrease rapidly with the size n of the objects.

Most objects of size $n \leq 4$ have a jamming density θ_j greater than 0.80, while θ_j for all objects of size $n = 5$ is in the interval 0.70–0.80. Jamming densities θ_j for all examined objects of size $n \geq 7$ have values below ≈ 0.70 . Noticeable drop in the jamming density θ_j is thus a clear consequence of the enhanced frustration of the spatial adsorption. However, adding a single node to large objects does not result in a significant increase in their size. Therefore, changing of the shape of the large objects has considerably more influence on the jamming density than increasing of the object size. For example, jamming densities for objects LA7b ($n = 7$) and LA12 ($n = 12$) with $m = 3$ possible orientations from Table XII are almost identical ≈ 0.67 , although they are of different sizes. The results presented in Tables IX–XII also suggest that there is no correlation between the number of possible orientations of the object and the corresponding values of the jamming density θ_j . Indeed, the jamming density of the object Xb6 with $m = 6$ possible orientations is $\theta_j \approx 0.68$, but objects I06 and Ba6 with a smaller number of possible orientations than six have, respectively, a higher and lower θ_j value than 0.68 (see Table XI). Similarly, the jamming density of the object LA7b with $m = 3$ possible orientations is $\theta_j \approx 0.67$.

TABLE VIII. Some lattice animals (x) of size $n \geq 7$ and their number of orientations m .

$(x), m$ shape	$(x), m$ shape	$(x), m$ shape
 (LA7a),1	 (LA7e),24	 (LA10),8
 (LA7b),3	 (LA8a),1	 (LA12),3
 (LA7c),6	 (LA8b),3	 (LA13),6
 (LA7d),8	 (LA8c),12	

However, objects LA7c and LA7d with a greater number of possible orientations than three have, respectively, a lower and higher θ_j value than 0.67 (see Table XII). Note that our results for the jamming densities of linear objects (k -mers: D, I3–I5, I06, LA7b) are in a good agreement with the results presented in reference [40] in which RSA of straight rigid rods on a simple cubic lattice is analyzed.

Figure 1 shows typical snapshot configurations at the jamming density obtained for objects (a) LA7a, (b) LA8b, (c) Ba6, (d) Xb6, (e) P4, (f) T15, and (g) LA7e. The snapshots of size $\Delta L^3 = 10^3$ are taken from the central part of the lattice. Figure 1 displays configurations for seven objects that match all values of the number of possible orientations ($m = 1, 3, 4, 6, 8, 12, 24$) for given objects.

B. RSA kinetics

Now, we report and discuss the numerical results regarding the influence of the number of possible orientations of the

shape on the kinetics of the deposition processes. Figures 2–6 show the plots of $\ln[\theta_j - \theta(t)]$ versus t for seven classes of the objects, i.e., for seven values $m = 1, 3, 4, 6, 8, 12, 24$ of the number of different orientations that lattice animals can take when placed on a cubic lattice. Each of these figures contains results for objects with the same number of possible orientations. For all examined objects plots of $\ln[\theta_j - \theta(t)]$ versus t are found to be straight lines at the late times of the deposition process, confirming the exponential approach to the jamming limit of the form Eq. (1), with parameters σ and θ_j that depend on the shape of a depositing object. Furthermore, for a given value of m , these plots are parallel lines in the late stages of the deposition process for lattice animals of very different sizes [e.g., see Fig. 3(b)]. Hence, for objects that have the same value of the parameter m , rapidity of the approach to the jamming state is not affected by the size of the object. The number of possible orientations m of the object has an essential influence in the late times of the deposition process. Lines with

TABLE IX. For each lattice animal (x) of size $n = 1, 2, 3, 4$ with m possible orientations, $\theta_j^{(x)}$ is the jamming coverage and σ is the relaxation time [Eq. (1)]. The numbers in parentheses are the numerical values of the standard uncertainty of $\theta_j^{(x)}$ referred to the last digits of the quoted value.

Shape (x), size n	m	σ	$\theta_j^{(x)}$
(M), $n = 1$	1	0.99	1.0000(0)
(D), $n = 2$	3	3.09	0.9184(1)
(I3), $n = 3$	3	3.16	0.8390(2)
(V3), $n = 3$	12	12.36	0.8788(2)
(A4), $n = 4$	12	12.45	0.8178(2)
(B4), $n = 4$	12	12.47	0.8178(2)
(I4), $n = 4$	3	3.19	0.7808(3)
(L4), $n = 4$	24	23.98	0.8339(2)
(O4), $n = 4$	3	3.06	0.8079(3)
(P4), $n = 4$	8	8.03	0.7941(3)
(S4), $n = 4$	12	12.08	0.8149(2)
(T4), $n = 4$	12	12.49	0.8114(3)

seven different slopes are plotted in Fig. 7, showing the late times of the deposition process corresponding to objects of

TABLE X. For each lattice animal (x) of size $n = 5$ with m possible orientations, $\theta_j^{(x)}$ is the jamming coverage and σ is the relaxation time [Eq. (1)]. The numbers in parentheses are the numerical values of the standard uncertainty of $\theta_j^{(x)}$ referred to the last digits of the quoted value.

Shape (x)	m	σ	$\theta_j^{(x)}$
(A5)	24	24.21	0.7716(2)
(F5)	24	24.29	0.7860(3)
(I5)	3	3.18	0.7369(4)
(J15)	12	11.95	0.7635(2)
(J25)	24	24.72	0.7839(2)
(J45)	24	24.12	0.7958(3)
(L5)	24	23.91	0.7695(3)
(L15)	12	12.20	0.7635(3)
(L25)	24	24.24	0.7839(2)
(L35)	24	24.42	0.7774(3)
(L45)	24	24.88	0.7957(2)
(N5)	24	24.34	0.7866(3)
(N15)	24	24.88	0.7842(2)
(N25)	24	24.35	0.7790(3)
(P5)	24	24.20	0.8017(3)
(Q5)	24	23.95	0.7826(3)
(S15)	24	24.41	0.7841(2)
(S25)	24	24.25	0.7790(3)
(T5)	12	12.76	0.7500(3)
(T15)	12	12.43	0.7582(3)
(T25)	24	24.58	0.7863(2)
(U5)	12	12.48	0.7611(3)
(V5)	12	11.94	0.7628(3)
(V15)	12	12.37	0.7647(3)
(V25)	12	12.64	0.7647(3)
(W5)	12	12.31	0.7615(3)
(X5)	3	3.08	0.7007(3)
(Y5)	24	24.62	0.7595(3)
(Z5)	12	12.79	0.7643(2)

TABLE XI. For lattice animal (x) of size $n = 6$ with m possible orientations, $\theta_j^{(x)}$ is the jamming coverage and σ is the relaxation time [Eq. (1)]. The numbers in parentheses are the numerical values of the standard uncertainty of $\theta_j^{(x)}$ referred to the last digits of the quoted value.

Shape (x)	m	σ	$\theta_j^{(x)}$
(I06)	3	3.06	0.7026(4)
(Ba6)	4	4.02	0.6683(3)
(Xb6)	6	6.03	0.6827(3)
(Tp6)	6	6.13	0.6879(4)
(Th6)	12	12.18	0.7179(3)
(Zf6)	12	12.25	0.7215(3)
(Te6)	24	24.55	0.7378(3)
(Ti6)	24	24.60	0.7369(3)

different number of possible orientations m , as indicated in the legend.

We have calculated the values of the parameter σ [Eq. (1)] from the slopes of the $\ln[\theta_j - \theta(t)]$ versus t curves in the late times of the process. The parameter σ determines how fast the lattice is filled up to the jamming coverage θ_j . The values of the relaxation time σ are given in Tables IX–XII for all examined lattice animals. Approximate values of the parameter σ for the seven classes of objects are found to be equal the number of possible orientations of the shape:

$$\sigma \simeq m \in \{1, 3, 4, 6, 8, 12, 24\}. \quad (5)$$

This means that the approach to the jamming limit is slower for objects with a larger number of possible orientations. At large times, adsorption events take place on islands of unoccupied sites. The individual islands act as selective targets for specific deposition events. In other words, there is only a restricted number of possible orientations in which an object can reach a vacant location, provided the location is small enough. Such difficult placement of an object in locations that allow only a small number of object orientations is a feature of the deposits near the jamming state. Namely, for an object

TABLE XII. For lattice animal (x) of size $n \geq 7$ with m possible orientations, $\theta_j^{(x)}$ is the jamming coverage and σ is the relaxation time [Eq. (1)]. The numbers in parentheses are the numerical values of the standard uncertainty of $\theta_j^{(x)}$ referred to the last digits of the quoted value.

Shape (x), size n	m	σ	$\theta_j^{(x)}$
(LA7a), $n = 7$	1	0.98	0.6225(4)
(LA7b), $n = 7$	3	2.97	0.6749(5)
(LA7c), $n = 7$	6	6.19	0.6336(4)
(LA7d), $n = 7$	8	8.06	0.6897(4)
(LA7e), $n = 7$	24	24.20	0.7006(3)
(LA8a), $n = 8$	1	0.98	0.6453(5)
(LA8b), $n = 8$	3	3.11	0.5858(4)
(LA8c), $n = 8$	12	12.18	0.6308(3)
(LA10), $n = 10$	8	8.08	0.5693(4)
(LA12), $n = 12$	3	3.04	0.6719(5)
(LA13), $n = 13$	6	6.12	0.4899(4)

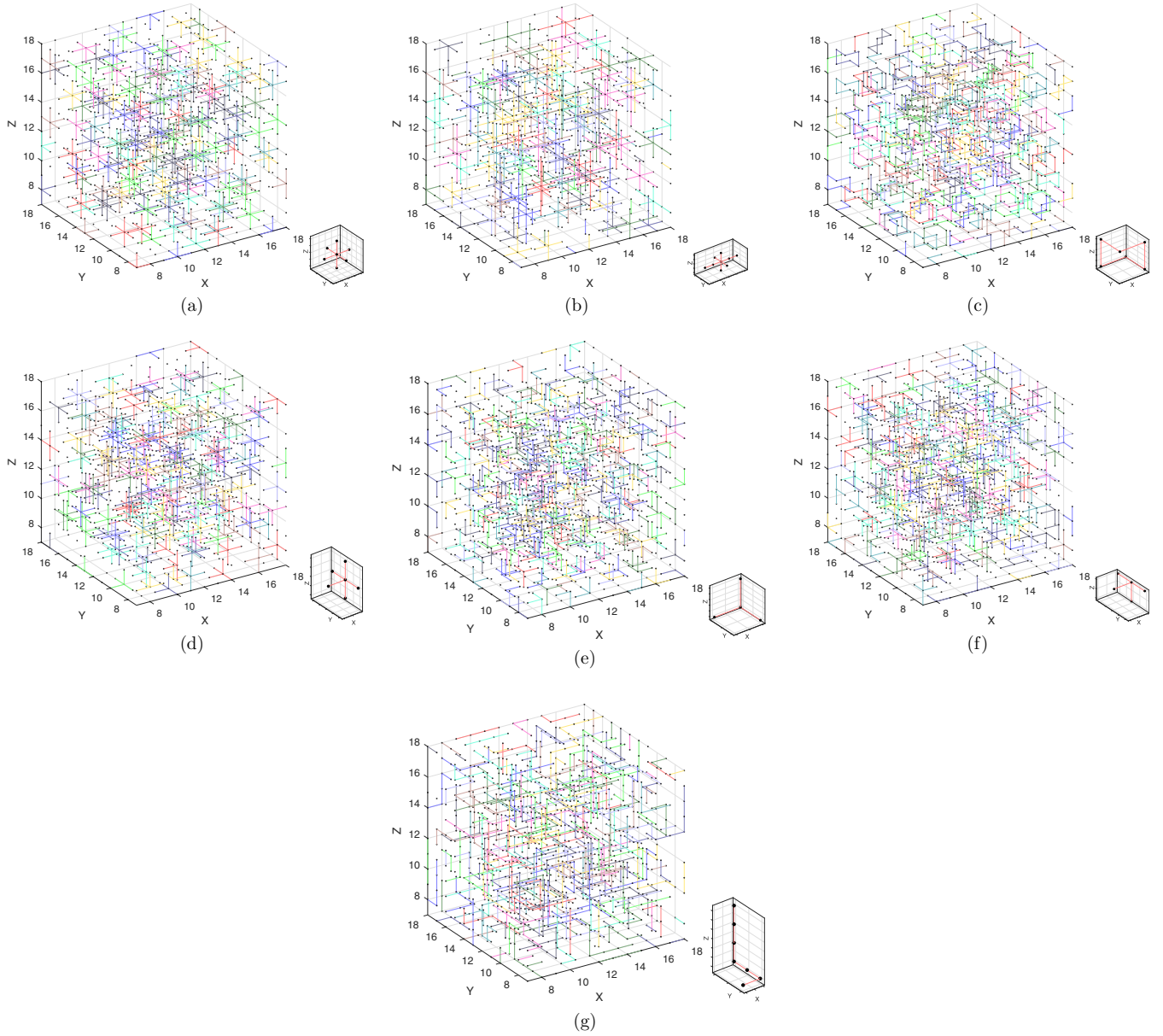


FIG. 1. Snapshots of patterns formed during the RSA of objects (a) LA7a, $m = 1$ (Tables VIII and XII), (b) LA8b, $m = 3$ (Tables VIII and XII), (c) Ba6, $m = 4$ (Tables VII and XI), (d) Xb6, $m = 6$ (Tables VII and XI), (e) P4, $m = 8$ (Tables V and IX), (f) T15, $m = 12$ (Tables VI and X), and (g) LA7e, $m = 24$ (Tables VIII and XII). The snapshots are taken from the central part of the lattice at times needed for the system to reach the jamming state. A corresponding lattice animal is shown in the lower right corner of each panel (a)–(g). The objects are colored with 12 colors randomly selected for each one.

with a larger number of possible placements, a longer time is needed to examine all isolated empty locations that are left in the late times of the process. Hence, the increase in the number of possible placements of the shape reduces the rate of single particle adsorption. This extends the mean waiting time between consecutive and successful deposition events, and the approach to the jamming state is slower.

IV. CONCLUDING REMARKS

In the case of irreversible deposition on planar lattices, it is well established that the kinetics of the late stage of deposition is determined exclusively with the symmetry properties of the

shapes. For the shapes made by self-avoiding lattice steps on the 2D triangular lattice, relaxation time σ [Eq. (1)] is inversely proportional to the order of symmetry axis n_s of the shape, $\sigma = 6/n_s$ [18,20]. However, for a planar shape with symmetry order n_s on a triangular lattice, the number of possible orientations is given exactly by the expression $6/n_n$. To generalise this result to 3D shapes, we have performed extensive numerical simulations of the RSA using large collections of objects (“lattice animals”) made by connected sites on a simple 3D cubic lattice.

As expected, the approach to the jamming limit θ_j was found to be exponential for all the lattice animals. It was shown that the relaxation time σ [Eq. (1)] is equal to the

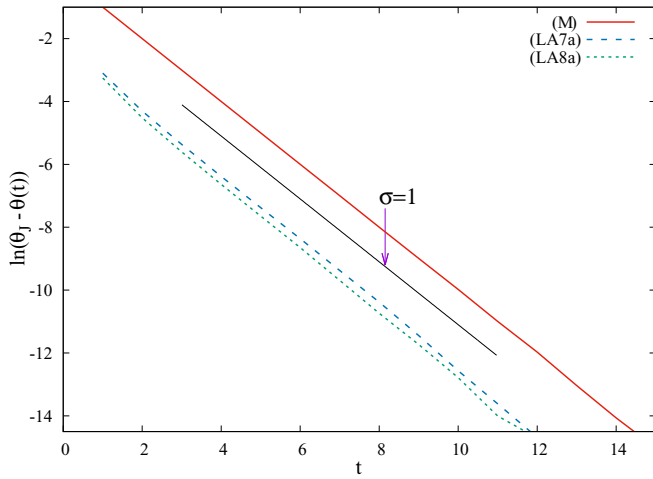


FIG. 2. Plots of $\ln[\theta_j - \theta(t)]$ versus t for objects (M), (LA7a), and (LA8a) with one possible placement (Tables V and VIII). Additionally, the slanted straight line with the slope $-1/\sigma = -1$ is shown, indicating the late-time RSA behavior and is guide to the eye.

number of different orientations m that lattice animals can take when placed on a cubic lattice [Eq. (5)]. To confirm this finding, we have analyzed all lattice animals of size $n = 1, 2, 3, 4,$ and 5 (41 different shapes), eight lattice animals of size $n = 6$ and eleven objects of size $n \geq 7$. In other words, the coverage kinetics is slowed down with the increase in the number of possible placements m of the shape. Indeed, the mean waiting time between consecutive deposition events

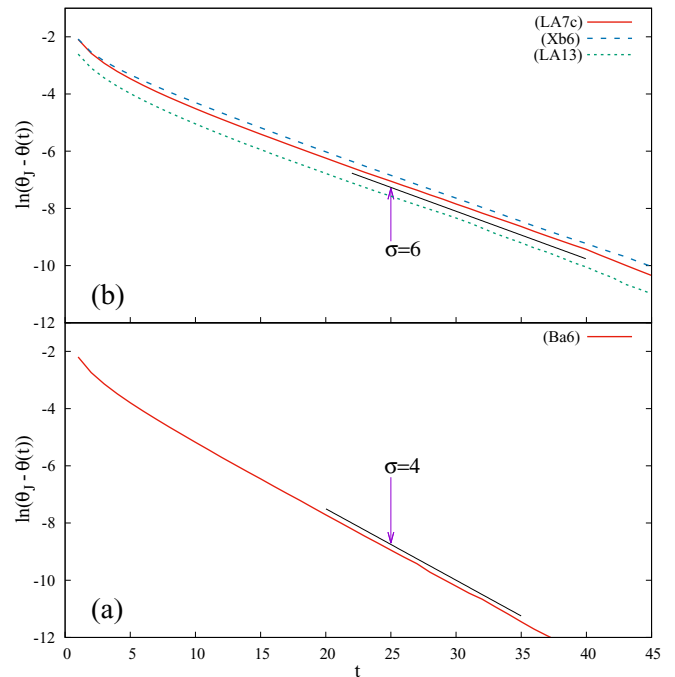


FIG. 4. Plots of $\ln[\theta_j - \theta(t)]$ versus t for: (a) object (Ba6) with four possible placements (Table VII); (b) objects (LA7c), (Xb6), and (LA13) with six possible placements (Tables VII and VIII). Additionally, the slanted straight lines with the slopes $-1/\sigma = -1/4$ (a), $-1/6$ (b) are shown, indicating the late-time RSA behavior and are guide to the eye.

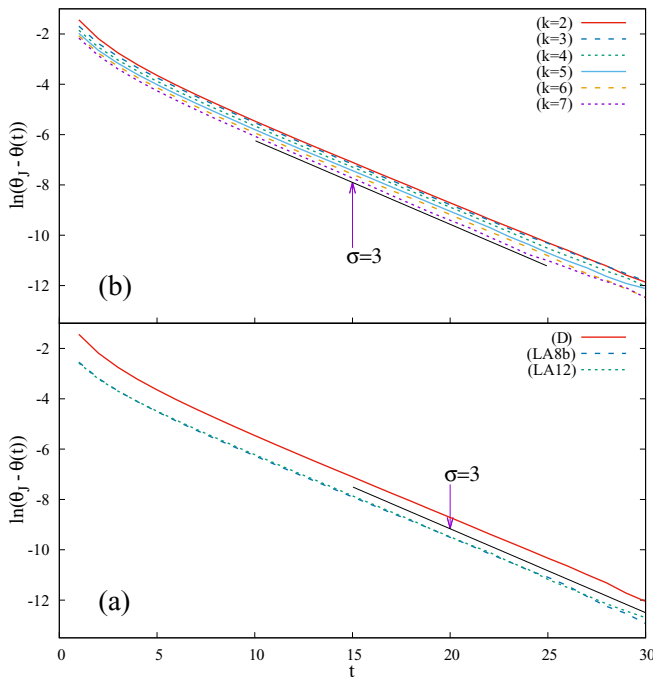


FIG. 3. Plots of $\ln[\theta_j - \theta(t)]$ versus t for: (a) objects (D), (LA8b), and (LA12) with three possible placements (Tables V and VIII); (b) k -mers ($k = 2, 3, 4, 5, 6, 7$). Additionally, the slanted straight lines with the slope $-1/\sigma = -1/3$ are shown, indicating the late-time RSA behavior and are guide to the eye.

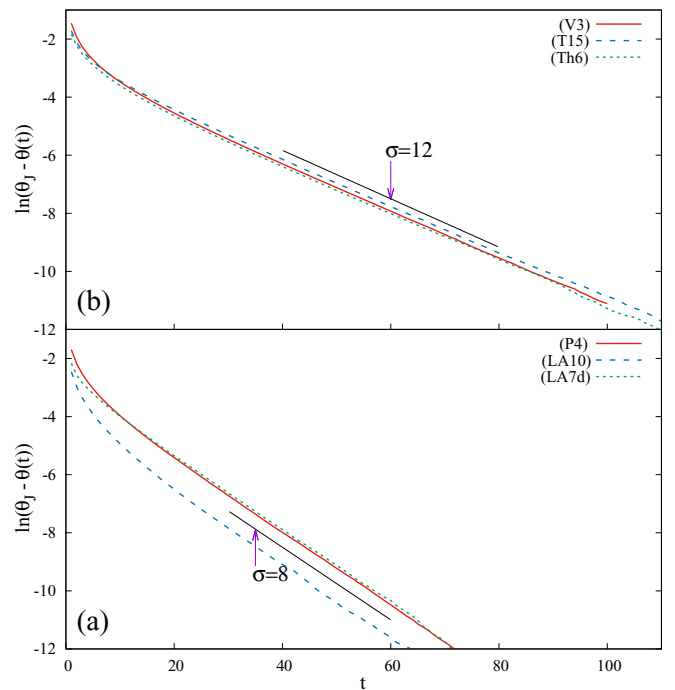


FIG. 5. Plots of $\ln[\theta_j - \theta(t)]$ versus t for: (a) objects (P4), (LA10), and (LA7d) with eight possible placements (Tables V and VIII); (b) objects (V3), (T15), and (Th6) with 12 possible placements (Tables V, VI, and VII). Additionally, the slanted straight lines with the slopes $-1/\sigma = -1/8$ (a), $-1/12$ (b) are shown, indicating the late-time RSA behavior and are guide to the eye.

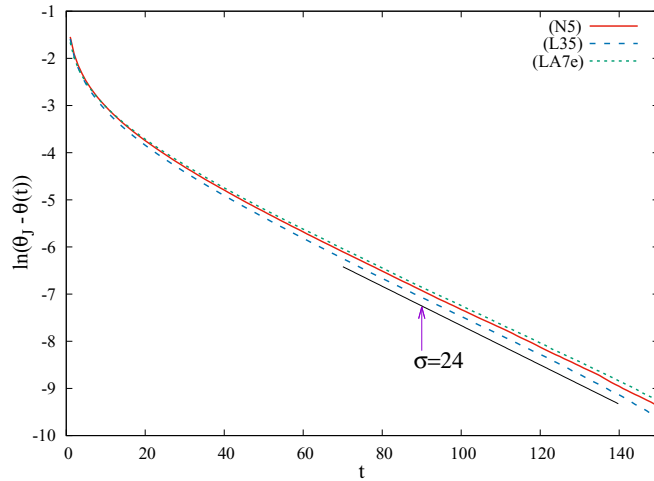


FIG. 6. Plots of $\ln[\theta_j - \theta(t)]$ versus t for objects (N5), (L35), and (LA7e) with 24 possible placements (Tables VI and VIII). Additionally, the slanted straight line with the slope $-1/\sigma = -1/24$ is shown, indicating the late-time RSA behavior and is guide to the eye.

extends with m , so that the approach to the jamming state is slower.

We have pointed out that for sufficiently large objects, changing of the shape has considerably more influence on the jamming density than increasing of the object size. These findings are in an excellent qualitative agreement with the results of Karayiannis and Laso [60,61]. They proposed a Monte Carlo scheme which is able to efficiently sample freely-jointed chains of hard spheres even up to the maximally random jammed (MRJ) state. In this model, chain connectivity imposes constraints that force bonded spheres to adopt specific local configurations. As an interesting result, the constraints imposed by chain connectivity were found to play a more important role in determining the MRJ states than the size of flexible chains. However, our results suggest that there is no correlation between the number of possible orientations of the object and the corresponding values of the jamming density θ_j . In Ref. [20], special attention is paid to the behavior of probability p_{insert} for the insertion of a new particle onto a planar triangular lattice during the deposition process. Shape factor, defined as the degree to which a particle is similar to

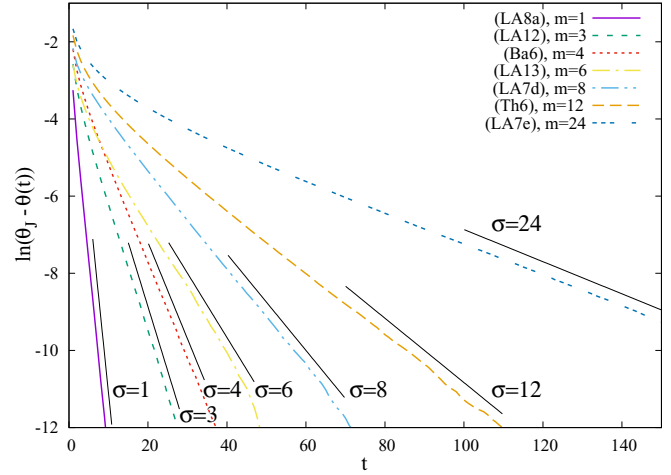


FIG. 7. Plots of $\ln[\theta_j - \theta(t)]$ versus t for objects (LA8a), (LA12), (Ba6), (LA13), (LA7d), (Th6), and (LA7e) from Tables VII and VIII. The curves correspond to objects with the various number of possible orientations, m , as indicated in the legend. Additionally, the slanted straight lines with the slope $-1/\sigma = -1, -1/3, -1/4, -1/6, -1/8, -1/12, -1/24$ are shown, indicating the late-time RSA behavior and are guides to the eye.

a circle, is associated with the evolution of probability p_{insert} . It would be interesting to perform a similar investigation with 3D objects of various shapes within the context of the shape descriptors, such as aspect ratios, compactness of the object, smoothness of the perimeter, and the shape factor. As an open possibility for the future, we think that the three-dimensional model presented in this work can be generalized to mixtures of several kinds of 3D objects.

ACKNOWLEDGMENTS

This work was supported by the Ministry of Education, Science, and Technological Development of the Republic of Serbia under Projects No. ON171017 and No. III45016, and by the European Commission under H2020 Project VI-SEEM, Grant No. 675121. Numerical simulations were run on the PARADOX supercomputing facility at the Scientific Computing Laboratory of the Institute of Physics Belgrade.

-
- [1] T. Aste, Variations around disordered close packing, *J. Phys.: Condens. Matter* **17**, S2361 (2005).
 - [2] S. Torquato and F. H. Stillinger, Jammed hard-particle packings: From Kepler to Bernal and beyond, *Rev. Mod. Phys.* **82**, 2633 (2010).
 - [3] P. M. Chaikin and T. C. Lubensky, *Principles of Condensed Matter Physics* (Cambridge University Press, New York, 1995).
 - [4] A. Donev, I. Cisse, D. Sachs, E. A. Variano, F. H. Stillinger, R. Connelly, S. Torquato, and P. M. Chaikin, Improving the density of jammed disordered packings using ellipsoids, *Science* **303**, 990 (2004).
 - [5] A. Dabrowski, Adsorption—From theory to practice, *Adv. Colloid Interface Sci.* **93**, 135 (2001).
 - [6] V. Privman (ed.), *Colloids Surf., A* **165**, 1 (2000) (a collection of review articles).
 - [7] A. Cadilhe, N. A. M. Araújo, and V. Privman, Random sequential adsorption: From continuum to lattice and pre-patterned substrates, *J. Phys.: Condens. Matter* **19**, 065124 (2007).
 - [8] J. W. Evans, Random and cooperative sequential adsorption, *Rev. Mod. Phys.* **65**, 1281 (1993).
 - [9] E. Ben-Naim and P. L. Krapivsky, On irreversible deposition on disordered substrates, *J. Phys. A: Math. Gen.* **27**, 3575 (1994).

- [10] M. C. Bartelt and V. Privman, Kinetics of irreversible multilayer adsorption: One-dimensional models, *J. Chem. Phys.* **93**, 6820 (1990).
- [11] R. H. Swendsen, Dynamics of random sequential adsorption, *Phys. Rev. A* **24**, 504 (1981).
- [12] J. Feder, Random sequential adsorption, *J. Theor. Biol.* **87**, 237 (1980).
- [13] Y. Pomeau, Some asymptotic estimates in the random parking problem, *J. Phys. A: Math. Gen.* **13**, L193 (1980).
- [14] B. Bonnier, Random sequential adsorption of binary mixtures on a line, *Phys. Rev. E* **64**, 066111 (2001).
- [15] M. Cieřla and J. Barbasz, Random packing of regular polygons and star polygons on a flat two-dimensional surface, *Phys. Rev. E* **90**, 022402 (2014).
- [16] S. S. Manna and N. M. Švrakić, Random sequential adsorption: Line segments on the square lattice, *J. Phys. A: Math. Gen.* **24**, L671 (1991).
- [17] Lj. Budinski-Petković and U. Kozmidis-Luburić, Jamming configurations for irreversible deposition on a square lattice, *Physica A: Stat. Mech. Appl.* **236**, 211 (1997).
- [18] Lj. Budinski-Petković and U. Kozmidis-Luburić, Random sequential adsorption on a triangular lattice, *Phys. Rev. E* **56**, 6904 (1997).
- [19] Lj. Budinski-Petković, S. B. Vrhovac, and I. Lončarević, Random sequential adsorption of polydisperse mixtures on discrete substrates, *Phys. Rev. E* **78**, 061603 (2008).
- [20] Lj. Budinski-Petković, I. Lončarević, D. Dujak, A. Karač, J. R. Šćepanović, Z. M. Jakšić, and S. B. Vrhovac, Particle morphology effects in random sequential adsorption, *Phys. Rev. E* **95**, 022114 (2017).
- [21] D. W. Cooper, Random-sequential-packing simulations in three dimensions for spheres, *Phys. Rev. A* **38**, 522 (1988).
- [22] J. Talbot, P. Schaaf, and G. Tarjus, Random sequential addition of hard spheres, *Mol. Phys.* **72**, 1397 (1991).
- [23] S. Torquato, O. U. Uche, and F. H. Stillinger, Random sequential addition of hard spheres in high euclidean dimensions, *Phys. Rev. E* **74**, 061308 (2006).
- [24] J. D. Sherwood, Random sequential adsorption of lines and ellipses, *J. Phys. A: Math. Gen.* **23**, 2827 (1990).
- [25] M. Cieřla, G. Pajak, and R. M. Ziff, In a search for a shape maximizing packing fraction for two-dimensional random sequential adsorption, *J. Chem. Phys.* **145**, 044708 (2016).
- [26] R. D. Vigil and R. M. Ziff, Kinetics of random sequential adsorption of rectangles and line segments, *J. Chem. Phys.* **93**, 8270 (1990).
- [27] W. Kasperek, P. Kubala, and M. Cieřla, Random sequential adsorption of unoriented rectangles at saturation, *Phys. Rev. E* **98**, 063310 (2018).
- [28] M. Cieřla and P. Karbowiczek, Random sequential adsorption of starlike particles, *Phys. Rev. E* **91**, 042404 (2015).
- [29] B. N. Aleksić, N. M. Švrakić, and M. Belić, Kinetics of deposition of oriented superdisks, *Phys. Rev. E* **88**, 062112 (2013).
- [30] P. Viot, G. Tarjus, S. M. Ricci, and J. Talbot, Random sequential adsorption of anisotropic particles. I. Jamming limit and asymptotic behavior, *J. Chem. Phys.* **97**, 5212 (1992).
- [31] M. Cieřla and P. Kubala, Random sequential adsorption of cubes, *J. Chem. Phys.* **148**, 024501 (2018).
- [32] M. Cieřla and P. Kubala, Random sequential adsorption of cuboids, *J. Chem. Phys.* **149**, 194704 (2018).
- [33] M. Cieřla, Continuum random sequential adsorption of polymer on a flat and homogeneous surface, *Phys. Rev. E* **87**, 052401 (2013).
- [34] N. I. Lebovka, N. N. Karmazina, Y. Yu. Tarasevich, and V. V. Laptev, Random sequential adsorption of partially oriented linear k -mers on a square lattice, *Phys. Rev. E* **84**, 061603 (2011).
- [35] N. I. Lebovka, Y. Yu. Tarasevich, D. O. Dubinin, V. V. Laptev, and N. V. Vygornitskii, Jamming and percolation in generalized models of random sequential adsorption of linear k -mers on a square lattice, *Phys. Rev. E* **92**, 062116 (2015).
- [36] Jian-Sheng Wang and Ras B. Pandey, Kinetics and Jamming Coverage in A Random Sequential Adsorption of Polymer Chains, *Phys. Rev. Lett.* **77**, 1773 (1996).
- [37] B. Bonnier, Y. Leroyer, and E. Pommiers, Random sequential adsorption of line segments: Universal properties of mixtures in 1, 2, and 3D lattices, *J. Phys. I France* **2**, 379 (1992).
- [38] Y. Tarasevich and V. Cherkasova, Dimer percolation and jamming on simple cubic lattice, *Eur. Phys. J. B* **60**, 97 (2007).
- [39] D. J. Burridge, Random packing of lines in a lattice cube, *Phys. Rev. E* **81**, 031107 (2010).
- [40] G. D. García, F. O. Sanchez-Varretti, P. M. Centres, and A. J. Ramirez-Pastor, Random sequential adsorption of straight rigid rods on a simple cubic lattice, *Physica A: Stat. Mech. Appl.* **436**, 558 (2015).
- [41] J. Wang, Z. Zhou, W. Zhang, T. M. Garoni, and Y. Deng, Bond and site percolation in three dimensions, *Phys. Rev. E* **87**, 052107 (2013).
- [42] M. I. González, P. M. Centres, W. Lebrecht, and A. J. Ramirez-Pastor, Site-bond percolation on simple cubic lattices: Numerical simulation and analytical approach, *J. Stat. Mech.* (2016) 093210.
- [43] K. Malarz, Simple cubic random-site percolation thresholds for neighborhoods containing fourth-nearest neighbors, *Phys. Rev. E* **91**, 043301 (2015).
- [44] R. M. Ziff and S. Torquato, Percolation of disordered jammed sphere packings, *J. Phys. A: Math. Theor.* **50**, 085001 (2017).
- [45] J.-F. Thovert, V. V. Mourzenko, and P. M. Adler, Percolation in three-dimensional fracture networks for arbitrary size and shape distributions, *Phys. Rev. E* **95**, 042112 (2017).
- [46] S. Torquato, T. M. Truskett, and P. G. Debenedetti, Is Random Close Packing of Spheres Well Defined? *Phys. Rev. Lett.* **84**, 2064 (2000).
- [47] A. B. Harris and T. C. Lubensky, Connection between percolation and lattice animals, *Phys. Rev. B* **23**, 3591 (1981).
- [48] A. R. Conway and A. J. Guttmann, On two-dimensional percolation, *J. Phys. A: Math. Gen.* **28**, 891 (1995).
- [49] M. F. Sykes and M. Glen, Percolation processes in two dimensions. I. Low-density series expansions, *J. Phys. A: Math. Gen.* **9**, 87 (1976).
- [50] T. C. Lubensky and J. Isaacson, Statistics of lattice animals and dilute branched polymers, *Phys. Rev. A* **20**, 2130 (1979).
- [51] S. Flesia, D. S. Gaunt, C. E. Soteros, and S. G. Whittington, Statistics of collapsing lattice animals, *J. Phys. A: Math. Gen.* **27**, 5831 (1994).
- [52] W. F. Lunnon, Counting polyominoes, in *Computers in Number Theory*, edited by A. O. L. Atkin and B. J. Birch (Academic Press, San Diego, CA, 1971), pp. 347–372.

- [53] D. S. Gaunt, M. F. Sykes, and H. Ruskin, Percolation processes in D-dimensions, *J. Phys. A: Math. Gen.* **9**, 1899 (1976).
- [54] G. Aleksandrowicz and G. Barequet, Counting polycubes without the dimensionality curse, *Discrete Math.* **309**, 4576 (2009).
- [55] I. Jensen, Enumerations of lattice animals and trees, *J. Stat. Phys.* **102**, 865 (2001).
- [56] D. H. Redelmeier, Counting polyominoes: Yet another attack, *Discrete Math.* **36**, 191 (1981).
- [57] W. F. Lunnon, Symmetry of cubical and general polyominoes, in *Graph Theory and Computing*, edited by Ronald C. Read (Academic Press, San Diego, CA, 1972), pp. 101–108.
- [58] OEIS Foundation Inc., Sequence A000162, in The On-Line Encyclopedia of Integer Sequences, edited by N. J. A. Sloane (2019), <http://oeis.org/A000162>.
- [59] H. Goldstein, C. Pole, and J. Safko, *Classical Mechanics*, 3rd ed. (Addison Wesley, San Francisco, CA, 2002).
- [60] N. Ch. Karayiannis and M. Laso, Dense and Nearly Jammed Random Packings of Freely Jointed Chains of Tangent Hard Spheres, *Phys. Rev. Lett.* **100**, 050602 (2008).
- [61] N. Ch. Karayiannis and M. Laso, Monte Carlo scheme for generation and relaxation of dense and nearly jammed random structures of freely jointed hard-sphere chains, *Macromolecules* **41**, 1537 (2008).



Long-term effects of abrupt environmental perturbations in model of group chase and escape with the presence of non-conservative processes

J.R. Šćepanović^{a,*}, Z.M. Jakšić^a, Lj. Budinski-Petković^b, S.B. Vrhovac^a

^a Institute of Physics Belgrade, University of Belgrade, Pregrevica 118, Zemun 11080, Belgrade, Serbia

^b Faculty of Engineering, Trg D. Obradovića 6, Novi Sad 21000, Serbia

ARTICLE INFO

Article history:

Received 14 October 2020

Received in revised form 27 April 2021

Available online 1 June 2021

Keywords:

Predator–prey model

Group chase and escape

Environmental perturbations

ABSTRACT

This paper examines the influence of environmental perturbations on dynamical regimes of model ecosystems. We study a stochastic lattice model describing the dynamics of a group chasing and escaping between predators and prey. The model includes smart pursuit (predators to prey) and evasion (prey from predators). Both species can affect their movement by visual perception within their finite sighting range. Non-conservative processes that change the number of individuals within the population, such as breeding and physiological dying, are implemented in the model. The model contains five parameters that control the breeding and physiological dying of predators and prey: the birth and two death rates of predators and two parameters characterizing the birth and death of prey. We study the response of our model of group chase and escape to sudden perturbations in values of parameters that characterize the non-conservative processes. Temporal dependencies of the number of predators and prey are compared for various perturbation events with different abrupt changes of probabilities affecting the non-conservative processes.

© 2021 Elsevier B.V. All rights reserved.

1. Introduction

Simulation of population dynamics is a central research theme in computational biology, which contributes to understanding the interactions between predators and prey. Classical models of predator–prey systems were developed first by Lotka and Volterra [1–3]. They showed that simple predator–prey models may exhibit limit cycles during which the populations of both species have periodic oscillations in time with a 1/4-period lag between predator and prey [4]. Such oscillations in species abundances have successfully been observed in real-world systems [5–8]. As the field developed, the commonly used model schemes shifted from continuous ones based on a differential equation towards discrete and agent-based models [9–13]. Furthermore, the predator–prey systems have been studied in various contexts, such as robotics, game theory and ecology [14–19].

Many complex systems have impulsive dynamical behavior due to abrupt jumps of some parameters affecting the system at specific instants during the evolving processes. Ecological systems are often affected by environmental changes and human activities, such as vaccination, medical treatment of disease, sterilization, etc. For example, numerous species are prone to extinction due to temperature fluctuations or climatic changes, and pollution events [20–26]. Discrete nature

* Corresponding author.

E-mail address: julija.scepanovic@ipb.ac.rs (J.R. Šćepanović).

of human actions or environmental changes lead to population densities changing very rapidly in a short time interval. The maintenance of existing population density requires information as to how organisms react to intended as well as unintended abrupt changes.

Short-term environmental perturbations (such as heavy rainfall, severe fires, or storms) are likely to cause the sudden death of healthy individuals within a population, which would not exhibit any changes in their biological variables within a population at a stable state. These perturbations are often assumed to be in the form of impulses in the modeling process. However, ecosystems can be exposed to various types of environmental perturbations for long periods of time, which may result in an enduring alteration of population and trait dynamics. Long-term effects of environmental perturbations frequently cause modification of the biological properties of species, such as species reproduction, mortality rates and other vital rates [23,27]. In this paper, we develop a stochastic lattice model describing the dynamics of a group chasing and escaping between predators and prey [28,29]. Non-conservative processes, such as breeding and physiological dying, are implemented in the model [30,31]. We study the dynamics of coexistence that arises due to the introducing of the abrupt changes in the values of parameters that characterize the non-conservative processes into the model.

Our model is based on the agent-based approach to simulate numerically collective chasing and escaping in a discrete space and time with periodic boundary conditions, similar to the model of hunting in groups proposed by Kamimura and Ohira [28,32–35]. In the following, we sketch the main features of our model, along the lines of Ref. [29]. Predators and prey are initially placed randomly on the sites of the lattice as pointlike particles. Thus, each site is either empty or occupied by a predator or a prey. Predators can sense the positions of the prey at an arbitrarily predefined distance and they try to move to one of the nearest neighboring sites in order to decrease the distance from the nearest prey. As predators move and approach their prey, the prey try to evade the capture by making a distance of one lattice spacing in a direction away from the nearest predator. Prey is caught upon the first encounter with a predator.

Distances in the present study are measured by the L^1 (“Manhattan”) metric. Manhattan distance between sites S_1 and S_2 on a square lattice is equal to the length of all paths connecting S_1 and S_2 sites along horizontal and vertical segments, without ever going back. In reality, predators search for prey in their vicinities. Similarly, prey can recognize the existence of nearby predators. Therefore, each species has its specific sighting range σ in which it can see the other species. Sighting range σ describes their skills at chasing or escaping. In that sense the model includes the smart pursuit of predators to prey and the escape of prey from predators. Analysis of the capture dynamics in the present study is limited to species with the same sighting ranges, i.e., $\sigma = 2$ [29]. If the value of σ equals zero, the movement is equivalent to the random walkers [28,31,36,37].

The model contains five parameters that control the breeding and physiological dying of predators and prey: the birth and two death rates of predators and two parameters characterizing the birth and death of prey. The goal of the present study is to investigate the short-time response of our model of group chase and escape to sudden perturbations in the values of parameters that characterize the non-conservative processes. In addition, we present and discuss the numerical results regarding the time evolution of the number of predators and prey for long periods of time after the abrupt changes of parameters affecting the non-conservative processes. In this paper we show that the short-time behavior is always linked to the forgetting of the initial conditions through the pursuit-evasion processes. Our numerical results suggest that this short-time evolving process is often accompanied with high amplitudes of population dynamics. The short-term memory effects observed in our model are reflected in the fact that the future evolution of the population densities after time $t_w > 0$ depends not only on the densities of predators and prey at the moment t_w , but also on the previous evolving history. This feature concerns the coding of the system history in various spatial configurations of predators and prey on the habitat. Furthermore, we try to demonstrate that the number of predators and prey in the long-term state are unambiguously determined by the probabilities for all nonconservative processes in the system. As consequence, quasi-steady state regime corresponding to perturbed probabilities does not depend on the moment of their introduction.

An outline of this paper is as follows. Section 2 describes the details of the model and simulations. In Section 3 results of numerical simulation are presented and discussed. Finally, Section 4 contains some additional comments and final remarks.

2. Definition of the model and the simulation method

The habitat where two interacting species survive and proliferate is represented by a two-dimensional square lattice of linear size L with periodic boundary conditions. In our model, the lattice is initially empty. To prepare the environment in the initially disordered state, we randomly distributed $N_1^{(0)}$ predators and $N_2^{(0)}$ prey as monomers. Spatial distribution of species on the lattice is generated using the random sequential adsorption (RSA) method [38,39]. Consequently, each site can be either empty or occupied by one particle: by a predator (chaser) or prey (escapee).

After placing the predators and the prey up to the chosen densities $\rho_1^{(0)} = N_1^{(0)}/L^2$ and $\rho_2^{(0)} = N_2^{(0)}/L^2$, we switch the species deposition events off and add the diffusive dynamics into the system. At this stage, apart from the hard core interaction between the species, there are rules governing the dynamic processes at the individual level. Movement within the lattice and the population dynamics are modeled as discrete time processes. At each Monte Carlo step a lattice site is selected at random. If the selected site is unoccupied, the configuration remains unchanged and a new site is selected at random. If the selected site is occupied by a predator or a prey, each species follow the hopping rules described below. After each Monte Carlo step, the time t is updated, $t \rightarrow t + 1/L^2$ and the process continues by choosing a new lattice site at random.

We assume that each species has its specific sighting range σ in which it can see the other species. In other words, predator has a certain pursuit region within which it can locate prey; simultaneously, prey has an escape zone inside which it can detect predators. The metric used in our model is L^1 , so e.g. the site (x, y) is at distance $|x| + |y|$ from the origin, with lattice spacing equal to unity. Here, unlike the previous model [29], both predators and prey have a sighting range $\sigma = 2$, which corresponds to the region around the individuals that includes the first and second neighbors. Accordingly, the decision for every step both of the predator and prey depends on the individuals that are found at the places of the first and second neighbors.

Suppose that predator is placed in a randomly selected site of the lattice. If the first neighbors of the selected site are entirely occupied with predators, the chosen predator stays at its original position. Then, the time t is updated, and the process continues by choosing a new lattice site at random. Suppose that some of the first neighbors of the selected site are occupied with prey. Then we randomly select a prey among them, remove the selected prey from the lattice, and move the chosen predator to this empty place. However, if the first neighbors of the chosen predator are not occupied with prey, the predator executes a jump as long as there is at least one empty nearest neighbor site. In this case, the predator moves to the empty adjacent site that is surrounded by the highest number of prey, $n_2^{(\max)}$, as its first neighbors. If two or more empty nearest neighbor sites correspond to the same highest number of prey $n_2^{(\max)}$, one of them is selected at random.

Now, suppose that a prey is placed in a randomly selected site of the lattice. If there are no empty nearest neighbors of the selected site, the chosen prey does not change its position, and the time increases by $1/L^2$. The process continues by choosing a new lattice site at random. If the selected site has empty adjacent sites, the chosen prey jumps to the empty nearest neighbor site that is surrounded by the lowest number of predators, $n_1^{(\min)}$, as its first neighbors. If two or more empty nearest neighbor sites correspond to the same lowest number of predators $n_1^{(\min)}$, one of them is selected at random. It must be emphasized that prey moves to the selected site only if $n_1^{(\min)}$ is less than or equal to the number of predators surrounding it in its original position.

The set of rules described above mimics the smart pursuit-evasion processes [29]. The competitive evolution of the populations of predators and prey is also governed by additional set of rules which defines the population dynamics. Non-conservative processes that change the number of individuals (size of the population), such as breeding and physiological dying, are also implemented in the model. We introduce the following five non-conservative processes into the model. For predators:

- Predators that have eaten a prey during the displacement can give an offspring in the previously occupied site, with probability P_{1r}^{fed} (birth probability of predators). In order to breed, it is considered that the predator must be strong enough, i.e., it must have food available in immediate surroundings.
- Predators that have not eaten a prey during the displacement can die with probability P_{1d}^{unfed} . It is assumed that the lack of food reduces the number of predators present in the habitat.
- Predators can suddenly die with probability P_{1d} (death probability of predators).

For prey:

- After displacement, prey can give an offspring filling an empty previously occupied site with probability P_{2r} (birth probability of prey).
- A prey has a probability P_{2d} of dying (death probability of prey).

Death probabilities of species describe quantitatively the dying that could be tied to any other factors and events in the eco-system, such as the old age of individuals or diseases.

Based on the above definitions we formulate the algorithm as follows. If a randomly selected site of the lattice is not empty, predator (prey) can die with probability P_{1d} (P_{2d}). If the predator (prey) died, it is removed from the lattice, and a new site is selected. Otherwise, we apply the rules for pursuit-evasion movement for individuals explained above. If the randomly selected predator survives, we check whether it ate the prey during the displacement. If so, the predator leaves an offspring in the previously occupied site, with probability P_{1r}^{fed} . However, if the predator did not eat the prey during the displacement, it dies with probability P_{1d}^{unfed} . Similarly, if the randomly selected prey survives, we check whether it moved into a new position. If so, the prey leaves an offspring in the previously occupied site, with probability P_{2r} .

The time t is counted by the number of attempts to select a lattice site and scaled by the total number of lattice sites $N = L^2$. Since in one Monte Carlo time step each lattice site is randomly checked once on the average, it can be considered that all predators and prey are active at all times and that none of the species have a priority in the number of attempts to make a move. In our study, the typical value of lattice size is $L = 128$, and the simulation data are averaged over 128 independent runs.

3. Results

At first, we present and discuss the numerical results regarding the time evolution of the normalized number of predators $\tilde{N}_1(t) = N_1(t)/N_1^{(0)}$ and prey $\tilde{N}_2(t) = N_2(t)/N_2^{(0)}$ on the lattice of size $L = 128$, for the representative set of probabilities $S_1 = \{P_{1r}^{\text{fed}} = 0.25, P_{1d}^{\text{unfed}} = 0.10, P_{1d} = 0.01; P_{2r} = 0.20, P_{2d} = 0.01\}$ that characterize the

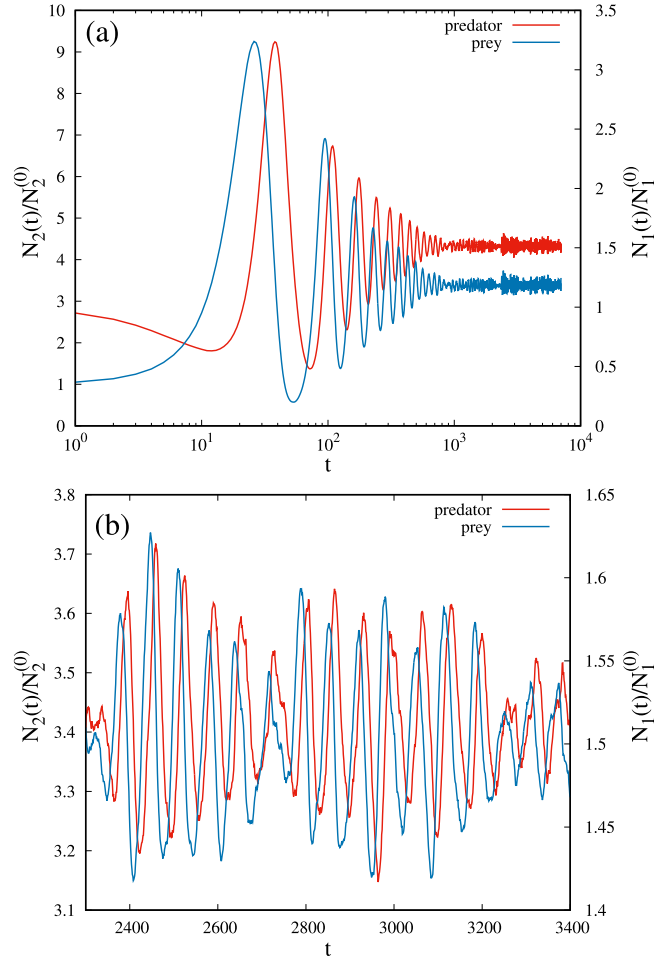


Fig. 1. (a) Time dependences of the number of the normalized number of predators $\tilde{N}_1 = N_1(t)/N_1^{(0)}$ and prey $\tilde{N}_2 = N_2(t)/N_2^{(0)}$ on the lattice of size $L = 128$. (b) Shown here are the temporal dependences of the \tilde{N}_1 and \tilde{N}_2 in the oscillatory region of the quasi-steady state, between $t_1 = 2300$ and $t_2 = 3400$, obtained for the same conditions as in panel (a). The values of probabilities that characterize the non-conservative processes are $S_1 = \{P_{1r}^{\text{fed}} = 0.25, P_{1d}^{\text{unfed}} = 0.10, P_{1d} = 0.01; P_{2r} = 0.20, P_{2d} = 0.01\}$. The initial numbers of species are chosen as $N_1^{(0)} = 720$ and $N_2^{(0)} = 800$.

non-conservative processes (see, Fig. 1(a)). The initial numbers of species were chosen as $N_1^{(0)} = 720$ and $N_2^{(0)} = 800$, corresponding to the initial densities $\rho_1^{(0)} = N_1^{(0)}/L^2 = 0.0439$ and $\rho_2^{(0)} = N_2^{(0)}/L^2 = 0.0488$, with the ratio $\rho_1^{(0)}/\rho_2^{(0)} = N_1^{(0)}/N_2^{(0)} = 0.9$. It can be seen that in the initial stage, during which the flocks of species are not formed, the number of predators and prey oscillates periodically with large amplitudes. However, the amplitude of oscillation decreases with time. After a short transient period, the system arrives at a quasi-steady state. This state corresponds to a coexisting state when the densities of predators and prey oscillate (fluctuate) around some “average” values, which do not change in time. More details about the temporal behavior of the number of predators and prey for the late stage of evolution, in a time range between $t_1 = 2300$ and $t_2 = 3400$, are shown in Fig. 1(b). A common prediction can be observed: prey oscillations precede predator oscillations by up to a quarter of the cycle period [4]. When predators are sparse, prey increase in the abundance. As the number of prey increases, predators also increase in the abundance. When the predators reach sufficiently high densities, the prey population is driven down to low densities. With a lack of prey, the predator population reduces, and the cycle repeats.

In addition, Fig. 2 shows the temporal evolution of the normalized number of predators $\tilde{N}_1(t) = N_1(t)/N_1^{(0)}$ and prey $\tilde{N}_2(t) = N_2(t)/N_2^{(0)}$ for the set of probabilities $S_2 = \{P_{1r}^{\text{fed}} = 0.09, P_{1d}^{\text{unfed}} = 0.05, P_{1d} = 0.01; P_{2r} = 0.15, P_{2d} = 0.01\}$, and initial numbers of species $N_1^{(0)} = 720$ and $N_2^{(0)} = 800$. For these conditions, we get qualitatively the same results as in Fig. 1. The results presented in Figs. 1 and 2 are used to establish the response in the evolution of the density of species to a change in the probabilities $S = \{P_{1r}^{\text{fed}}, P_{1d}^{\text{unfed}}, P_{1d}; P_{2r}, P_{2d}\}$ at a given moment t_w .

It is interesting to compare the oscillatory behavior of the number of predators and prey obtained using the two different sets (S_1, S_2) of probabilities that characterize the non-conservative processes (see, Figs. 1(b) and 2(b)). In the

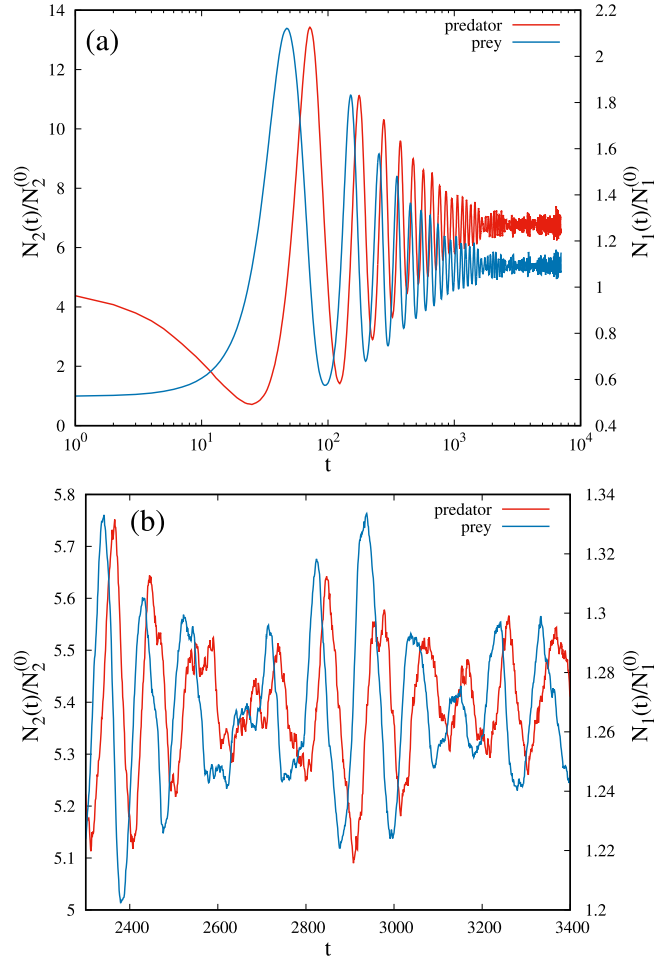


Fig. 2. (a) Time dependences of the number of the normalized number of predators $\tilde{N}_1 = N_1(t)/N_1^{(0)}$ and prey $\tilde{N}_2 = N_2(t)/N_2^{(0)}$ on the lattice of size $L = 128$. (b) Shown here are the temporal dependences of the \tilde{N}_1 and \tilde{N}_2 in the oscillatory region of the quasi-steady state, between $t_1 = 2300$ and $t_2 = 3400$, obtained for the same conditions as in panel (a). The values of probabilities that characterize the non-conservative processes are $S_2 = \{P_{1r}^{\text{fed}} = 0.09, P_{1d}^{\text{unfed}} = 0.05, P_{1d} = 0.01; P_{2r} = 0.15, P_{2d} = 0.01\}$. The initial numbers of species are chosen as $N_1^{(0)} = 720$ and $N_2^{(0)} = 800$.

second set of parameters S_2 , the probabilities P_{1r}^{fed} and P_{1d}^{unfed} for the non-conservative processes related to predator feeding are significantly reduced. The predator–prey cycles are based on a feeding relationship between two species. Therefore, we can consider that the coupling of the predator and prey systems is much stronger in the case of parameters from the set S_1 . Consequently, the amplitude of oscillations of predators in the quasi-stationary regime corresponding to the set of parameters S_2 is significantly smaller than in the case of the set of parameters S_1 .

In Fig. 3 we show the temporal dependence of the normalized number of predators $\tilde{N}_1(t) = N_1(t)/N_1^{(0)}$ and prey $\tilde{N}_2(t) = N_2(t)/N_2^{(0)}$ on the lattices of size $L = 64$ and 128 . It is important to note that the initial densities of predators $\rho_1^{(0)}$ and prey $\rho_2^{(0)}$ have not changed with the lattice size L . Numerical results for $\tilde{N}_1(t)$ and $\tilde{N}_2(t)$ in Fig. 3 are given for the initial densities $\rho_1^{(0)} = 0.0439$ and $\rho_2^{(0)} = 0.0488$ for both lattices. It is evident that the time evolution of the normalized number of species does not depend on the lattice size L . However, for the lattice of fixed size L , time evolution of $\tilde{N}_1(t)$ and $\tilde{N}_2(t)$ depends on the initial number of predators $N_1^{(0)}$ and prey $N_2^{(0)}$. Fig. 4 shows the dependence of the mean number of predators $\langle N_1 \rangle$ and prey $\langle N_2 \rangle$ in a quasi-stationary state on their initial number. It can be seen that the behavior of the system in the quasi-steady state ceases to depend on the initial conditions if the initial density of predators and prey is high enough. Indeed, the lower is the concentration of the targets (prey), the longer is the mean distance that a chaser (predator) crosses to find a target and catch it. Thus, at low densities of species, group chase with sight-limited chasers becomes very inefficient. Consequently, in the present paper, sufficiently large initial densities of species are chosen so that the average values of the number of predators and prey in the long-term state are unambiguously determined by the probabilities for all nonconservative processes in the system.

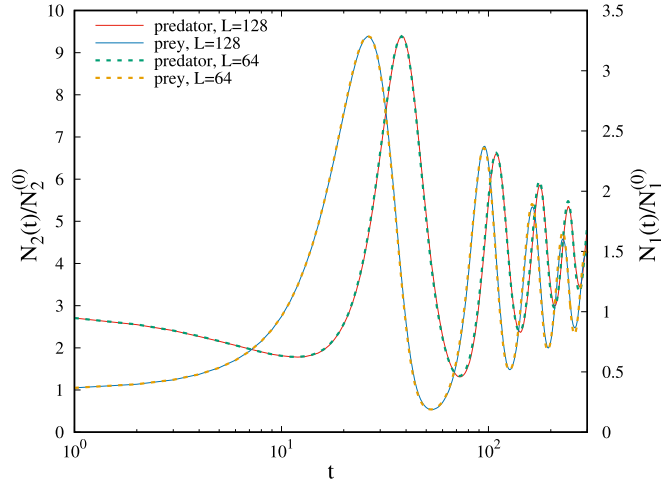


Fig. 3. Time dependences of the normalized number of predators $\tilde{N}_1 = N_1(t)/N_1^{(0)}$ and prey $\tilde{N}_2 = N_2(t)/N_2^{(0)}$ on the lattices of size $L = 64$ and 128 , as indicated in the legend. Results shown here are obtained for the same initial densities $\rho_1^{(0)} = 0.0439$ and $\rho_2^{(0)} = 0.0488$, for both lattices. Initial values for the number of predators/prey are $N_1^{(0)}/N_2^{(0)} = 180/200, 720/800$ for $L = 64, 128$, respectively. The values of probabilities that characterize the non-conservative processes are $\mathcal{S}_1 = \{P_{1r}^{\text{fed}} = 0.25, P_{1d}^{\text{unfed}} = 0.10, P_{1d} = 0.01; P_{2r} = 0.20, P_{2d} = 0.01\}$.

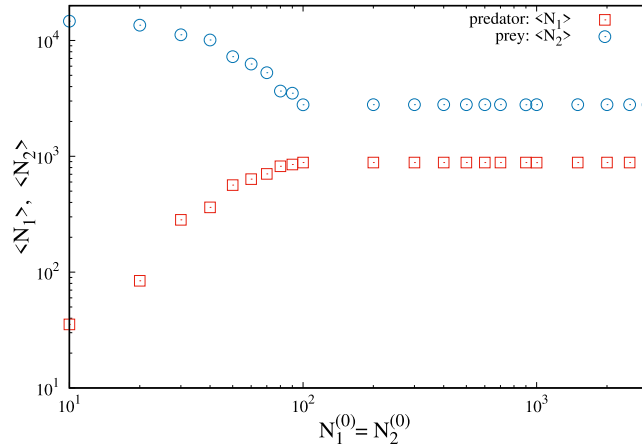


Fig. 4. Shown here is the dependence of the mean number of predators and prey in a quasi-stationary state on their initial number. The values of probabilities that characterize the non-conservative processes are: $\mathcal{S} = \{P_{1r}^{\text{fed}} = 0.25, P_{1d}^{\text{unfed}} = 0.10, P_{1d} = 0.01; P_{2r} = 0.20, P_{2d} = 0.01\}$. The lattice size value is $L = 128$.

One of the aims of our study were the properties of the long-term state attained by a population. We have found three possible states: (S1) the coexisting one with prey and predators, (S2) the absorbing one with prey only, and (S3) the empty one where no individual survived. Which one is the final state of a given population depends on the parameters characterizing the population dynamics. In the following example, we demonstrate the described behavior of the model. From the set of probabilities $\mathcal{S} = \{P_{1r}^{\text{fed}}, P_{1d}^{\text{unfed}}, P_{1d}; P_{2r}, P_{2d}\}$, three of them are fixed, i.e. we put $P_{1d} = 0.05, P_{2r} = 0.20$ and $P_{2d} = 0.05$. Probabilities P_{1r}^{fed} and P_{1d}^{unfed} are varied in $[0, 1]$ range, with a step of 0.1 . In Fig. 5 we show the average values of the normalized number of predators $\tilde{N}_1(t) = N_1(t)/N_1^{(0)}$ and prey $\tilde{N}_2(t) = N_2(t)/N_2^{(0)}$ in the long-term state for the full range of probabilities $P_{1r}^{\text{fed}}, P_{1d}^{\text{unfed}} \in [0, 1]$. An absorbing state (S2) can be reached for each probability value $P_{1r}^{\text{fed}} \in [0, 1]$ if the probability P_{1d}^{unfed} is large enough. It corresponds to the part of the surface in Fig. 5(a) for which the number of predators is equal to zero. Figs. 5(a) and 5(b) show that the system asymptotically tends to the state (S3) when $P_{1r}^{\text{fed}} \rightarrow 1$ and $P_{1d}^{\text{unfed}} \rightarrow 0$. It can be seen from Fig. 5 that all other areas correspond to the coexisting state (S1). In order to show different possible states in a more clear manner, we presented our results also in Fig. 6 which is a two-dimensional plot where we highlighted the states (S1), (S2), (S3), and (S1&2) which is an area of both (S1) and (S2) states. In other words, the individual simulation runs corresponding to the domain (S1&S2) can be finished in one of the two final states: adsorbing or coexisting one. In the case of coexisting final state (S1), the number of prey is very high; it covers a large part

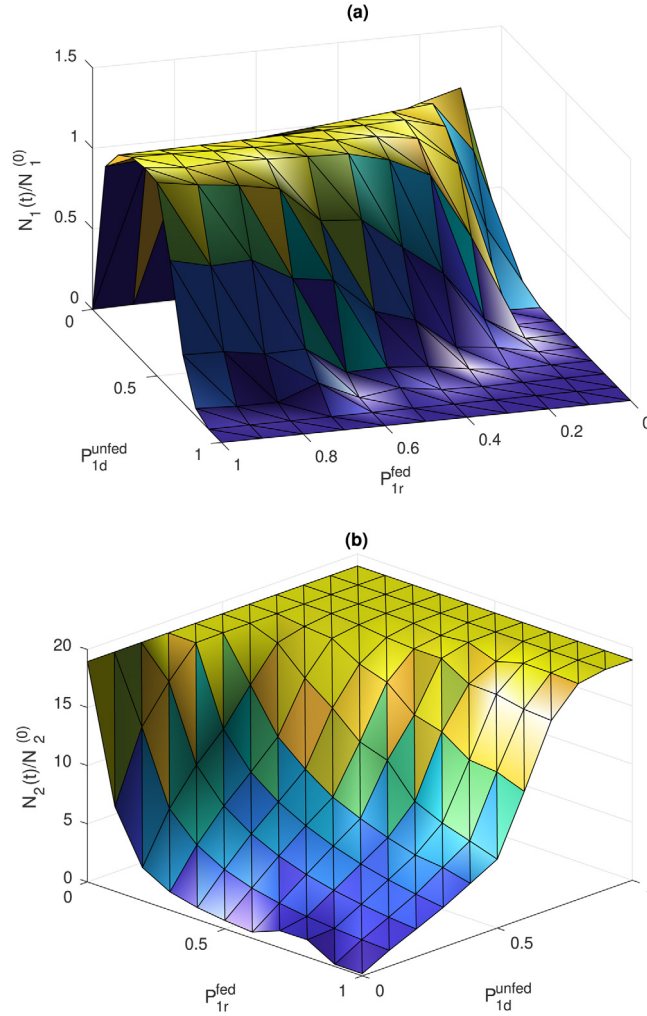


Fig. 5. Shown here is the surface plot of the normalized number of (a) predators $\tilde{N}_1 = N_1(t)/N_1^{(0)}$ and (b) prey $\tilde{N}_2 = N_2(t)/N_2^{(0)}$ in the long-term state for the full range of the probabilities $p_{1r}^{fed}, p_{1d}^{unfed} \in [0, 1]$. Initial densities of both species on the lattice of size $L = 128$ are the same, $\rho_1^{(0)} = \rho_2^{(0)} = 0.0488$, which corresponds to $N_1^{(0)} = N_2^{(0)} = 800$ predators and prey at $t = 0$.

of the lattice, but they coexist with a small number of predators. Clear boundaries between the states could be obtained by performing many more simulations with step that is less than 0.1.

3.1. Response properties of the model

In this section, we present the results of the simulations for the previously described model subject to abrupt changes in the values of probabilities $\{p_{1r}^{fed}, p_{1d}^{unfed}, P_{1d}; P_{2r}, P_{2d}\}$ that characterize the non-conservative processes. Starting from an initially disordered state, with randomly distributed predators and prey on the lattice, the system evolves at fixed probabilities $\mathcal{S} = \{p_{1r}^{fed}, p_{1d}^{unfed}, P_{1d}; P_{2r}, P_{2d}\}$. At a certain time, t_w , probability value for some selected non-conservative process $P \in \mathcal{S}$ changes from $P(I)$ to another value $P(II)$. During the further evolution of the system, the perturbed probability value $P(II)$ does not change.

At first, we present the results of simulations for the cases with abrupt changes of probabilities P_{2r} and P_{2d} that characterize the non-conservative processes of prey. In both cases, the system evolves to the time $t_w = 2500$ with constant probabilities $\mathcal{S}_1 = \{p_{1r}^{fed} = 0.25, p_{1d}^{unfed} = 0.10, P_{1d} = 0.01; P_{2r} = 0.20, P_{2d} = 0.01\}$. Fig. 7 shows the response in the evolution of the normalized number of predators $\tilde{N}_1(t)$ and prey $\tilde{N}_2(t)$ to an abrupt decrease in the birth probability of prey $P_{2r}(I) = 0.20 \rightarrow P_{2r}(II) = 0.10$ at instant $t_w = 2500$. When P_{2r} is abruptly lowered, the first effect is a sharp drop in the number of prey. This is followed by a significant reduction in the number of predators due to a lack of food. After the transient oscillatory regime, the system arrives at a quasi-steady state when the average number of predators remains reduced, but the average number of prey has slightly increased for the chosen parameter set.

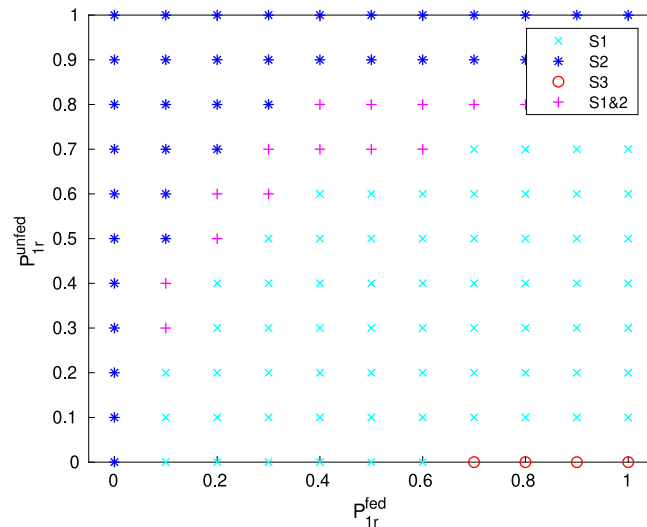


Fig. 6. Two-dimensional representation of full range of probabilities $p_{1r}^{fed}, p_{1d}^{unfed} \in [0, 1]$ that shows possible states of the model, (S1) – the coexisting one, (S2) – with prey only, (S3) – the empty one, and (S1&S2) – with both (S1) and (S2) states.

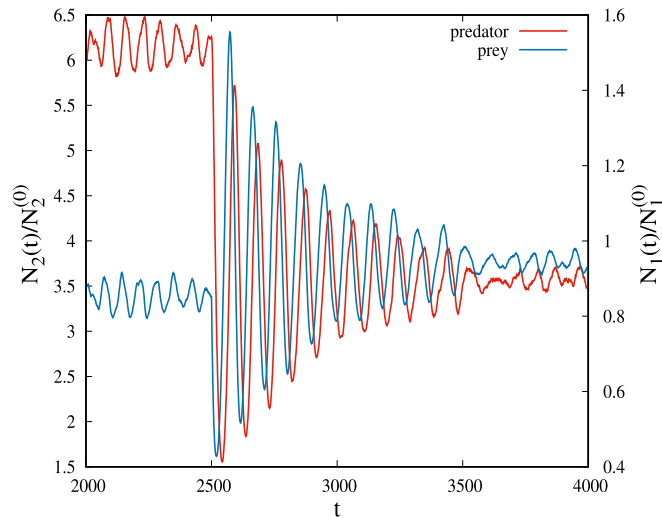


Fig. 7. Response in the evolution of the normalized number of predators $\tilde{N}_1(t) = N_1(t)/N_1^{(0)}$ and prey $\tilde{N}_2(t) = N_2(t)/N_2^{(0)}$ to an abrupt change of the probability $P_{2r}(I) = 0.20 \rightarrow P_{2r}(II) = 0.10$ at $t_w = 2500$. The values of probabilities that characterize the non-conservative processes before t_w are $S_1 = \{p_{1r}^{fed} = 0.25, p_{1d}^{unfed} = 0.10, P_{1d} = 0.01; P_{2r} = 0.20, P_{2d} = 0.01\}$.

Fig. 8 shows the response in the evolution of the normalized number of predators $\tilde{N}_1(t)$ and prey $\tilde{N}_2(t)$ to an abrupt increase in the death probability of prey $P_{2d}(I) = 0.01 \rightarrow P_{2d}(II) = 0.05$ at instant $t_w = 2500$. These results were obtained for the initial probability set $S_1 = \{p_{1r}^{fed} = 0.25, p_{1d}^{unfed} = 0.10, P_{1d} = 0.01; P_{2r} = 0.20, P_{2d} = 0.01\}$, which is identical to the previous one. Comparing **Figs. 7** and **8**, it can be seen that the response of the system to an increase in the death probability is very similar to its behavior when reducing the birth probability of prey. At short times after the probability P_{2d} is suddenly increased, we observe an abrupt decrease in the number of prey, followed by the reduction of the number of predators. After the transient oscillatory regime, the average number of predators is decreased because there is not enough available food. However, the average number of prey remains the same because there are fewer predators to catch them.

In the following, we present the results of simulations for the cases with the abrupt changes of probabilities $\{p_{1r}^{fed}, p_{1d}^{unfed}, P_{1d}\}$ that characterize the non-conservative processes of predators. These simulations are performed for two sets of initial probabilities, $S_1 = \{p_{1r}^{fed} = 0.25, p_{1d}^{unfed} = 0.10, P_{1d} = 0.01; P_{2r} = 0.20, P_{2d} = 0.01\}$ and $S_2 = \{p_{1r}^{fed} = 0.09, p_{1d}^{unfed} = 0.05, P_{1d} = 0.01; P_{2r} = 0.15, P_{2d} = 0.01\}$ (see **Figs. 1** and **2** showing the unperturbed evolution of the system).

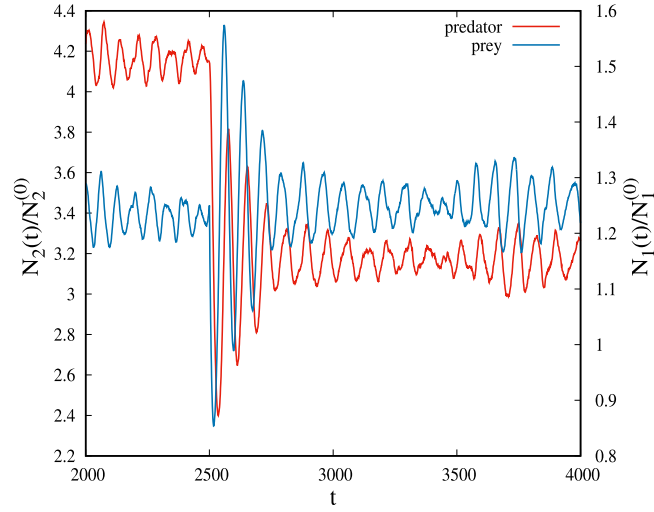


Fig. 8. Response in the evolution of the normalized number of predators $\tilde{N}_1(t) = N_1(t)/N_1^{(0)}$ and prey $\tilde{N}_2(t) = N_2(t)/N_2^{(0)}$ to an abrupt change of the probability $P_{2d}(I) = 0.01 \rightarrow P_{2d}(II) = 0.05$ at $t_w = 2500$. The values of probabilities that characterize the non-conservative processes before t_w are $S_1 = \{P_{1r}^{fed} = 0.25, P_{1d}^{unfed} = 0.10, P_{1d} = 0.01; P_{2r} = 0.20, P_{2d} = 0.01\}$.

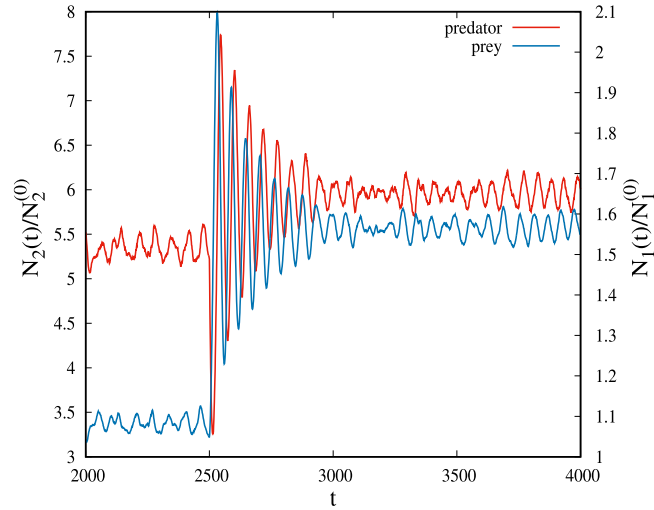


Fig. 9. Response in the evolution of the normalized number of predators $\tilde{N}_1(t) = N_1(t)/N_1^{(0)}$ and prey $\tilde{N}_2(t) = N_2(t)/N_2^{(0)}$ to an abrupt change of the probability $P_{1d}(I) = 0.01 \rightarrow P_{1d}(II) = 0.05$ at $t_w = 2500$. The values of probabilities that characterize the non-conservative processes before t_w are $S_1 = \{P_{1r}^{fed} = 0.25, P_{1d}^{unfed} = 0.10, P_{1d} = 0.01; P_{2r} = 0.20, P_{2d} = 0.01\}$.

In Fig. 9 we show the time evolution of the normalized number of predators $\tilde{N}_1(t)$ and prey $\tilde{N}_2(t)$ for the first set of initial probabilities S_1 , when the death probability of predators P_{1d} is changed from $P_{1d}(I) = 0.01$ to $P_{1d}(II) = 0.05$ at instant $t_w = 2500$. We can see that for short times after an abrupt change of P_{1d} the decay of the number of predators is fast. At short times, predator deficiency leads to a rapid increase in the number of prey. However, the increased food availability and the better nutrition of predators maintain their presence on the habitat after the transient oscillatory regime with almost the same average number as before the system perturbation. In other words, increasing the probability P_{1d} has not reduced the number of predators on the habitat, but it increased the average number of prey.

It must be stressed that the density evolution of predators and prey at short times after initialization ($t = 0$), or after an abrupt change of probabilities $S = \{P_{1r}^{fed}, P_{1d}^{unfed}, P_{1d}, P_{2r}, P_{2d}\}$ at instant $t = t_w$, depends not only on their density at these instants, but also on the corresponding spatial distribution of agents on the lattice. Initial spatial distribution of agents on the lattice depends on the method used to build an initial distribution of individuals within the population on the lattice. Spatial distribution of agents generated at moment $t_w = 2500$ represents the initial condition for further evolution of the system with new (perturbed) probabilities that characterize the non-conservative processes. It is clear that the spatial distributions of system agents in time $t_w = 2500$ are quite different from the spatial distributions generated by the RSA

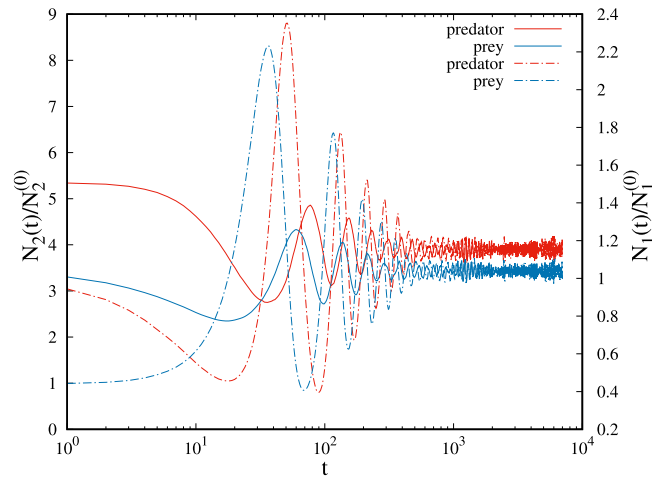


Fig. 10. Time dependences of the number of the normalized number of predators $\tilde{N}_1 = N_1(t)/N_1^{(0)}$ and prey $\tilde{N}_2 = N_2(t)/N_2^{(0)}$ on the lattice of size $L = 128$. The values of probabilities that characterize the non-conservative processes are $\mathcal{S} = \{P_{1r}^{fed} = 0.25, P_{1d}^{unfed} = 0.10, P_{1d} = 0.01; P_{2r} = 0.20, P_{2d} = 0.05\}$. Solid lines: The results from Fig. 8, which are translated along the x-axis, $t \rightarrow t - t_w$. Dashed lines: Results obtained in the case when the initial configuration of agents are generated by the RSA method.

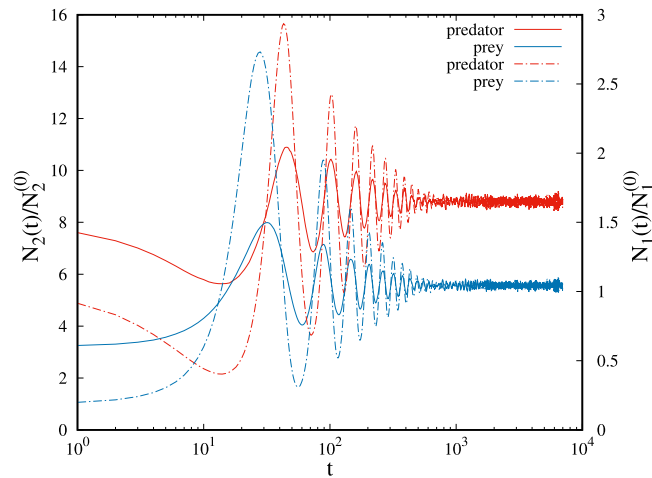


Fig. 11. Time dependences of the number of the normalized number of predators $\tilde{N}_1 = N_1(t)/N_1^{(0)}$ and prey $\tilde{N}_2 = N_2(t)/N_2^{(0)}$ on the lattice of size $L = 128$. The values of probabilities that characterize the non-conservative processes are $\mathcal{S} = \{P_{1r}^{fed} = 0.25, P_{1d}^{unfed} = 0.10, P_{1d} = 0.05; P_{2r} = 0.20, P_{2d} = 0.01\}$. Solid lines: The results from Fig. 9, which are translated along the x-axis, $t \rightarrow t - t_w$. Dashed lines: Results obtained in the case when the initial configuration of agents are generated by the RSA method.

method. Therefore, the responses of the system at short times after initialization ($t = 0$) and after an abrupt change of the any of probabilities $\mathcal{S} = \{P_{1r}^{fed}, P_{1d}^{unfed}, P_{1d}; P_{2r}, P_{2d}\}$ at the time $t_w = 2500$ are quite different. In Figs. 10 and 11 we show such comparisons. This can be explained by the memory effect, which is a common phenomenon in out-of-equilibrium systems. It is well known that the system can be found in states, characterized by the same density of predators and prey, that have different spatial distribution of agents on the lattice. Memory of the hunting history up to the densities $\rho_1(t)$ and $\rho_2(t)$ is encoded in the arrangement of the agents in the environment. This implies that the knowledge of the density of agents $\rho_1(t)$ and $\rho_2(t)$ is not sufficient to predict the further evolution of the system. This feature concerns the coding of the system history in the “microscopic” configurations.

Furthermore, a quasi-steady state regime corresponding to perturbed probabilities does not depend on the moment of their introduction. This conclusion is confirmed by the results shown in Figs. 10 and 11. It can be seen that using different moments ($t = 0$ or $t = t_w = 2500$) of introducing the perturbed values of probabilities for non-conservative processes give quantitatively the same results for the temporal evolution of $\tilde{N}_1(t)$ and $\tilde{N}_2(t)$ in the quasi-steady state regime.

In order to gain a better insight into the effect of a sudden increase in P_{1d} on the population dynamics, the same set of numerical experiments is carried out as in Fig. 9, with the only difference that the set of initial probabilities for the non-conservative processes is changed from \mathcal{S}_1 to \mathcal{S}_2 . These results are shown in Fig. 12. By comparing the results shown

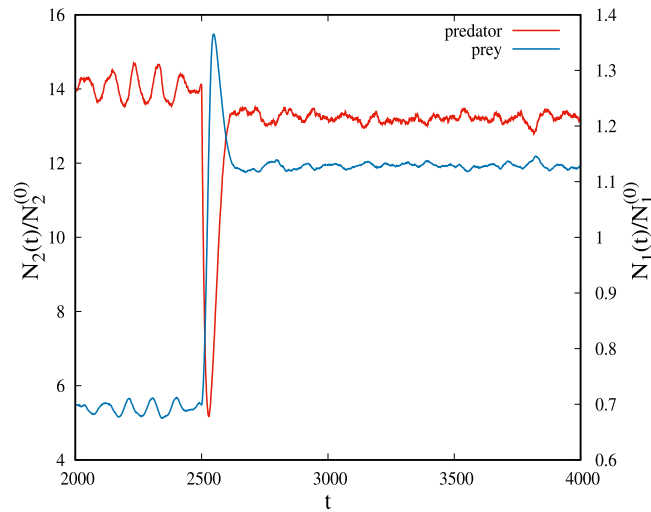


Fig. 12. Response in the evolution of the normalized number of predators $\tilde{N}_1(t) = N_1(t)/N_1^{(0)}$ and prey $\tilde{N}_2(t) = N_2(t)/N_2^{(0)}$ to an abrupt change of the probability $P_{1d}(I) = 0.01 \rightarrow P_{1d} = 0.05$ at $t_w = 2500$. The values of probabilities that characterize the non-conservative processes before t_w are $S_2 = \{P_{1r}^{fed} = 0.09, P_{1d}^{unfed} = 0.05, P_{1d} = 0.01; P_{2r} = 0.15, P_{2d} = 0.01\}$.

in Figs. 9 and 12, it is obvious that the same kind of numerical experiments for different initial probabilities S_1 and S_2 produce qualitatively similar results for the time evolution of the number of predators and prey. However, small changes in the system behavior are possible. From Fig. 12, it is evident that the change in the initial probabilities $S_1 \rightarrow S_2$ has led to a shortening of the transient oscillatory regime. The sudden increase in the death probability of predators P_{1d} causes an increase in the number of prey. However, after the transient regime, the number of predators slightly decreased, in the contrary to the behavior of the system shown in Fig. 9.

In the following, we shall demonstrate that an abrupt decrease in the birth probability of predators P_{1r}^{fed} has a very similar effect on the systems evolution as an abrupt increase of their death probability P_{1d} . Fig. 13 shows the response in the evolution of the normalized number of predators $\tilde{N}_1(t)$ and prey $\tilde{N}_2(t)$ for the set of initial probabilities S_1 , when the birth probability of predators P_{1r}^{fed} is decreased from $P_{1r}^{fed}(I) = 0.25$ to $P_{1r}^{fed}(II) = 0.15$ at instant $t_w = 2500$. Fig. 14 shows the same time dependences, but for the system whose initial probabilities are given by S_2 and the birth probability of predators P_{1r}^{fed} is abruptly changed from $P_{1r}^{fed}(I) = 0.09$ to $P_{1r}^{fed}(II) = 0.05$. Similarly to the results presented in Figs. 9 and 12, here we observe a fast decay of the number of predators for short times after an abrupt change of P_{1r}^{fed} . At short times this leads to a rapid increase in the number of prey. As previously mentioned, better food availability favorably affects the presence of predators in the habitat, so that their number increases slightly after the transient regime.

Inadequate and insufficient nutrition can lead to increased predator mortality. In our model, the predators that have not eaten any prey in the previous MC step can die with probability P_{1d}^{unfed} . In Figs. 15 and 16 we show the time evolution of the normalized number of predators $\tilde{N}_1(t)$ and prey $\tilde{N}_2(t)$, when the death probability of predators P_{1d}^{unfed} is abruptly doubled at instant $t_w = 2500$. In Figs. 15 and 16, the results are shown for the sets of initial probabilities S_1 and S_2 , respectively. After an abrupt increase of the probability P_{1d}^{unfed} , large and long-lasting oscillations in the number of predators occur, followed by large oscillations in the number of prey. As expected, the average number of prey is increased compared to the one observed before the perturbation, but the average number of predators stays almost the same. An increase in the number of prey makes the food more available, which maintains the number of predators.

4. Concluding remarks

In this paper, we have developed an intuitively clear framework for understanding the impacts of environmental perturbations on the population dynamics of the predator–prey systems. We have studied a stochastic lattice model describing a group chase and escape with sight-limited predators and prey by numerical simulations. Five probabilities that control the breeding and physiological dying of predators and prey were introduced into the model. Although the probability values used in the simulations were not taken from any specific research, our results highlight some possible consequences of perturbations in the predator–prey systems. Our MC simulations have shown that there are three possible final states into which the dynamics could lead the populations: coexistence of predator and prey, prey only, and an empty state in which both populations are extinct.

In the model, a perturbation was introduced at a specific instant during the evolving process by the abrupt change of the birth and death rates. In short times, after an abrupt change probability that characterizes the chosen non-conservative process, we have observed a sharp drop or jump in the numbers of predators and prey. Sudden changes in their number

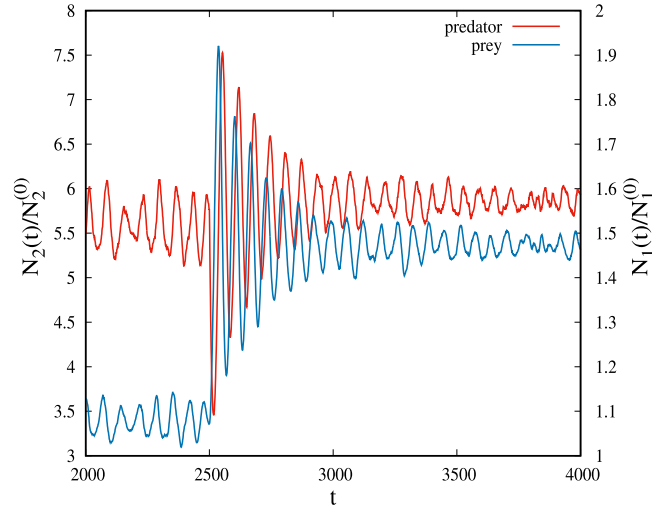


Fig. 13. Response in the evolution of the normalized number of predators $\tilde{N}_1(t) = N_1(t)/N_1^{(0)}$ and prey $\tilde{N}_2(t) = N_2(t)/N_2^{(0)}$ to an abrupt change of the probability $P_{1r}^{\text{fed}}(I) = 0.25 \rightarrow P_{1r}^{\text{fed}}(II) = 0.15$ at $t_w = 2500$. The values of probabilities that characterize the non-conservative processes before t_w are $\mathcal{S}_1 = \{P_{1r}^{\text{fed}} = 0.25, P_{1d}^{\text{unfed}} = 0.10, P_{1d} = 0.01; P_{2r} = 0.20, P_{2d} = 0.01\}$.

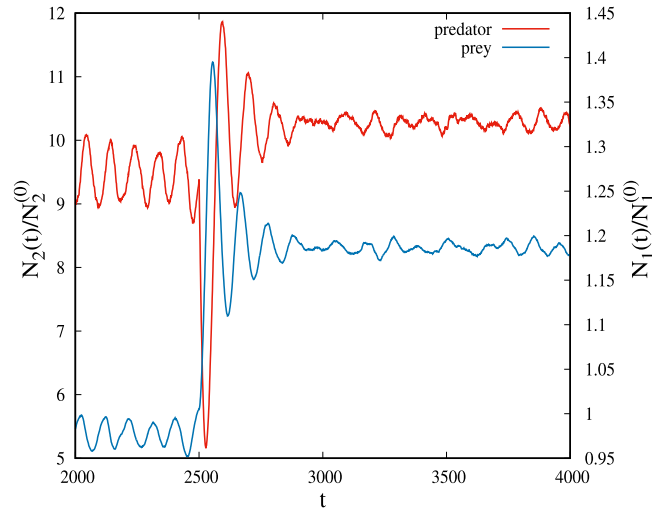


Fig. 14. Response in the evolution of the normalized number of predators $\tilde{N}_1(t) = N_1(t)/N_1^{(0)}$ and prey $\tilde{N}_2(t) = N_2(t)/N_2^{(0)}$ to an abrupt change of the probability $P_{1r}^{\text{fed}}(I) = 0.09 \rightarrow P_{1r}^{\text{fed}}(II) = 0.05$ at $t_w = 2500$. The values of probabilities that characterize the non-conservative processes before t_w are $\mathcal{S}_2 = \{P_{1r}^{\text{fed}} = 0.09, P_{1d}^{\text{unfed}} = 0.05, P_{1d} = 0.01; P_{2r} = 0.15, P_{2d} = 0.01\}$.

are stabilized during the transient oscillatory regime. After the transient oscillatory regime, the system arrives at a quasi-steady state when the densities of predators and prey oscillate (fluctuate) around some “average” values, which do not change in time. Our simulations predict the oscillations with a 1/4-period lag between predator and prey during and after the transient oscillatory regime. We have demonstrated that perturbation of a selected non-conservative process in numerical experiments with different initial probabilities produces qualitatively similar results for the time evolution of the number of predators and prey.

Our results suggest that the response of the system to an increase in the death probability of prey is very similar to its behavior when reducing the birth probability of prey. In both cases, the average number of predators is decreased after the transient oscillatory regime due to the lack of food. Further, we have found that an abrupt decrease in the birth probability of predators affects the evolution of the system similarly to an abrupt increase of their death probability. Decreasing (increasing) the birth (death) probability of predators changes their number slightly, but considerably increases the number of prey in the quasi-steady state regime. Such perturbations lead to a rapid increase in the number of prey at short times. Consequently, increased food availability maintains the presence of predators on the habitat after the transient oscillatory regime.

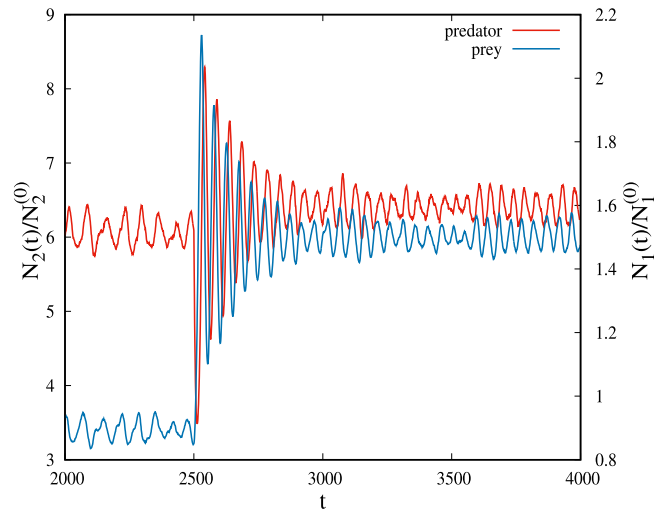


Fig. 15. Response in the evolution of the normalized number of predators $\tilde{N}_1(t) = N_1(t)/N_1^{(0)}$ and prey $\tilde{N}_2(t) = N_2(t)/N_2^{(0)}$ to an abrupt change of the probability $P_{1d}^{unfed}(I) = 0.10 \rightarrow P_{1d}^{unfed}(II) = 0.20$ at $t_w = 2500$. The values of probabilities that characterize the non-conservative processes before t_w are $S_1 = \{P_{1r}^{fed} = 0.25, P_{1d}^{unfed} = 0.10, P_{1d} = 0.01; P_{2r} = 0.20, P_{2d} = 0.01\}$.

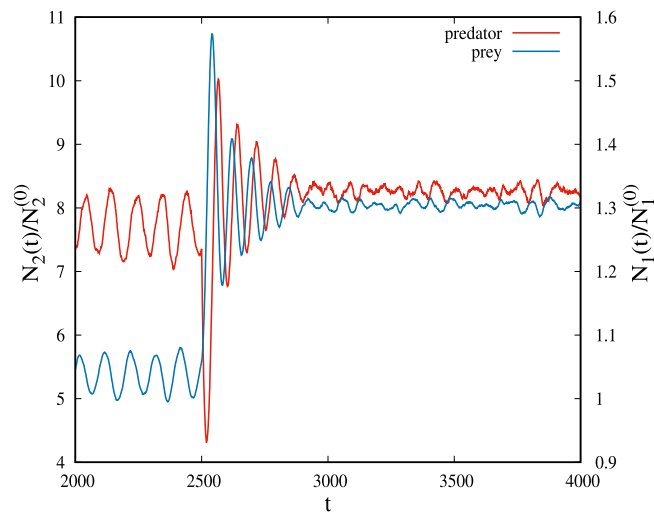


Fig. 16. Response in the evolution of the normalized number of predators $\tilde{N}_1(t) = N_1(t)/N_1^{(0)}$ and prey $\tilde{N}_2(t) = N_2(t)/N_2^{(0)}$ to an abrupt change of the probability $P_{1d}^{unfed}(I) = 0.05 \rightarrow P_{1d}^{unfed}(II) = 0.10$ at $t_w = 2500$. The values of probabilities that characterize the non-conservative processes before t_w are $S_2 = \{P_{1r}^{fed} = 0.09, P_{1d}^{unfed} = 0.05, P_{1d} = 0.01; P_{2r} = 0.15, P_{2d} = 0.01\}$.

This study could serve as a good basis for further studies of the dynamics of multi-species communities that are exposed to sudden environmental perturbations. It would be interesting to perform a similar investigation in a heterogeneous landscape, i.e., in an environment that contains obstacles [29]. This would allow us to study the role that rapid changes in the spatial structure of the natural habitat play in the time evolution of the number of predators and prey.

CRediT authorship contribution statement

J.R. Šćepanović: Conceptualization, Methodology, Software, Validation, Formal analysis, Writing - original draft, Writing - review & editing, Visualization. **Z.M. Jakšić:** Methodology, Validation, Formal analysis, Writing - review & editing, Supervision. **Lj. Budinski-Petković:** Methodology, Validation, Formal analysis, Writing - review & editing, Supervision. **S.B. Vrhovac:** Methodology, Software, Validation, Formal analysis, Visualization, Writing - review & editing, Supervision.

Declaration of competing interest

The authors declare that they have no known competing financial interests or personal relationships that could have appeared to influence the work reported in this paper.

Acknowledgments

This work was supported by the Ministry of Education, Science and Technological Development of the Republic of Serbia. Numerical simulations were run on the PARADOX supercomputing facility at the Scientific Computing Laboratory of the Institute of Physics Belgrade.

References

- [1] Alfred J. Lotka, Elements of physical biology, *Sci. Prog. Twentieth Century* (1919-1933) 21 (1926) 341–343.
- [2] Vito Volterra, Variations and fluctuations of the number of individuals in animal species living together, *ICES J. Mar. Sci.* 3 (1928) 3–51.
- [3] M.L. Rosenzweig, R.H. MacArthur, Graphical representation and stability conditions of predator–prey interactions, *Am. Nat.* 97 (1963) 209–223.
- [4] M.G. Bulmer, The theory of prey–predator oscillations, *Theor. Popul. Biol.* 9 (1976) 137–150.
- [5] Charles Elton, Mary Nicholson, The ten-year cycle in numbers of the lynx in Canada, *J. Anim. Ecol.* 11 (1942) 215–244.
- [6] Syunro Utida, Cyclic fluctuations of population density intrinsic to the host–parasite system, *Ecology* 38 (1957) 442–449.
- [7] Leo S. Luckinbill, The effects of space and enrichment on a predator–prey system, *Ecology* 55 (1974) 1142–1147.
- [8] Olivier Gilg, Ilkka Hanski, Benoît Sittler, Cyclic dynamics in a simple vertebrate predator–prey community, *Science* 302 (2003) 866–868.
- [9] A. Pekalski, A short guide to predator–prey lattice models, *Comput. Sci. Eng.* 6 (2004) 62–66.
- [10] Tibor Antal, Michel Droz, Adam Lipowski, Géza Ódor, Critical behavior of a lattice prey–predator model, *Phys. Rev. E* 64 (2001) 036118.
- [11] A.F. Rozenfeld, E.V. Albano, Study of a lattice–gas model for a prey–predator system, *Physica A* 266 (1999) 322–329.
- [12] Tamás Vicsek, András Czirók, Eshel Ben-Jacob, Inon Cohen, Ofer Shochet, Novel type of phase transition in a system of self-driven particles, *Phys. Rev. Lett.* 75 (1995) 1226–1229.
- [13] Masahide Sato, Chasing and escaping by three groups of species, *Phys. Rev. E* 85 (2012) 066102.
- [14] Ankush Sengupta, Tobias Kruppa, Hartmut Löwen, Chemotactic predator–prey dynamics, *Phys. Rev. E* 83 (2011) 031914.
- [15] Tongfeng Weng, Huijie Yang, Changgui Gu, Jie Zhang, Pan Hui, Michael Small, Predator–prey games on complex networks, *Commun. Nonlinear Sci. Numer. Simul.* 79 (2019) 104911.
- [16] Jacopo A. Baggio, Kehinde Salau, Marco A. Janssen, Michael L. Schoon, Örjan Bodin, Landscape connectivity and predator–prey population dynamics, *Landsc. Ecol.* 26 (2010) 33–45.
- [17] Luciano Stucchi, Javier Galeano, Desiderio A. Vasquez, Pattern formation induced by intraspecific interactions in a predator–prey system, *Phys. Rev. E* 100 (2019) 062414.
- [18] Dipanjan Chakraborty, Sanchayan Bhunia, Rumi De, Survival chances of a prey swarm: how the cooperative interaction range affects the outcome, *Sci. Rep.* 10 (2020).
- [19] Siddharth Patwardhan, Rumi De, K. Panigrahi, Survival probability of a lazy prey on lattices and complex networks, *Eur. Phys. J. E* 43 (53) (2020).
- [20] Russell Lande, Risks of population extinction from demographic and environmental stochasticity and random catastrophes, *Amer. Nat.* 142 (1993) 911–927.
- [21] David Tilman, John A. Downing, Biodiversity and stability in grasslands, *Nature* 367 (1994) 363–365.
- [22] Alex Kamenev, Baruch Meerson, Boris Shklovskii, How colored environmental noise affects population extinction, *Phys. Rev. Lett.* 101 (2008) 268103.
- [23] Peter Yodzis, The indeterminacy of ecological interactions as perceived through perturbation experiments, *Ecology* 69 (1988) 508–515.
- [24] Ashley Shade, Jordan S. Read, Nicholas D. Youngblut, Noah Fierer, Rob Knight, Timothy K. Kratz, Noah R. Lottig, Eric E. Roden, Emily H. Stanley, Jesse Stombaugh, Rachel J. Whitaker, Chin H. Wu, Katherine D. McMahon, Lake microbial communities are resilient after a whole-ecosystem disturbance, *ISME J.* 6 (2012) 2153–2167.
- [25] Vincent Bretagnolle, Julien Terraube, Predator–prey interactions and climate change, in: *Effects of Climate Change on Birds*, Oxford University Press, 2019, pp. 199–220.
- [26] Qihua Huang, Hao Wang, Mark A. Lewis, The impact of environmental toxins on predator–prey dynamics, *J. Theoret. Biol.* 378 (2015) 12–30.
- [27] Edward A. Bender, Ted J. Case, Michael E. Gilpin, Perturbation experiments in community ecology: Theory and practice, *Ecology* 65 (1984) 1–13.
- [28] Atsushi Kamimura, Toru Ohira, Group chase and escape, *New J. Phys.* 12 (2010) 053013.
- [29] J.R. Šćepanović, A. Karač, Z.M. Jakšić, Lj. Budinski-Petković, S.B. Vrhovac, Group chase and escape in the presence of obstacles, *Physica A* 525 (2019) 450–465.
- [30] N. Boccara, O. Roblin, M. Roger, Automata network predator–prey model with pursuit and evasion, *Phys. Rev. E* 50 (1994) 4531–4541.
- [31] Alejandro F. Rozenfeld, Ezequiel V. Albano, Critical and oscillatory behavior of a system of smart preys and predators, *Phys. Rev. E* 63 (2001) 061907.
- [32] Atsushi Kamimura, Toru Ohira, Group Chase and Escape: Fusion of Pursuits-Escapes and Collective Motions, Springer, Singapore, 2019.
- [33] Milá Janosov, Csaba Virá, Gábor Vásárhelyi, Tamás Vicsek, Group chasing tactics: how to catch a faster prey, *New J. Phys.* 19 (2017) 053003.
- [34] Luca Angelani, Collective predation and escape strategies, *Phys. Rev. Lett.* 109 (2012) 118104.
- [35] Sicong Yang, Shijie Jiang, Li Jiang, Geng Li, Zhangang Han, Aggregation increases prey survival time in group chase and escape, *New J. Phys.* 16 (2014) 083006.
- [36] Ryosuke Nishi, Atsushi Kamimura, Katsuhiko Nishinari, Toru Ohira, Group chase and escape with conversion from targets to chasers, *Physica A* 391 (2012) 337–342.
- [37] Huodong Wang, Wenchen Han, Junzhong Yang, Group chase and escape with sight-limited chasers, *Physica A* 465 (2017) 34–39.
- [38] J.W. Evans, Random and cooperative sequential adsorption, *Rev. Modern Phys.* 65 (1993) 1281–1329.
- [39] Lj. Budinski-Petković, I. Lončarević, D. Dujak, A. Karač, J.R. Šćepanović, Z.M. Jakšić, S.B. Vrhovac, Particle morphology effects in random sequential adsorption, *Phys. Rev. E* 95 (2017) 022114.

PAPER

Consequences for predator–prey dynamics caused by the presence of obstacles

To cite this article: J R Šćepanović *et al* *J. Stat. Mech.* (2023) 083406

View the [article online](#) for updates and enhancements.

You may also like

- [Modeling the fear effect on a stochastic prey–predator system with additional food for the predator](#)
Amartya Das and G P Samanta
- [Stability of a stage-structure Rosenzweig-MacArthur model incorporating Holling type-II functional response](#)
Lazarus Kalvein Beay, Agus Suryanto, Isnani Darti et al.
- [Stability and Optimal Harvesting of Modified Leslie-Gower Predator-Prey Model](#)
S Toaha and M I Azis

PAPER: Interdisciplinary statistical mechanics

Consequences for predator–prey dynamics caused by the presence of obstacles

J R Šćepanović^{1,*}, Lj Budinski-Petković², Z M Jakšić¹,
A Belić¹ and S B Vrhovac¹

¹ Institute of Physics Belgrade, University of Belgrade, Pregrevica 118, Zemun, 11080 Belgrade, Serbia

² Faculty of Engineering, Trg D. Obradovića 6, Novi Sad 21000, Serbia
E-mail: julija@ipb.ac.rs

Received 5 June 2023

Accepted for publication 27 July 2023

Published 22 August 2023



Online at stacks.iop.org/JSTAT/2023/083406
<https://doi.org/10.1088/1742-5468/aceb58>

Abstract. In order to understand how a heterogeneous habitat affects the population dynamics of the predator–prey system, a spatially explicit lattice model consisting of predators, prey and obstacles is constructed. The model includes smart pursuit (predators to prey) and evasion (prey from predators). Both species can affect their movement by visual perception within their finite sighting range. Non-conservative processes that change the number of individuals within the population, such as breeding and physiological dying, are implemented in the model. Obstacles are represented by non-overlapping lattice shapes that are randomly placed on the lattice. In the absence of obstacles, numerical simulations reveal regular, coherent oscillations with a nearly constant predator–prey phase difference. Numerical simulations have shown that changing the probabilities for non-conservative processes can increase or decrease the period of coherent oscillations in species abundances and change the relative lag between coherent components. After introducing obstacles into the model, we observe random transitions between coherent and non-coherent oscillating regimes. In the non-coherent regime, predator and prey abundances continue to oscillate, but without a well-defined phase relationship. Our model suggests that stochasticity introduced by density fluctuations of obstacles is responsible for the reversible shift from coherent to non-coherent oscillations.

* Author to whom any correspondence should be addressed.

Keywords: predator–prey model, group chase and escape, square lattice, obstacles, wavelet analysis

Contents

1. Introduction	2
2. Definition of the model and the simulation method	4
2.1. Movement of predators and prey	5
2.2. Non-conservative processes	6
2.3. Algorithm	6
3. Results and discussion	7
3.1. Dynamics of the system without obstacles	7
3.1.1. Coherence of the fluctuations	12
3.2. Dynamics of the system with obstacles	14
3.2.1. Coherence of the fluctuations	16
4. Concluding remarks	22
Acknowledgments	24
Appendix. Wavelet analysis	24
References	25

1. Introduction

In predator–prey modeling, a system is modeled as a collection of autonomous decision-making entities called agents. Basically, two types of agents are present in the system: chasers (predators) and escapees (prey). A predator–prey model consists of a system of agents and the relationships between them. Each agent individually assesses its situation and makes decisions on the basis of a set of rules. Predator–prey models can exhibit complex behavior patterns and provide valuable information about the dynamics of real-world systems. For example, simple predator–prey models may exhibit limit cycles during which the populations of both species have periodic oscillations in time with a 1/4-period lag between predator and prey [1–4]. These oscillations in species abundances have been successfully observed in nature [5–8]. Furthermore, the predator–prey systems have been studied in various contexts, such as robotics, game theory and ecology [9–15].

Habitat heterogeneity has long been recognized as a major factor in ecological dynamics. Animal habitats include natural physical obstacles, such as lakes, rivers or high mountains and areas of avoidance due to increased predation risk such as open

areas without refuge. In addition, habitats are often intersected by long human-made structures, such as roads, railways, power lines and pipe lines [16, 17]. These spatial heterogeneities can affect predator–prey interactions in two qualitatively different ways, by providing refuge for the prey or obstacles that interfere with the movements of both prey and predators. Predation is a consequence of predators and prey overlapping (i.e. encounters) in time and space. Animals regulate the encounter process by deciding which parts of resource to use, how long to use these parts, and how to travel among them. However, anthropogenic landscape changes can alter the animals' ability to access resources and avoid predation, with consequences for predator–prey dynamics [18–20]. In this paper, we aim to explore how habitat spatial obstacles may affect the predator–prey dynamics. Special attention is paid to the changes in the oscillatory properties of species abundances caused by the presence of obstacles.

In the following, we sketch the main features of our numerical model, along the lines of [21, 22]. Our model is an agent-based approach to simulate numerically collective chasing and escaping in a discrete space with periodic boundary conditions. Our approach is similar to the model of hunting in groups proposed by Kamimura and Ohira [23–25]. The problem of group chase and escape in various situations and extensions has been studied by computer simulations and by theoretical analysis. Examples include the model with conversion of caught escapees into chasers [26], the group chase and escape by three groups [27], the models with fast chasers [28], the group chase and escape model with the chaser's interaction [29], the off-lattice model [30], the three aggregation strategies for the prey [31], etc. Predators and prey are initially placed randomly on the sites of the square lattice as pointlike particles. Distances in the present study are measured by the L^1 ('Manhattan') metric. For example, the site (x, y) is at distance $|x| + |y|$ from the origin, with the lattice spacing equal to unity. Both species perform independent nearest-neighbor walks on a lattice following simple dynamical rules, increasing or decreasing the distance from the nearest particle of the opposite group. Each species has its specific sighting range σ in which it can see the other species. Predators (prey) can sense the position of the prey (predator) at a predefined distance σ and they try to move to one of the nearest neighboring sites in order to decrease (increase) the distance from the nearest prey (predator). Therefore, the sighting range σ describes their skills at chasing or escaping. Prey is caught upon the first encounter with a predator. Analysis of the capture dynamics in the present study is limited to species with the same sighting ranges, i.e. $\sigma = 2$ [21, 22]. If the value of σ is equal to zero, the movement is equivalent to that of random walkers [23, 26, 32, 33]. It has been confirmed that the idea of animals using blind search strategies does not seem to be usable since it neglects the role of animal intelligence and experience in guiding them [34]. Consequently, we have not considered species with zero sighting range.

Non-conservative processes that change the number of individuals (size of the population), such as breeding and physiological dying, are also implemented in the model [22, 32, 35–38]. The model contains five parameters that control the non-conservative processes. The birth and two death rates of predators and two parameters characterizing the birth and death of prey. In the presence of non-conservative processes, the dominant type of dynamics can be characterized by regular, coherent oscillations in time with a nearly constant predator–prey phase difference [1–4]. These oscillations in

species abundances have been successfully observed in real-world systems or laboratory studies with fast-reproducing organisms [5–8, 39, 40].

Furthermore, an element of stochasticity of the environment, such as obstacles present in any natural system, is incorporated into the model. Lattice-based models allow easy handling of obstacles of various shapes and sizes. We study the case when the lattice is initially covered with obstacles at various concentrations. Depositing objects (obstacles) of various shapes are formed by a small number of lattice steps on the square lattice. The spatial distribution of the obstacles on the lattice is created using the random sequential adsorption (RSA) method [41, 42].

In addition to the empirical data, long-running experiments with fast-reproducing organisms also support the sustained nature of predator–prey cycles [6, 39, 40, 43–45]. Since these experiments can be carried out under controlled conditions, they are suitable for finding the most important parameters that influence the species dynamics and coexistence. Recently, the potential for long-term persistence of predator–prey cycles has been experimentally studied with a planktonic predator–prey system [45]. Experiments were conducted with parthenogenetic rotifers as predators and unicellular algae as prey under constant environmental conditions. Although the experiments were not perturbed by external influences, transitions between two different dynamic regimes were identified. Periods in which the predator densities follow the prey densities with a phase lag of about $\pi/2$ (coherent oscillations) were intersected by non-coherent oscillation regimes in which a well-defined phase relationship between the measured signals is lost. We show that the stochasticity introduced by the presence of obstacles can be responsible for the reversible shift from coherent to non-coherent oscillations.

We organized the paper as follows. Section 2 describes the details of the model and simulations. In section 3, results of numerical simulations are presented and discussed. Section 4 contains some additional comments and final remarks. Some technical details of the calculations are given in the appendices.

2. Definition of the model and the simulation method

The environment where two interacting species coexist is represented by a two-dimensional square lattice of linear size $L=256$ with periodic boundary conditions. The lattice is initially occupied by obstacles of various shapes and sizes. Their spatial distribution at density ρ_0 is generated using the RSA method [41, 42]. This density ρ_0 is defined as the fraction of sites of the lattice that are occupied by the obstacles. Linear obstacles are k -mers of length $\ell = 0, 1, \dots, 8$, shown in table 1 as objects (A_1) – (A_9) .

To initialize the numerical simulations, $N_1^{(0)}$ predators and $N_2^{(0)}$ prey are randomly distributed as monomers in the lattice up to the chosen densities $\rho_1^{(0)} = N_1^{(0)}/L^2$ and $\rho_2^{(0)} = N_2^{(0)}/L^2$. Again, the initial spatial distribution of species on the lattice is generated using the RSA method [41, 42]. Accordingly, each site can be either empty or occupied by one particle: a chaser (predator), an escapee (prey) or a particle that belongs to an obstacle.

Table 1. Jamming coverages $\rho_j^{(x)}$ for various k -mers (x) of length $\ell^{(x)}$ on a square lattice [46].

(x)	k -mer	$\ell^{(x)}$	$\rho_j^{(x)}$
(A_1)	•	0	1.0
(A_2)	—	1	0.9067
(A_3)	—•	2	0.8465
(A_4)	—•—	3	0.8102
(A_5)	—•—•	4	0.7867
(A_6)	—•—•—	5	0.7699
(A_7)	—•—•—•	6	0.7578
(A_8)	—•—•—•—	7	0.7479
(A_9)	—•—•—•—•	8	0.7405

2.1. Movement of predators and prey

The movement of individuals with escape and pursuit behavior within the lattice is modeled as a discrete-time process. At this stage, apart from the hard-core interaction between the species and between the species and the obstacles, there are simple rules governing the dynamic processes at an individual level. At each Monte Carlo step, a lattice site is selected at random. If the chosen site is unoccupied, the positions of predators and prey remain unchanged, and a new site is randomly selected. If a predator or prey occupies the chosen site, each species follows the hopping rules described below. After each Monte Carlo step, the time t is updated, $t \rightarrow t + 1/L^2$, and the process continues by randomly choosing a new lattice site. The present model includes species with the same sighting range, $\sigma = 2$. Accordingly, the decision for every step, both of the predator and prey depends on the individuals and obstacles that are found at the places of the first and second neighbors.

Suppose that the predator is placed in a randomly selected site of the lattice. If the first neighbors of the selected site are entirely occupied by obstacles and predators, the chosen predator stays at its original position. Then, the time t is updated, and the process continues by selecting a new lattice site at random. Suppose that some of the first neighbors of the selected site are occupied by prey. Then, we randomly select a prey among them, remove it from the lattice, and move the chosen predator to this empty place. However, if the first neighbors of the selected predator are not occupied by prey, the predator executes a jump as long as there is at least one empty nearest neighbor site. In this case, the predator moves to the vacant adjacent site surrounded by the highest number of prey, $n_2^{(\max)}$, as its first neighbors. If two or more empty nearest neighbor sites correspond to the same highest number of prey, $n_2^{(\max)}$, one of them is selected at random.

Suppose that the prey is placed in a randomly selected lattice site. If there are no empty nearest neighbors of the selected site, the chosen prey does not change its position, and the time increases by $1/L^2$. The process continues by choosing a new lattice site at random. If the selected site has empty adjacent sites, the chosen prey jumps to

the vacant nearest neighbor site surrounded by the lowest number of predators, $n_1^{(\min)}$, as its first neighbors. If two or more empty nearest neighbor sites correspond to the same lowest number of predators, $n_1^{(\min)}$, one of them is selected at random. It must be emphasized that a prey moves to the selected site only if $n_1^{(\min)}$ is less than or equal to the number of predators surrounding it in its original position.

2.2. Non-conservative processes

We introduce into the model the following non-conservative processes and an additional set of rules that define the population dynamics.

Rules intended for predators:

1. Predators that have eaten prey during the displacement can leave offspring at the previously occupied site, with probability P_{1b}^{fed} (birth probability of predators). To breed, the predator must be strong enough, i.e. it must have food available in the immediate vicinity.
2. Predators that have not eaten prey during the displacement can die with probability P_{1d}^{unfed} . It is assumed that the lack of food reduces the number of predators in the habitat.
3. Predators can suddenly die with probability P_{1d} (death probability of predators).

Rules intended for prey:

1. After displacement, prey can leave offspring filling an empty previously occupied site with probability P_{2b} (birth probability of prey).
2. Prey has a probability P_{2d} of dying (death probability of prey).

Species mortality probabilities P_{1d} and P_{2d} quantitatively describe dying that could be related to various factors and events in the ecosystem, such as the age of individuals or diseases. Here, we list the probability values that characterize non-conservative processes as sequences of numbers with the following structure: $\mathcal{S} = \{P_{1b}^{\text{fed}}, P_{1d}^{\text{unfed}}, P_{1d}; P_{2b}, P_{2d}\}$.

2.3. Algorithm

Based on the above definitions and rules, we formulate the algorithm as follows. If a randomly selected site of the lattice is not empty, the predator (prey) can die with probability P_{1d} (P_{2d}). If the predator (prey) dies, it is removed from the lattice, and a new site is selected. Otherwise, we apply the rules for the pursuit–evasion movement for individuals explained above (section 2.1). If the randomly selected predator survives, we check whether it ate the prey during the displacement. If so, the predator leaves an offspring at the previously occupied site, with probability P_{1b}^{fed} . However, if the predator did not eat the prey during the displacement, it dies with probability P_{1d}^{unfed} . Similarly, if the randomly selected prey survives, we check whether it moved into a new position. If so, the prey leaves an offspring at the previously occupied site, with probability P_{2b} .

3. Results and discussion

In the first part of this section, the group spatial chase and escape phenomena are analyzed in the environment without heterogeneities. Then, population dynamics are studied in an environment that contains spatial obstacles.

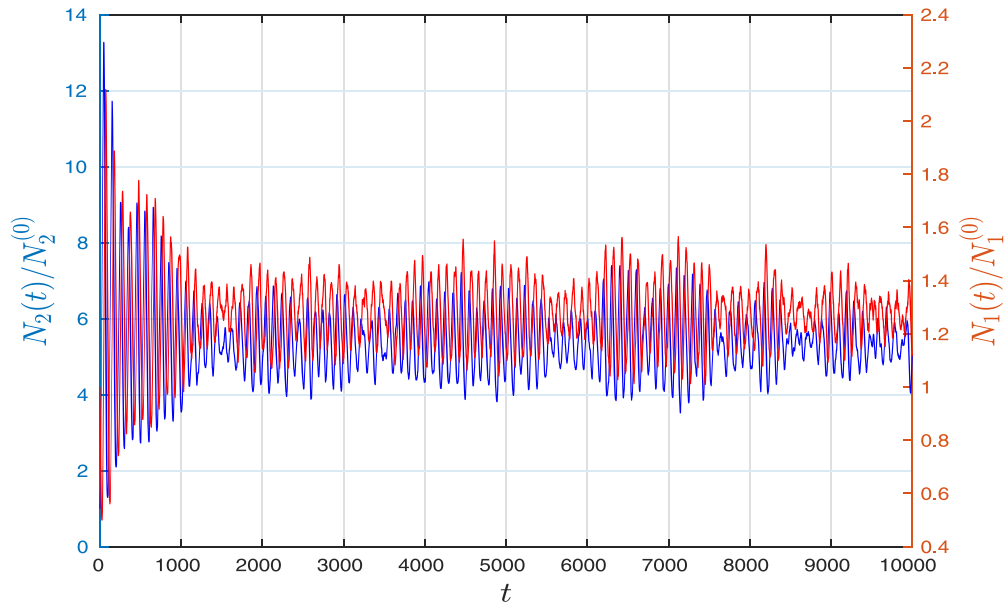
3.1. Dynamics of the system without obstacles

In figures 1 and 2, we present numerical results regarding the time evolution of the normalized number of predators, $\tilde{N}_1(t) = N_1(t)/N_1^{(0)}$, and prey, $\tilde{N}_2(t) = N_2(t)/N_2^{(0)}$, for the two representative sets of probabilities that characterize the non-conservative processes: $\mathcal{S}_1 = \{0.09, 0.05, 0.01; 0.15, 0.01\}$ and $\mathcal{S}_2 = \{0.25, 0.10, 0.01; 0.20, 0.01\}$. For both cases, the initial numbers of species were chosen as $N_1^{(0)} = 2880$ and $N_2^{(0)} = 3200$, corresponding to the initial densities $\rho_1^{(0)} = N_1^{(0)}/L^2 = 0.0439$ and $\rho_2^{(0)} = N_2^{(0)}/L^2 = 0.0488$, with the ratio $\rho_1^{(0)}/\rho_2^{(0)} = N_1^{(0)}/N_2^{(0)} = 0.90$. It is important to note that the time evolution of the normalized number of species $\tilde{N}_1(t)$ and $\tilde{N}_2(t)$ does not depend on the lattice size L if the initial densities $\rho_1^{(0)}$ and $\rho_2^{(0)}$ of species do not change with L [22]. However, for a lattice of fixed size L , the time evolution of $\tilde{N}_1(t)$ and $\tilde{N}_2(t)$ depends on the initial number (density) of predators $N_1^{(0)}$ and prey $N_2^{(0)}$.

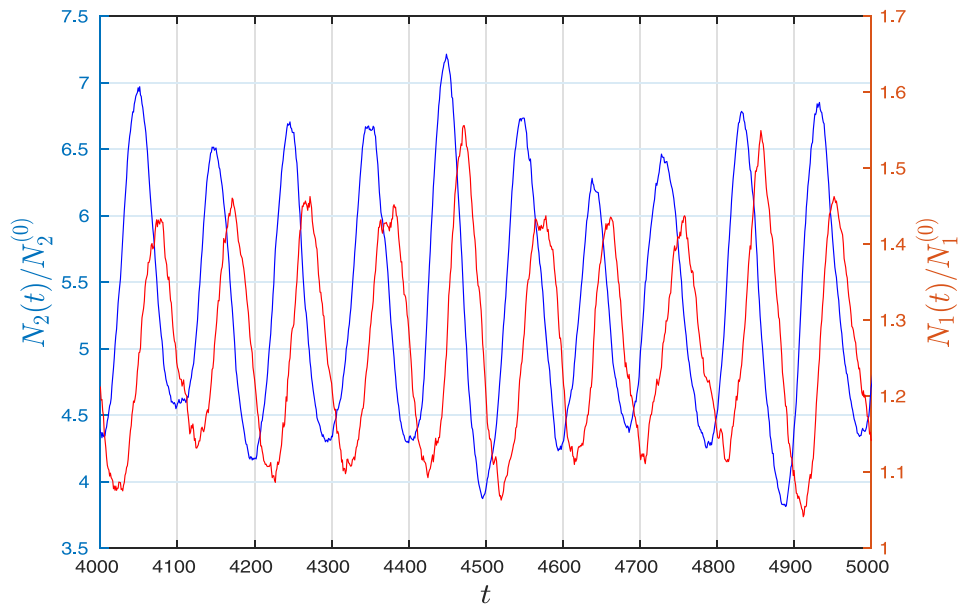
Let us compare the results for two different sets of probabilities \mathcal{S}_1 and \mathcal{S}_2 , shown in figures 1(a) and 2(a). We show that the time dependencies of the normalized number of species $\tilde{N}_1(t)$ and $\tilde{N}_2(t)$ are qualitatively similar. In the initial stage, the number of predators and prey oscillates periodically with large amplitudes, rapidly decreasing in time. After a short transient period, the system arrives at a quasi-steady state. This state corresponds to coexisting populations of predators and prey when their densities oscillate around some average values, which do not change over time.

More details about the temporal behavior of the number of predators and prey for the quasi-steady state stage of evolution, in the time range between $t_1 = 4000$ u.t. and $t_2 = 5000$ u.t. are shown in figures 1(b) and 2(b). Our model provides the usual prediction that in predator–prey cycles, the peaks in prey abundance precede the peaks in predator abundance [4]. When predators are sparse, prey increase and are in abundance. As the number of prey increases, predators also increase and are in abundance. When the predators reach sufficiently high densities, the prey population is driven down to low densities. With a lack of prey, the predator population reduces, and the cycle repeats.

It is interesting to compare the oscillatory behavior of the number of predators $\tilde{N}_1(t)$ and prey $\tilde{N}_2(t)$ in the quasi-steady state regime obtained for two different sets of probabilities, \mathcal{S}_1 and \mathcal{S}_2 , that characterize the non-conservative processes (see figures 1(b) and 2(b)). It is obvious that the change of probabilities from \mathcal{S}_1 to \mathcal{S}_2 leads to an increase in the frequency of oscillations of the number of predators and prey. We investigate the species fluctuations in further detail using a wavelet analysis, which reveals statistically significant associations between the dynamics of the predator and prey densities [47, 48]. Details of the power analysis and the phase analysis (in particular, cross-wavelet analysis and wavelet coherence (WCO)) are given in the [appendix](#).

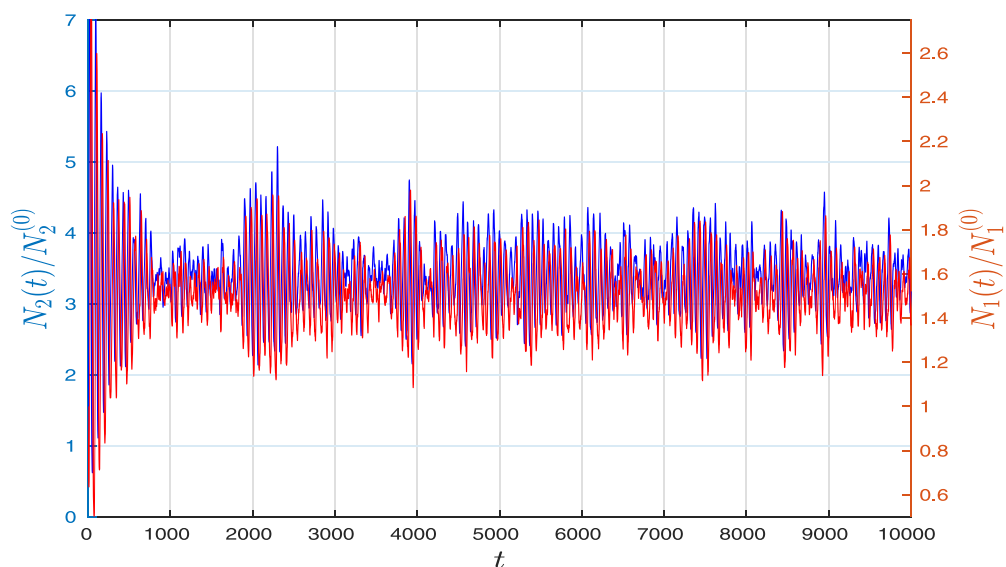


(a)

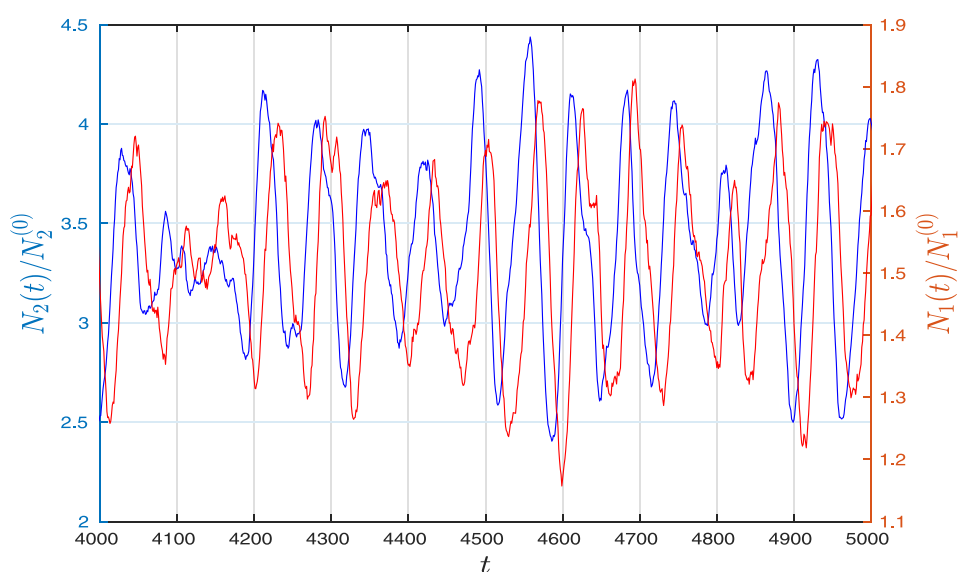


(b)

Figure 1. (a) Time dependencies of the number of the normalized number of predators $\tilde{N}_1 = N_1(t)/N_1^{(0)}$ (red lines) and prey $\tilde{N}_2 = N_2(t)/N_2^{(0)}$ (blue lines) on the lattice of size $L=256$. Initial numbers of species are chosen as $N_1^{(0)} = 2880$ and $N_2^{(0)} = 3200$. Probabilities that characterize the non-conservative processes are $\mathcal{S}_1 = \{0.09, 0.05, 0.01, 0.15, 0.01\}$. (b) Shown here are the temporal dependencies of the \tilde{N}_1 and \tilde{N}_2 in the oscillatory region of the quasi-steady state, between $t_1 = 4000$ u.t. and $t_2 = 5000$ u.t., taken from the panel (a).



(a)



(b)

Figure 2. (a) Time dependencies of the number of the normalized number of predators $\tilde{N}_1 = N_1(t)/N_1^{(0)}$ (red lines) and prey $\tilde{N}_2 = N_2(t)/N_2^{(0)}$ (blue lines) on the lattice of size $L=256$. Initial numbers of species are chosen as $N_1^{(0)} = 2880$ and $N_2^{(0)} = 3200$. Probabilities that characterize the non-conservative processes are $\mathcal{S}_2 = \{0.25, 0.10, 0.01, 0.20, 0.01\}$. (b) Shown here are the temporal dependencies of the \tilde{N}_1 and \tilde{N}_2 in the oscillatory region of the quasi-steady state, between $t_1 = 4000$ u.t. and $t_2 = 5000$ u.t., taken from the panel (a).

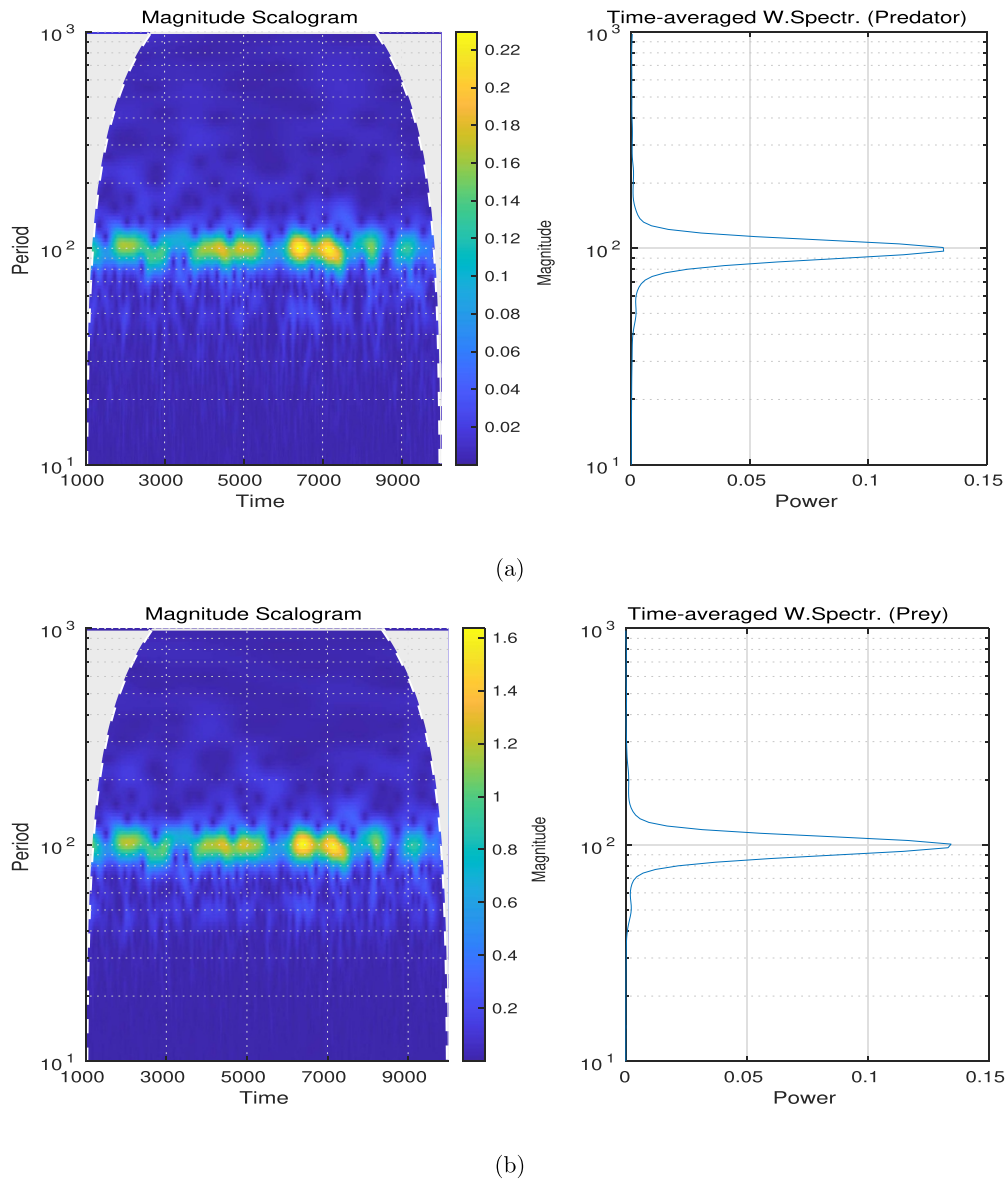


Figure 3. Scalograms and time-averaged wavelet power spectra of the predator and prey time series, $\tilde{N}_1(t)$ (a) and $\tilde{N}_2(t)$ (b) respectively, corresponding to the quasi-steady state regime of evolution ($t > 1000$ u.t.). Probabilities that characterize the non-conservative processes are $\mathcal{S}_1 = \{0.09, 0.05, 0.01, 0.15, 0.01\}$.

In figure 3, we show the scalograms and the time-averaged power spectra of the signals $\tilde{N}_1(t)$ and $\tilde{N}_2(t)$ obtained for the same conditions as in figure 1. The scalogram is the absolute value of the continuous wavelet transform (CWT) plotted as a function of time and frequency (i.e. period). Time-averaged power spectra are obtained by time-averaging the magnitude-squared scalogram over all times. The period is plotted on a logarithmic scale. The cone of influence showing where edge effects become significant is also plotted. Gray regions outside the dashed white line delineate regions where edge

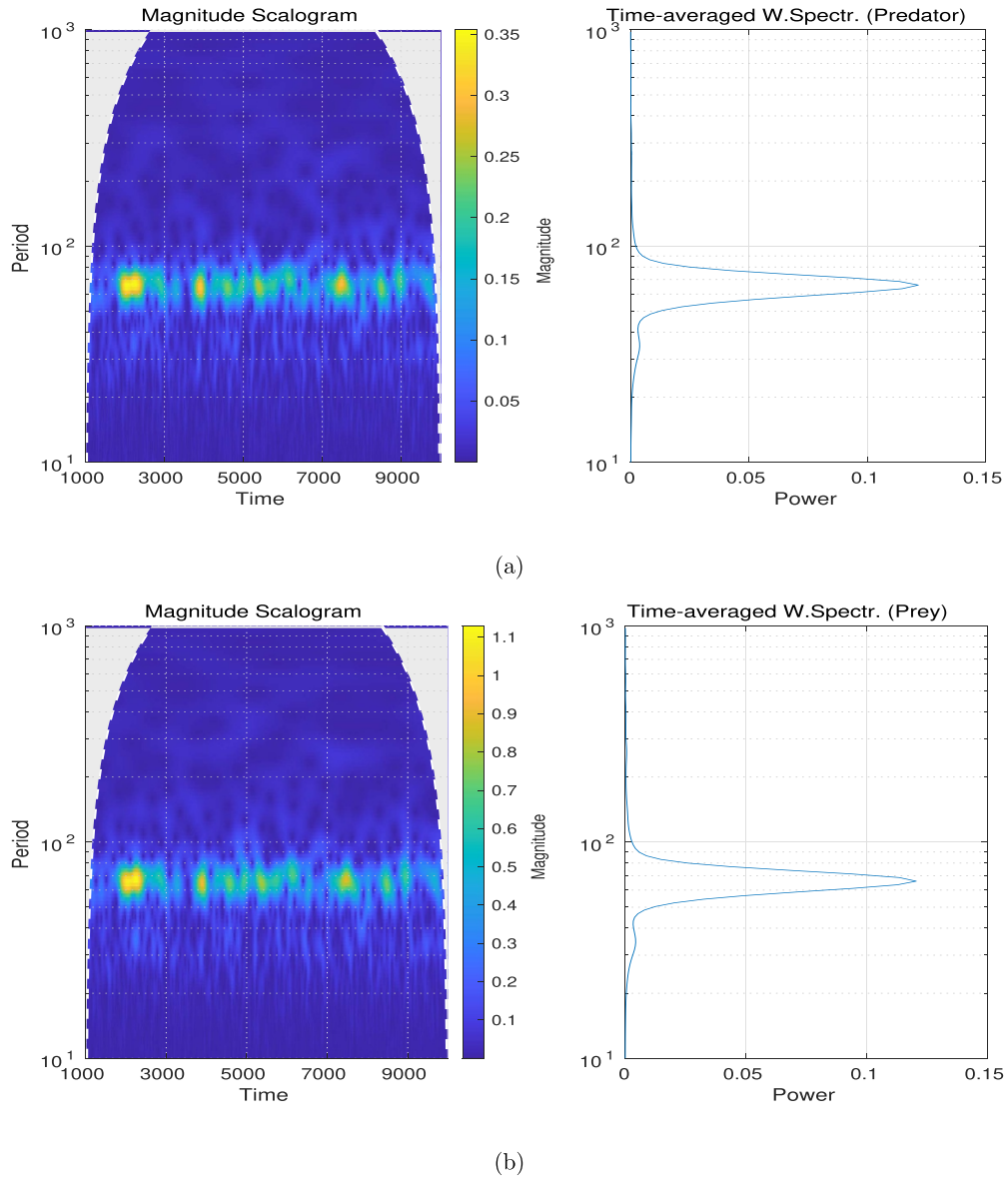


Figure 4. Scalograms and time-averaged wavelet power spectrum of the predator and prey time series, $\tilde{N}_1(t)$ (a) and $\tilde{N}_2(t)$ (b) respectively, corresponding to the quasi-steady state regime of evolution ($t > 1000$ u.t.). Probabilities that characterize the non-conservative processes are $\mathcal{S}_2 = \{0.25, 0.10, 0.01, 0.20, 0.01\}$.

effects are significant. Here, we normalize the power of the time-averaged wavelet spectrum as a probability density function. CWT gives a time-frequency representation that accurately captures the instantaneous frequencies of the signals $\tilde{N}_1(t)$ and $\tilde{N}_2(t)$. Both for predators and prey, the CWT shows nearly steady-state oscillations with the same period of about $T_1 = 97$ u.t.. This value corresponds to the position of the maximum in the time-averaged wavelet spectra (see the right-hand-side panels in figure 3).

The scalograms and the time-averaged power spectra of the signals $\tilde{N}_1(t)$ and $\tilde{N}_2(t)$ from figure 2, which correspond to the set of probabilities \mathcal{S}_2 , are presented in figure 4.

Figures 3 and 4 enable a quantitative comparison of the oscillatory behavior of the number of predators and prey for the two sets of probability values \mathcal{S}_1 and \mathcal{S}_2 that characterize the non-conservative processes. For the set \mathcal{S}_2 , numerical simulations revealed sustained oscillations with a shorter period length of $T_2 = 64$ u.t.. In the second set of parameters \mathcal{S}_2 , the probabilities P_{1b}^{fed} , P_{1d}^{unfed} and P_{2b} for the non-conservative processes related to predator feeding and prey reproduction are significantly enhanced. The predator–prey cycles are based on a feeding relationship between two species. We consider the case where the coupling between the predator and prey systems is much stronger in the case of parameters from set \mathcal{S}_2 . Consequently, the period of oscillations of species in the quasi-stationary regime corresponding to the set of parameters \mathcal{S}_2 is smaller than in the case of the set of parameters \mathcal{S}_1 .

The previously mentioned reasons for the change of the period of oscillations in species abundances are confirmed by the results of additional numerical simulations. For instance, numerical simulations have shown that increasing the probability P_{2b} is a sufficient condition for decreasing the period of oscillations. Increasing the probability P_{2b} tends to hasten the growth of the prey population. The increased food availability and better nutrition hasten the growth of the number of predators. Faster growth of the predator population shortens the time required for the number of prey to reach the maximum value. Then, the increased number of predators leads to an accelerated decrease in the prey number. The resulting lack of food shortens the time needed for the number of predators to reach a maximum value and begin to decline.

3.1.1. Coherence of the fluctuations Often the two signals are related in some way, e.g. one signal may determine behavior in another. The signals may also be correlated due to some influence intrinsic to both signals. Fourier-domain coherence is a well-established technique for measuring the linear correlation between two stationary processes as a function of frequency. Since wavelets provide local information about data in time and scale (frequency), wavelet-based coherence allows us to measure the time-varying correlation as a function of frequency. Consequently, a WCO is suitable for nonstationary processes, such as predator–prey coexistence. The WCO measures the correlations between the fluctuations of two time series (i.e. the coherence of the fluctuations). Wavelet coherency is defined as the wavelet cross-spectrum (WCS) normalized by the spectrum of each signal (see [appendix](#)).

In figure 5, we show the WCO between predators and prey obtained from the numerical data shown in figure 1(a). Color coding indicates the WCO, while arrows indicate the phase angles between the fluctuations of the two time series. The black contour lines enclose significant areas (95% significance level). The red dots show the instantaneous oscillation period $\tilde{s}(t)$ of the highest WCO within these areas (coherent oscillation regimes). To clarify the diagram, only in regions of the time-frequency (period) plane where WCO exceeds 0.85, is the phase of the WCS used to indicate the relative lag between coherent components. Note that a 1/4 cycle lag between the two signals at a particular frequency is indicated by an arrow pointing vertically down. The white dashed line shows a cone of influence where edge effects become significant at different frequencies (scales). It is evident that oscillations corresponding to the set of probabilities \mathcal{S}_1 are persistently coherent, meaning that the ups and downs of the different species in the

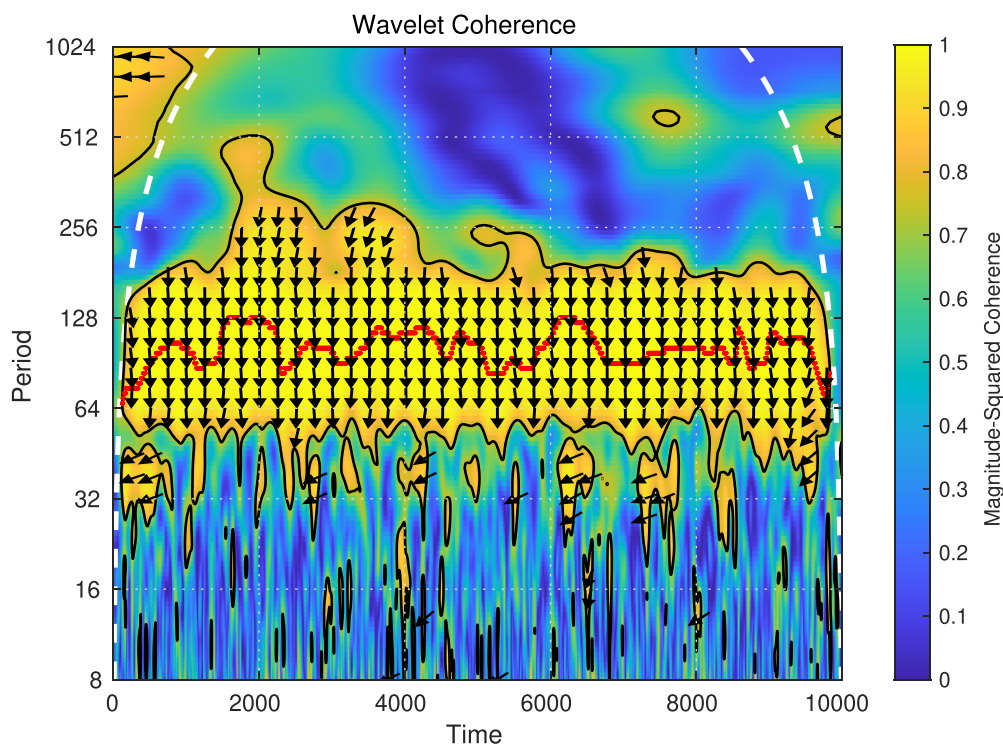


Figure 5. WCO between predators and prey, corresponding to time series $\tilde{N}_1(t)$ and $\tilde{N}_2(t)$ shown in figure 1(a). Values range from 0 (blue) to 1 (yellow). Cone of influence is indicated by the dashed white lines. Red dots indicate the instantaneous oscillation period $\tilde{s}(t)$ of the highest WCO within the prefixed period length band (64–256 u.t.). Significant areas (95% significance level) are enclosed by thin solid lines. Arrows indicate the phase angles between the fluctuations of the two species. Arrows pointing down represent a $1/4$ cycle delay between the two time series. Clockwise (counterclockwise) arrow rotation corresponds to an increase (decrease) in phase lag between them. We use the phase display threshold of 0.85, which shows phase arrows only where the coherence is greater than or equal to 0.85.

predator–prey community are indeed related to each other. For the whole quasi-state regime, we observe oscillations of period of about $T_1 = 97$ u.t. both for predators and prey, with a significantly coherent, nearly constant phase relationship. These sustained cycles are also reflected in the clockwise motion in the predator–prey phase plane. More precisely, the predator densities follow the prey densities with a phase lag of about $\pi/2$ at frequencies $1/T_1$. A quarter delay (phase angle of $\pi/2$) between the fluctuations of predator and prey species is typical for many predator–prey models (e.g. [49]).

Figure 6 shows the WCO between predators and prey obtained from the time series shown in figure 2(a). The dominant type of dynamics is characterized by regular, coherent oscillations with a nearly constant predator–prey phase difference. In fact, the two species fluctuate at a significant periodicity of $T_2 = 64$ u.t. but the arrows now indicate a phase angle noticeably smaller than $\pi/2$. These phase differences are notably constant over all different numerical simulation replicates. An increase in the probability of predator breeding P_{1b}^{fed} tends to accelerate the growth of the number of predators. The

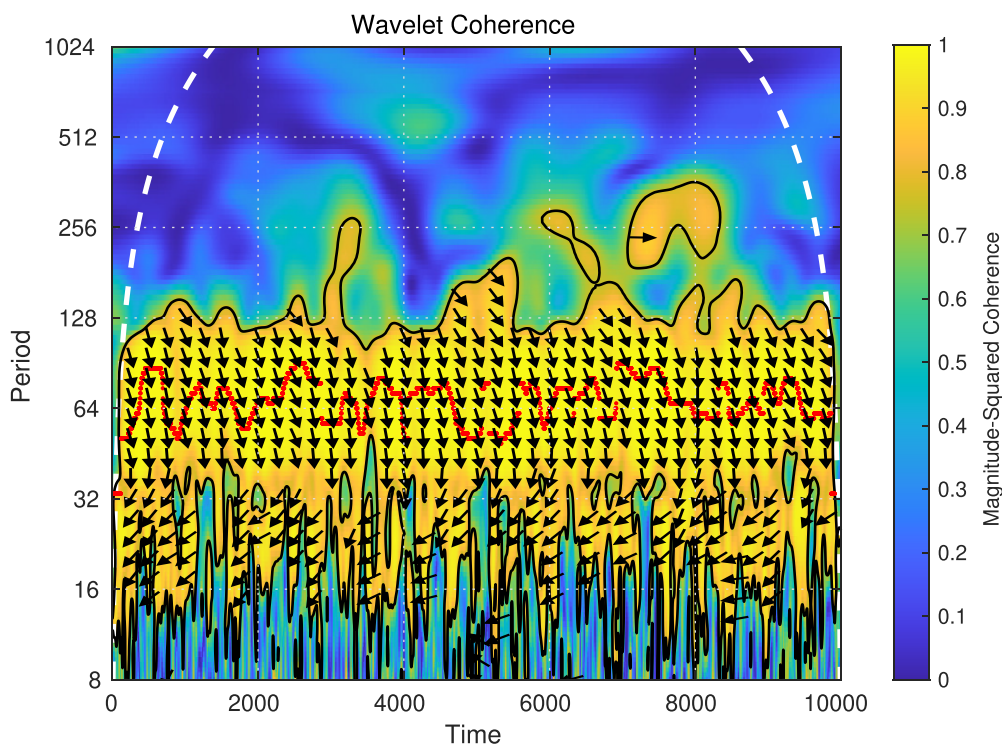


Figure 6. WCO between predators and prey, corresponding to time series $\tilde{N}_1(t)$ and $\tilde{N}_2(t)$ shown in figure 2(a). Values range from 0 (blue) to 1 (yellow). Cone of influence is indicated by the dashed white lines. Red dots indicate the instantaneous oscillation period $\tilde{s}(t)$ of the highest WCO within the prefixed period length band (32–256 u.t.). Significant areas (95% significance level) are enclosed by thin solid lines. Arrows indicate the phase angles between the fluctuations of the two species. Arrows pointing down represent a 1/4 cycle delay between the two time series. Clockwise (counterclockwise) arrow rotation corresponds to an increase (decrease) in phase lag between them. We use the phase display threshold of 0.85, which shows phase arrows only where the coherence is greater than or equal to 0.85.

faster growth of the predator population slows the growth of the number of prey. These processes shorten the time between reaching two successive maxima, i.e. the maxima for the time dependencies of predators $\tilde{N}_1(t)$ and prey $\tilde{N}_2(t)$.

3.2. Dynamics of the system with obstacles

Here, we consider in more detail the influence of the length ℓ and density ρ_0 of the linear segments that cause the obstacles on the temporal behavior of the number of predators $\tilde{N}_1(t)$ and prey $\tilde{N}_2(t)$. Simulations have been performed for linear segments (k -mers) of lengths $\ell = k - 1$, $k = 1, 2, \dots, 9$ (see, table 1), and for a wide range of obstacle densities, $\rho_0 = 0 - 0.25$, below the corresponding percolation thresholds [50, 51]. As the density of obstacles is increased above a percolation threshold p_c^* , the initial large cluster of empty lattice space breaks into tiny non-communicating components so that connectivity between both sides of the lattice disappears. In this case, spatially separated groups

of predators and prey can be formed on the lattice during the initialization process. These artificial situations will not be considered in this paper.

We begin the analysis of habitat heterogeneity's impact on predator–prey coexistence dynamics with a quantitative description of the interaction of individuals with obstacles. In our model, there is a hard-core interaction between the individuals and the obstacles. We consider that grid nodes that form the obstacles are inaccessible to predators and prey. When the obstacle is located at the place of the first neighbor, it affects the individual's decision about where to go. Accordingly, predators and prey will never choose a direction of movement towards a neighboring node where an obstacle is located. They 'see' the obstacles and 'wisely' determine the direction of their movement, following the movement rules provided in section 2.1. It is stated that prey always move towards lower predator concentration. Predators, in the absence of prey as their immediate neighbors, move towards higher prey concentration. Although collisions of individuals with obstacles (in the sense of particle collision with a wall) do not formally exist, it is necessary to quantitatively characterize their interaction with obstacles. Therefore, we count the movements of predators and prey in which at least one first neighbor is occupied by an obstacle while selecting the direction of their motion. The number of such 'encounters' between predators (prey) and obstacles per unit of time normalized to one individual, is called the collision frequency, ν .

The temporal behavior of the collisional frequencies of predators (ν_1) and prey (ν_2) for the quasi-steady state stage of evolution ($t = 4000 - 6000$) in the presence of obstacles (4-mers) are shown in figure 7. The numerical results correspond to a set of probabilities $\mathcal{S}_1 = \{0.09, 0.05, 0.01, 0.15, 0.01\}$, and two densities of 4-mers, $\rho_0 = 0.15, 0.25$. At both densities of the obstacles, the collision frequency of prey ν_2 is higher than the collision frequency of predator ν_1 . Indeed, when avoiding predators, prey move towards areas where the predator population is smaller. These areas often contain a higher concentration of obstacles. The movement of prey towards regions of higher concentration of obstacles increases the collision frequency of ν_2 . As expected, increasing the density of obstacles ρ_0 increases the collision frequencies of both species with obstacles.

In figure 8, we show the time-averaged wavelet power spectrum (WPS) of the time-series $\tilde{N}_1(t)$ and $\tilde{N}_2(t)$ obtained for the set of probabilities $\mathcal{S}_1 = \{0.09, 0.05, 0.01, 0.15, 0.01\}$, in the presence of obstacles (9-mers) at various densities $\rho_0 = 0, 0.10, 0.15, 0.20, 0.25$. It is observed that the maximum of the global WPS shifts to higher values with the increase in the density of obstacles ρ_0 . This shift indicates an increase in the mean oscillation period T of the time series $\tilde{N}_1(t)$ and $\tilde{N}_2(t)$. The period T grows from $T \approx 97$ u.t. to $T \approx 112$ u.t. when the density of obstacles ρ_0 increases from 0 to 0.25. Hence, the presence of obstacles in the habitat slightly slows down the dynamics of a group chasing and escaping between predators and prey. In addition, increasing the density of obstacles ρ_0 leads to a broadening of the peak in the global WPS. Time-averaged WPS measures the averaged variance of the time-series $\tilde{N}_1(t)$ and $\tilde{N}_2(t)$ at scale s (see appendix). Accordingly, the presence of obstacles increases the deviations of the oscillatory period T of the time-series $\tilde{N}_1(t)$ and $\tilde{N}_2(t)$ from its mean value.

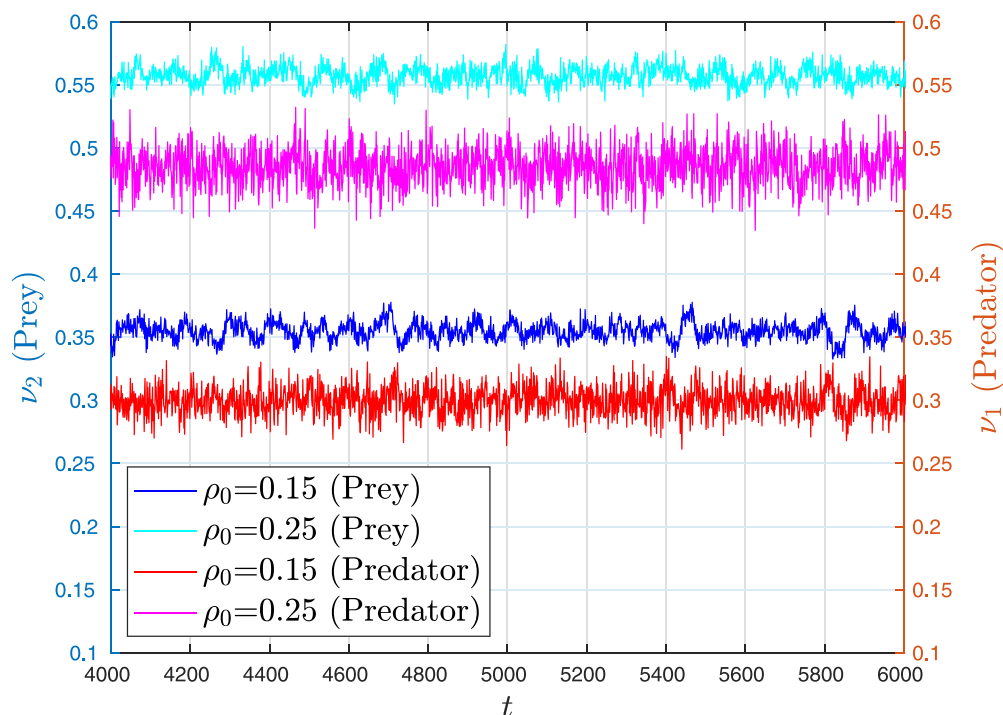


Figure 7. Collisional frequencies of predators (ν_1) and prey (ν_2) in the presence of obstacles (4-mers) at densities $\rho_0 = 0.15, 0.25$. Numerical results correspond to the set of probabilities $\mathcal{S}_1 = \{0.09, 0.05, 0.01, 0.15, 0.01\}$, and two densities $\rho_0 = 0.15, 0.25$ of 4-mers. Shown here are the temporal dependences of the ν_1 and ν_2 in the oscillatory region of the quasi-steady state, between $t_1 = 4000$ u.t. and $t_2 = 6000$ u.t..

Comparisons of the time-averaged WPS obtained for various obstacle lengths $k = 1, 2, 4, 8$ are shown in figure 9. We note that changing the length and shape of obstacles at a fixed density $\rho_0 = 0.15$ has almost no effect on the global WPS.

3.2.1. Coherence of the fluctuations In the absence of obstacles, the oscillations are persistently coherent, without the non-coherent breaks in the time-series $\tilde{N}_1(t)$ and $\tilde{N}_2(t)$ (see figures 5 and 6). In the following, we present the results of our analysis of the WCO between predators and prey obtained in the cases when the habitat is covered with obstacles at various concentrations $\rho_0 \leq 0.25$. We show that the presence of obstacles is responsible for the reversible shift from coherent to non-coherent oscillations.

In figure 10, we compare WCO for the two values of obstacle density, $\rho_0 = 0.15, 0.25$. For comparison, we show the results obtained for obstacles of very different lengths, namely, for monomers and 8-mers (table 1). The numerical results correspond to the set $\mathcal{S}_1 = \{0.09, 0.05, 0.01, 0.15, 0.01\}$ of probabilities that characterize the non-conservative processes. Thick solid lines indicate the 95% significance level. Arrows that indicate phase angles between fluctuations of the two species are only shown where the value of the WCO is greater than or equal to the threshold of 0.85. For lower density $\rho_0 = 0.15$, the dynamics can be characterized by regular oscillations in time with a nearly constant

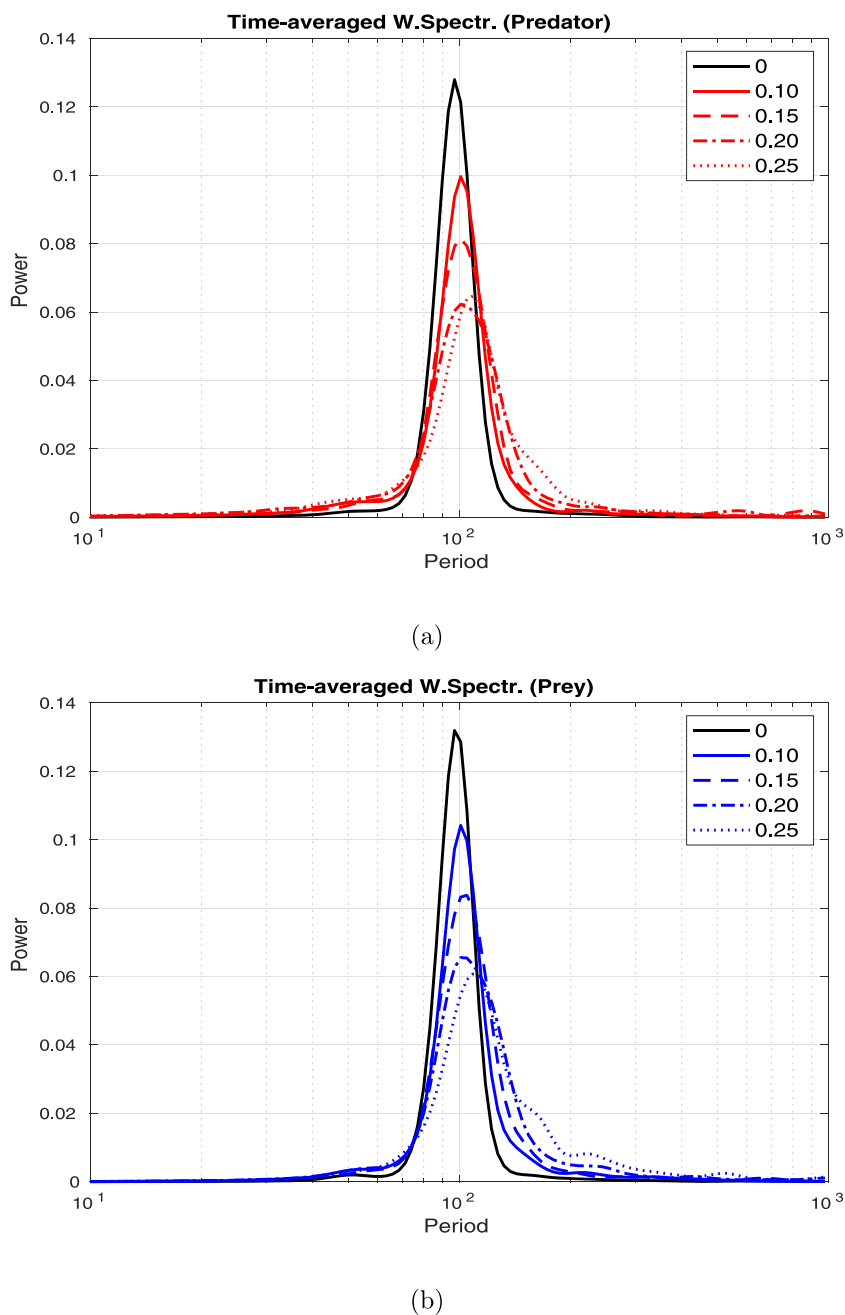
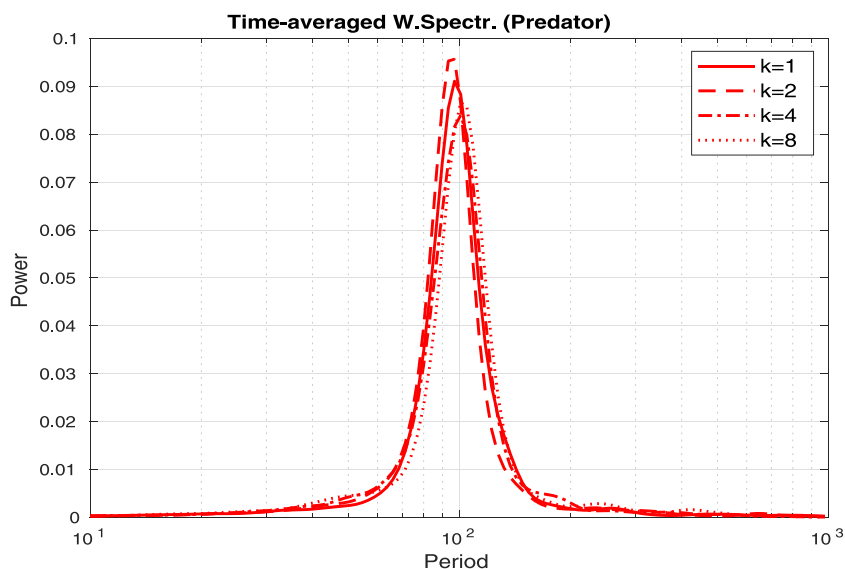
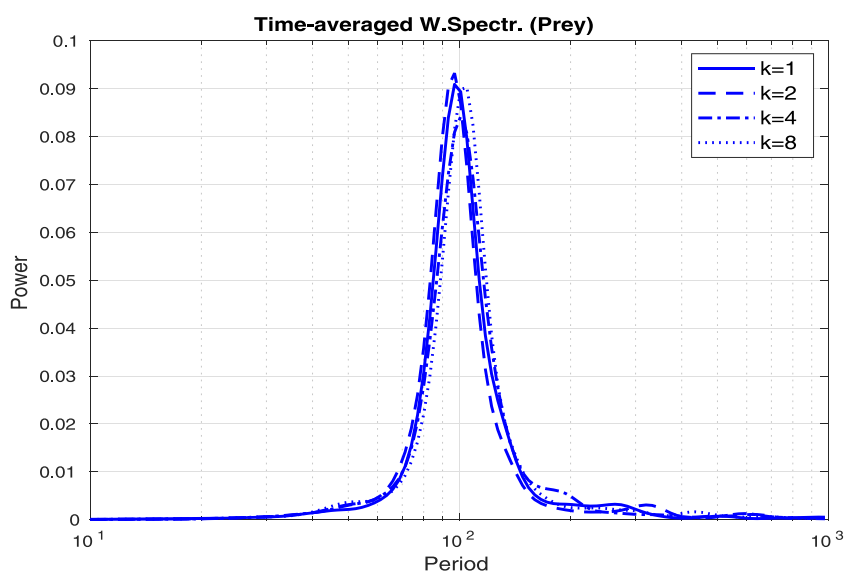


Figure 8. Time-averaged WPS of the predator and prey time-series, $\tilde{N}_1(t)$ (a) and $\tilde{N}_2(t)$ (b) respectively, obtained for 9-mers ($k = 9$) as obstacles at densities $\rho_0 = 0, 0.10, 0.15, 0.20, 0.25$. Probabilities that characterize the non-conservative processes are $\mathcal{S}_1 = \{0.09, 0.05, 0.01, 0.15, 0.01\}$.

predator–prey phase lag of about $\pi/2$ at frequencies corresponding to maximum WCO values (i.e. around $T_1 = 97$ u.t.). For higher density of obstacles $\rho_0 = 0.25$, significant regions of the time-frequency (period) plane reveals a wide distribution of different phase



(a)



(b)

Figure 9. Time-averaged WPS of the predator and prey time-series, $\tilde{N}_1(t)$ (a) and $\tilde{N}_2(t)$ (b) respectively, obtained for various k -mers ($k = 1, 2, 4, 8$) as obstacles at density $\rho_0 = 0.15$. Probabilities that characterize the non-conservative processes are $\mathcal{S}_1 = \{0.09, 0.05, 0.01, 0.15, 0.01\}$.

angles. We also note a tendency for regions with significant WCO to be decomposed into disjoint areas, especially in the case of long obstacles (see figure 10(d)).

A representative example of the occurrence of short episodes of irregular, non-coherent oscillations without any significant phase relationship induced by the presence

Consequences for predator–prey dynamics caused by the presence of obstacles

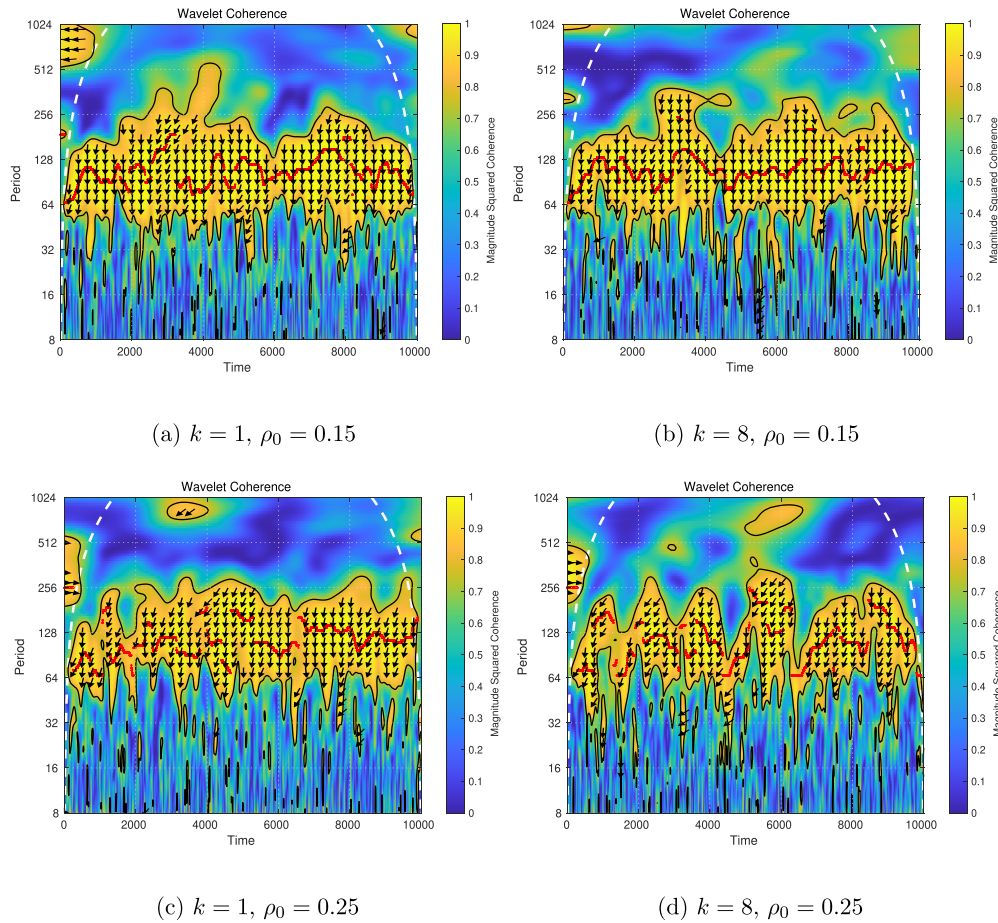


Figure 10. WCO between predators and prey, corresponding to time-series $\tilde{N}_1(t)$ and $\tilde{N}_2(t)$, obtained for monomers ($k = 1$) and 8-mers ($k = 8$) as obstacles, at two densities ρ_0 : (a) $k = 1, \rho_0 = 0.15$; (b) $k = 8, \rho_0 = 0.15$; (c) $k = 1, \rho_0 = 0.25$; (d) $k = 8, \rho_0 = 0.25$. Values range from 0 (blue) to 1 (yellow). Cone of influence is indicated by the dashed white lines. Red dots indicate the instantaneous oscillation period $\tilde{s}(t)$ of the highest WCO within the prefixed period length band (64–256 u.t.). Significant areas (95% significance level) are enclosed by thin solid lines. Arrows indicate the phase angles between the fluctuations of the two species. We use the phase display threshold of 0.85, which shows phase arrows only where the coherence is greater than or equal to 0.85.

of obstacles is given in figure 11. The numerical results correspond to the set of probabilities $\mathcal{S}_1 = \{0.09, 0.05, 0.01, 0.15, 0.01\}$ and a high density $\rho_0 = 0.25$ of 9-mers as obstacles. Figure 11(a) shows the WCO between predators and prey obtained from the time-series shown in figure 11(b). In order to make it easier to connect the results on both panels, dashed vertical lines border an arbitrarily chosen time interval $t = 4770 - 5540$ u.t.

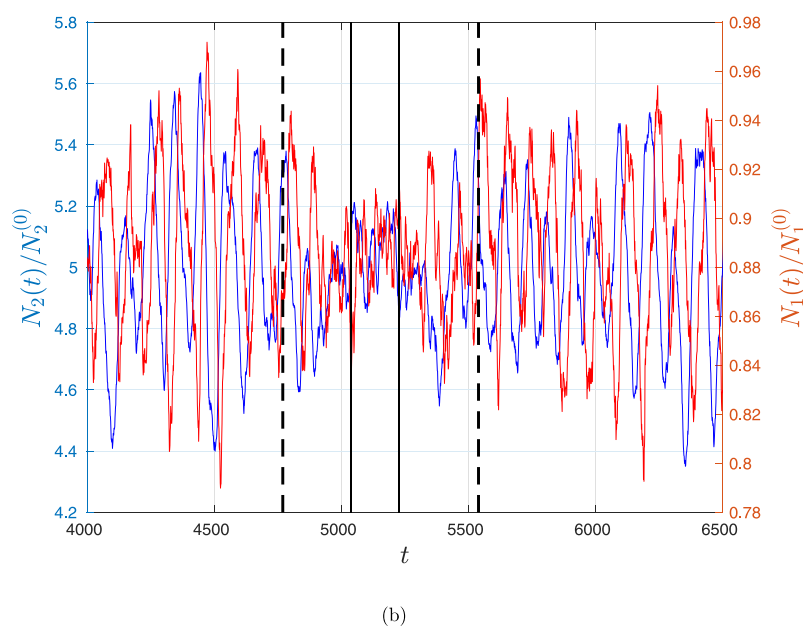
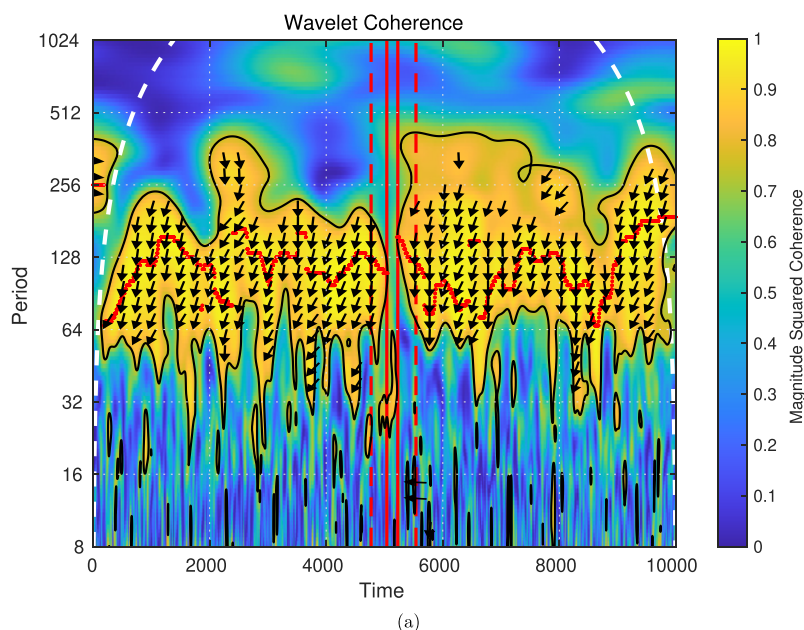


Figure 11. (a) WCO between predators and prey, corresponding to time-series $\tilde{N}_1(t)$ and $\tilde{N}_2(t)$, obtained for 9-mers ($k=9$) as obstacles, at density $\rho_0 = 0.25$. Red dots indicate the instantaneous oscillation period $\tilde{s}(t)$ of the highest WCO within the prefixed period length band (64–256 u.t.). Significant areas (95% significance level) are enclosed by thin solid lines. Arrows indicate the phase angles between the fluctuations of the two species. We use the phase display threshold of 0.85, which shows phase arrows only where the coherence is greater than or equal to 0.85. (b) Shown here are the temporal dependencies of the normalized number of predators \tilde{N}_1 (red lines) and prey \tilde{N}_2 (blue lines) in the oscillatory region of the quasi-steady state, between $t_1 = 4000$ u.t. and $t_2 = 6500$ u.t. obtained under the same conditions as in panel (a). Dashed vertical lines on both panel border a time interval $t = 4770 - 5540$ u.t. Solid vertical lines at $t_1 = 5040$ u.t. and $t_2 = 5228$ u.t. indicate the time span of irregular oscillations.

Coherent oscillation regime is a contiguous time interval for which the dominant scale $\tilde{s}(t)$ is within a statistically significant area in the time-scale plane (see [appendix](#)). The time intervals that do not meet this condition constitute the non-coherent oscillation regimes. Solid vertical lines in [figure 11](#) border a time interval without significant WCO between predator and prey. Non-coherent oscillations arise between $t_1 = 5040$ u.t. and $t_2 = 5228$ u.t. Indeed, the appearance of more irregular time-series can be observed in [figure 11\(b\)](#), in which the phase relationship between prey and predator is lost in oscillatory regions between solid vertical lines, although both populations continue to oscillate. Within significant regions of the time-frequency (period) plane, we observe that the predator density follows the prey density with a phase difference of $\Delta > \pi/2$. Dominant phase difference values $\tilde{\Delta}(t)$ (see [appendix](#)) range from 90° to $\approx 120^\circ$, with a mean value of $\langle \tilde{\Delta} \rangle = 105^\circ \pm 15^\circ$ for the entire time interval. Since the dominant scale $\tilde{s}(t)$ constitutes the line of the strongest co-oscillating component of both signals in the time-scale plane, it can be concluded that value $\langle \tilde{\Delta} \rangle = 105^\circ \pm 15^\circ$ is the dominant predator–prey phase difference that characterizes coherent regions.

In the time range between dashed vertical lines in [figure 11](#) ($\delta t = 4770 - 5540$ u.t.), we observe a reversible shift from coherent to non-coherent oscillations that are triggered by the presence of obstacles. Outside this region, oscillations with a dominant predator–prey phase difference $\langle \tilde{\Delta} \rangle \approx 105^\circ$ are established. The central part inside this region corresponds to the regime of incoherent oscillations. However, inside significant areas that are enclosed between dashed vertical lines we detect predator–prey cycles with phase shift of $\pi/2$. Here, we observe that the regime of coherent oscillations gives way to a noncoherent time-series spontaneously, but the system also shows a tendency to return to the dominant dynamical regime with a defined phase relationship. It is important to note that the regime of incoherent oscillations also appears when another parameter set, \mathcal{S}_2 , determines non-conservative processes. As in the case of parameter set \mathcal{S}_1 , decoherence of oscillations occurs if the obstacle density is sufficiently high. This is confirmation that the presence of obstacles can induce incoherent oscillations, regardless of the characteristics of the non-conservative processes.

In [figure 12](#), we show the scalograms and scale-averaged power spectra (SAWS) of the signals $\tilde{N}_1(t)$ and $\tilde{N}_2(t)$ obtained under the same conditions as in [figure 11](#). Scale-averaged WPS is obtained by scale-averaging the magnitude-squared scalogram over all scales. In fact, the SAWS is a time-series of the average variance in a certain band [[47](#)]. In the case of [figure 11](#), it is the 16–1024 u.t. band on the period scale. Thus, SAWS can be used to examine modulation of one time-series by another, or modulation of one frequency by another within the same time-series. The variance plot for predators and prey (2nd and 4th panel in [figure 12](#)) shows a distinct period between vertical lines when variance is low. Both time series show consistent changes over time. According to [figures 11](#) and [12](#), we can see that periods with low values of SAWS coincide with regions without significant WCO between predator and prey.

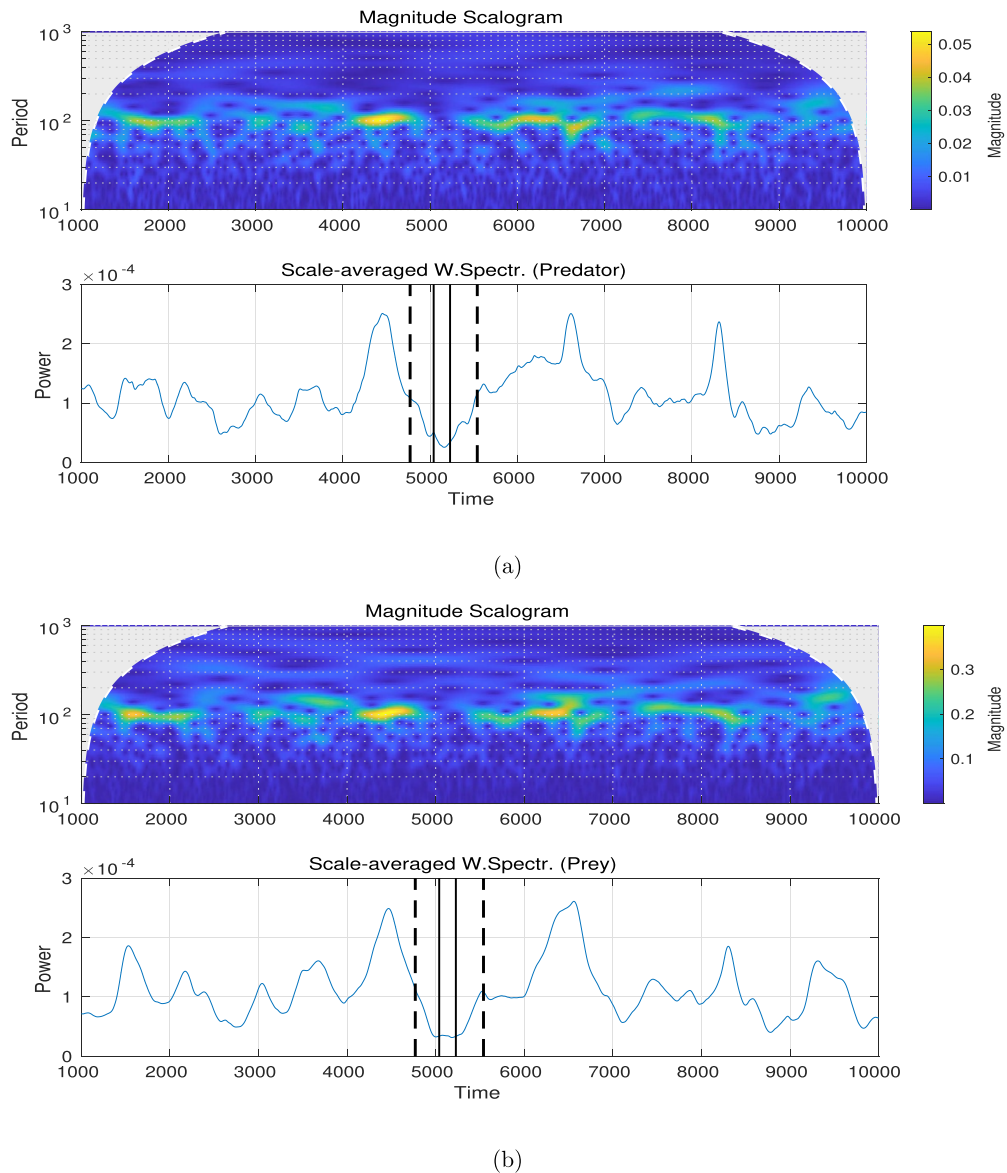


Figure 12. Scalograms and SAWS of the predator and prey time-series, $\tilde{N}_1(t)$ (a) and $\tilde{N}_2(t)$ (b) respectively, obtained for 9-mers ($k=9$) as obstacles at density $\rho_0=0.25$. Data correspond to the quasi-steady state regime of evolution ($t>1000$ u.t.). SAWS is obtained by scale-averaging the magnitude-squared scalogram over all scales. As in figure 11, dashed vertical lines on both panels border a time interval $t=4770-5540$ u.t.. Solid vertical lines at $t_1=5040$ u.t. and $t_2=5228$ u.t. indicate time span of irregular oscillations.

4. Concluding remarks

In this paper, we have developed an intuitively plausible model for understanding the impact of habitat spatial heterogeneities on the population dynamics of predator–prey

systems. We study a stochastic lattice model describing group chase and escape with sight-limited predators and prey using numerical simulations. Five probabilities that control the breeding and physiological dying of predators and prey were introduced into the model. The habitat heterogeneities are built by randomly selecting a fraction of the sites of the square lattice that are considered forbidden for the species.

In the absence of obstacles, numerical simulations reveal sustained oscillations with a nearly constant predator–prey phase difference. Numerical simulations have shown that changing the probabilities for non-conservative processes can increase or decrease the period of coherent oscillations in the abundance of species and change the relative lag between coherent components. After introducing obstacles into the model, we observe the breaks in the oscillation regimes, with random transitions between coherent and non-coherent oscillating regimes. Our model suggests that stochasticity introduced by obstacles is probably responsible for the reversible shift from coherent to non-coherent oscillations. At a sufficiently small scale, heterogeneities in the environment can decrease the ability of predators to catch prey by modifying the movement of individuals. Indeed, obstacles reduce the spatial spread of particles. By changing the trajectory of predators, obstacles increase the probability that a predator explores a place he had already gone through and previously cleared of prey. Therefore, obstacles decrease the encounter rate of the predator with prey. Furthermore, predators could lose time to handle obstacles they encounter during their search for prey. Accumulation of a high number of obstacles encountered could decrease the time available to search for prey. Consequently, the handling of obstacles could also decrease the attack rate. We consider that obstacles, at sufficiently high densities, decompose the habitat into areas of various sizes and shapes, where predators and prey are partially isolated from the rest of the habitat. The local dynamics in these areas are determined by the size and shape of these regions, due to the influence of obstacles on, for example, encounter and attack rates. Impaired communication among individuals in different habitat areas further promotes the development of different dynamics within these isolated units. In other words, the spatial separation of habitats leads to the development of local oscillatory regimes with different phase relationships. Consequently, density fluctuations of obstacles make predator–prey dynamics in different parts of the habitat very heterogeneous. This heterogeneity of the coexistence dynamics reduces or even prevents the establishment of overall oscillations with a defined phase relationship. Note that we have shown that periods with low values of SAWS coincide with short episodes of irregular, non-coherent oscillations (figure 12). If the signal of interest is contaminated by noise or interference, it can affect the wavelet analysis and result in small scale-averaged power values. Noisy signals often have components that may not contribute significantly to the overall power at each scale, leading to smaller values in the scale-averaged spectra. In general, stochasticity or external perturbations can obscure or prevent predator–prey oscillations, and our simulations suggest that stochasticity introduced by obstacles is probably responsible for the reversible shifts from coherent to more-erratic oscillations that we observe in our model.

Here, obstacles are represented by non-overlapping k -mers that are randomly placed on the lattice. It would be interesting to perform a similar investigation with obstacles of various shapes. We can introduce anisotropy in the deposition procedure for obstacle

shapes. This simple modification introduces a preferential direction in the obstacle orientations and, depending on the aspect ratio of the deposited shapes, imposes specific ‘patterning’ on the habitat. This would allow us to study the role that the spatial structure of the habitat plays in the pursuit–evasion processes.

Acknowledgments

This study was supported by the Ministry of Education, Science and Technological Development of the Republic of Serbia. Numerical simulations were run on the PARADOX supercomputing facility at the Scientific Computing Laboratory of the Institute of Physics Belgrade.

Appendix. Wavelet analysis

The wavelet transform decomposes signals over dilated and translated functions called ‘mother wavelets’ $\psi(\tau)$. Throughout our analysis, we used the Morlet wavelet $\psi(\tau) = \pi^{-1/4} \exp(i\omega_0\tau) \exp(-\tau^2/2)$. The CWT of a signal $x(t)$ is calculated as the convolution of the signal with a localized complex-valued wavelet function $\psi(\tau)$ centered at time t and dilated by the scale parameter s :

$$W_x(s, t) = \frac{1}{s^{1/2}} \int dt' x(t') \psi^* \left(\frac{t' - t}{s} \right). \quad (\text{A1})$$

Here, the asterisk denotes the complex conjugate. The wavelet coefficients, $W_x(s, t)$, represent the contribution of the scales (the s values) to the signal at different time positions (the t values).

To quantify the statistical relationship between two non-stationary signals $x(t)$ and $y(t)$, the WCS is defined as the smoothed product of the corresponding wavelet transforms:

$$W_{x,y}(s, t) = \langle W_x(s, t) W_y^*(s, t) \rangle. \quad (\text{A2})$$

Here, $\langle \dots \rangle$ denotes a smoothing operator in both scale and time. The WCS is a measure of the distribution of power of two signals. Local WPS of a signal $x(t)$ at time t and scale s is defined as $W_{x,x}(s, t) = \langle W_x(s, t) W_x^*(s, t) \rangle$. The global (time-averaged) WPS is defined as the time average of the local WPS and measures the averaged variance of the signal $x(t)$ at scale s . We use the maximum of global WPS to estimate the mean oscillation period of the signal.

WCO is defined as the amplitude of the WCS divided by the square roots of the two local WPS:

$$\text{WCO}_{x,y}(s, t) = \frac{|W_{x,y}(s, t)|}{\sqrt{W_{x,x}(s, t)} \sqrt{W_{y,y}(s, t)}}. \quad (\text{A3})$$

The WCO estimates the relationship between the two signals at time t and scale s , normalized into the range $0 \leq \text{WCO} \leq 1$.

The dominant scale $\tilde{s}(t)$ is defined for every time instance t as the scale parameter that has maximum WCO at time t over all scales in a prefixed band $[s_1, s_2]$. The statistical significance of the WCO is tested against red noise using Monte Carlo (MC) methods [52, 53]. Surrogate time series ($N = 1000$) are generated with the same first-order autoregression coefficients as the original time series. For each pair, the WCO is calculated and then the significance level is estimated for each scale from the ensemble of MC results, using a 95% significance level. As a coherent oscillation regime, we define a maximum contiguous time interval for which the dominant scale $\tilde{s}(t)$ is inside a statistically significant area (95% significance level) in the time-scale plane. Inserting dominant scale $\tilde{s}(t)$ into the WCS yields the dominant phase difference $\tilde{\Delta}(t)$ between the two signals at every time instance.

References

- [1] Lotka A J 1926 *Elements of Physical Biology (Science Progress in the Twentieth Century (1919–1933))* vol 21 (Springer) p 341
- [2] Volterra V 1928 Variations and fluctuations of the number of individuals in animal species living together *ICES J. Mar. Sci.* **3** 3
- [3] Rosenzweig M L and MacArthur R H 1963 Graphical representation and stability conditions of predator-prey interactions *Am. Nat.* **97** 209
- [4] Bulmer M 1976 The theory of prey-predator oscillations *Theor. Popul. Biol.* **9** 137
- [5] Elton C and Nicholson M 1942 The ten-year cycle in numbers of the lynx in Canada *J. Anim. Ecol.* **11** 215
- [6] Utida S 1957 Cyclic fluctuations of population density intrinsic to the host-parasite system *Ecology* **38** 442
- [7] Luckinbill L S 1974 The effects of space and enrichment on a predator-prey system *Ecology* **55** 1142
- [8] Gilg O, Hanski I and Sittler B 2003 Cyclic dynamics in a simple vertebrate predator-prey community *Science* **302** 866
- [9] Sengupta A, Kruppa T and Löwen H 2011 Chemotactic predator-prey dynamics *Phys. Rev. E* **83** 031914
- [10] Weng T, Yang H, Gu C, Zhang J, Hui P and Small M 2019 Predator-prey games on complex networks *Commun. Nonlinear Sci. Numer. Simul.* **79** 104911
- [11] Baggio J A, Salau K, Janssen M A, Schoon M L and Bodin Orjan 2010 Landscape connectivity and predator-prey population dynamics *Landscape Ecol.* (Springer) **26** 33
- [12] Stucchi L, Galeano J and Vasquez D A 2019 Pattern formation induced by intraspecific interactions in a predator-prey system *Phys. Rev. E* **100** 062414
- [13] Chakraborty D, Bhunia S and De R 2020 Survival chances of a prey swarm: how the cooperative interaction range affects the outcome *Sci. Rep.* **10** 8362
- [14] Patwardhan S, De R and Panigrahi P K 2020 Survival probability of a lazy prey on lattices and complex networks *Eur. Phys. J. E* **43** 53
- [15] Samhouri J F, Stier A C, Hennessey S M, Novak M, Halpern B S and Levin P S 2017 Rapid and direct recoveries of predators and prey through synchronized ecosystem management *Nat. Ecol. Evol.* **1** 0068
- [16] Keim J L, DeWitt P D, Wilson S F, Fitzpatrick J J, Jenni N S and Lele S R 2021 Managing animal movement conserves predator–prey dynamics *Front. Ecol. Evol.* **19** 379
- [17] Guiden P W, Bartel S L, Byer N W, Shipley A A and Orrock J L 2019 Predator–prey interactions in the anthropocene: Reconciling multiple aspects of novelty *Trends Ecol. Evol.* **34** 616
- [18] Brown J S 1988 Patch use as an indicator of habitat preference, predation risk and competition *Behav. Ecol. Sociobiol.* **22** 37
- [19] Holt R D 1984 Spatial heterogeneity, indirect interactions and the coexistence of prey species *Am. Nat.* **124** 377
- [20] Serrouya R, Seip D R, Hervieux D, McLellan B N, McNay R S, Steenweg R, Heard D C, Hebblewhite M, Gillingham M and Boutin S 2019 Saving endangered species using adaptive management *Proc. Natl Acad. Sci.* **116** 6181
- [21] Šćepanović J R, Karač A, Jakšić Z M, Budinski-Petković L and Vrhovac S B 2019 Group chase and escape in the presence of obstacles *Physica A* **525** 450

- [22] Šćepanović J, Jakšić Z, Budinski-Petković L and Vrhovac S 2021 Long-term effects of abrupt environmental perturbations in model of group chase and escape with the presence of non-conservative processes *Physica A* **580** 126156
- [23] Kamimura A and Ohira T 2010 Group chase and escape *New J. Phys.* **12** 053013
- [24] Kamimura A and Ohira T 2019 *Group Chase and Escape: Fusion of Pursuits-Escapes and Collective Motions* (Springer)
- [25] Janosov M, Virágh C, Vásárhelyi G and Vicsek T 2017 Group chasing tactics: how to catch a faster prey *New J. Phys.* **19** 053003
- [26] Nishi R, Kamimura A, Nishinari K and Ohira T 2012 Group chase and escape with conversion from targets to chasers *Physica A* **391** 337
- [27] Sato M 2012 Chasing and escaping by three groups of species *Phys. Rev. E* **85** 066102
- [28] Iwama T and Sato M 2012 Group chase and escape with some fast chasers *Phys. Rev. E* **86** 067102
- [29] Saito T, Nakamura T and Ohira T 2016 Group chase and escape model with chasers' interaction *Physica A* **447** 172
- [30] Angelani L 2012 Collective predation and escape strategies *Phys. Rev. Lett.* **109** 118104
- [31] Yang S, Jiang S, Jiang L, Li G and Han Z 2014 Aggregation increases prey survival time in group chase and escape *New J. Phys.* **16** 083006
- [32] Rozenfeld A F and Albano E V 2001 Critical and oscillatory behavior of a system of smart preys and predators *Phys. Rev. E* **63** 061907
- [33] Wang H, Han W and Yang J 2017 Group chase and escape with sight-limited chasers *Physica A* **465** 34
- [34] Travis J 2007 Do wandering albatrosses care about math? *Science* **318** 742
- [35] Pekalski A 2004 A short guide to predator-prey lattice models *Comput. Sci. Eng.* **6** 62
- [36] Rozenfeld A and Albano E 1999 Study of a lattice-gas model for a prey–predator system *Physica A* **266** 322
- [37] Boccara N, Roblin O and Roger M 1994 Automata network predator-prey model with pursuit and evasion *Phys. Rev. E* **50** 4531
- [38] Droz M and Pekalski A 2001 Coexistence in a predator-prey system *Phys. Rev. E* **63** 051909
- [39] Fussmann G F, Ellner S P, Shertzer K W and Hairston N G Jr 2000 Crossing the hopf bifurcation in a live predator-prey system *Science* **290** 1358
- [40] Benincà E, Jöhnk K D, Heerkloss R and Huisman J 2009 Coupled predator–prey oscillations in a chaotic food web *Ecol. Lett.* **12** 1367
- [41] Evans J W 1993 Random and cooperative sequential adsorption *Rev. Mod. Phys.* **65** 1281
- [42] Budinski-Petković L, Lončarević I, Dujak D, Karač A, Šćepanović J R, Jakšić Z M and Vrhovac S B 2017 Particle morphology effects in random sequential adsorption *Phys. Rev. E* **95** 022114
- [43] Luckinbill L S 1973 Coexistence in laboratory populations of paramecium aurelia and its predator didinium nasutum *Ecology* **54** 1320
- [44] Hauzy C, Tully T, Spataro T, Paul G and Arditi R 2010 Spatial heterogeneity and functional response: an experiment in microcosms with varying obstacle densities *Oecologia* **163** 625
- [45] Blasius B, Rudolf L, Weithoff G, Gaedke U and Fussmann G F 2020 Long-term cyclic persistence in an experimental predator–prey system *Nature* **577** 226
- [46] Tarasevich Y Y, Laptev V V, Vygornitskii N V and Lebovka N I 2015 Impact of defects on percolation in random sequential adsorption of linear k -mers on square lattices *Phys. Rev. E* **91** 012109
- [47] Torrence C and Compo G P 1998 A practical guide to wavelet analysis *Bull. Am. Meteorol. Soc.* **79** 61
- [48] Cazelles B, Chavez M, Berteaux D, Ménard F, Vik J O, Jenouvrier S and Stenseth N C 2008 Wavelet analysis of ecological time series *Oecologia* **156** 287
- [49] Begon M, Townsend C R and Harper J L 2006 *Ecology: From Individuals to Ecosystems* 4th edn (Blackwell Publishing)
- [50] Vandewalle N, Galam S and Kramer M 2000 A new universality for random sequential deposition of needles *Eur. Phys. J. B* **14** 407
- [51] Cornette V, Ramirez-Pastor A J and Nieto F 2003 Percolation of polyatomic species on a square lattice *Eur. Phys. J. B* **36** 391
- [52] Grinsted A, Moore J C and Jevrejeva S 2004 Application of the cross wavelet transform and wavelet coherence to geophysical time series *Nonlinear Process. Geophys.* **11** 561
- [53] Si B C 2008 Spatial scaling analyses of soil physical properties: a review of spectral and wavelet methods *Vadose Zone J.* **7** 547



Research paper

Percolation in random sequential adsorption of lattice animals on a three-dimensional cubic lattice

D. Stojiljković^{a,*}, J.R. Šćepanović^a, Z.M. Jakšić^a, Lj. Budinski-Petković^b, S.B. Vrhovac^a^a Institute of Physics Belgrade, University of Belgrade, Pregrevica 118, Belgrade 11080, Serbia^b Faculty of Technical Sciences, University of Novi Sad, Trg D. Obradovića 6, Novi Sad 21000, Serbia

ARTICLE INFO

Keywords:

Random sequential adsorption
Three-dimensional (3D) lattice
Lattice animals
Percolations

ABSTRACT

Percolation properties of the Random Sequential Adsorption (RSA) of objects of various shapes on simple three-dimensional (3D) cubic lattice are studied numerically by means of Monte Carlo simulations. Depositing objects are “lattice animals”, made of a certain number of nearest neighbor sites on a lattice. The aim of this work is to investigate the impact of the geometrical properties of the shapes on the values of percolation threshold θ_p^* . We analyzed all lattice animals of size $n \leq 5$.

Thanks to an extensive database of studied objects, we found that the number of nearest neighbors N_1 and the radius of gyration R_g of the objects are correlated with the values of percolation threshold θ_p^* . For lattice animals of the same size, the percolation threshold θ_p^* decreases with an increase in the number of the object's nearest neighbors N_1 . If objects of the same size n have the same number of nearest neighbors N_1 , their percolation threshold θ_p^* decreases with an increase in the radius of gyration R_g .

1. Introduction

A connected subgraph of a lattice is called a lattice animal. It can also be viewed as a finite set of lattice sites connected by a network of nearest neighbor bonds. In mathematics, and combinatorics in particular, terms polyominoes and polycubes are frequently used. A polyomino of size n is an edge-connected set of n squares on the square lattice \mathcal{Z}^2 (the set of integers is denoted by \mathcal{Z}). A polycube of size n is a face-connected set of n cubes in the cubic lattice \mathcal{Z}^3 . Because the square (cubic) lattice is self-dual, polyominoes (polycubes) are equivalent to lattice animals on the dual lattice.

Depending on the problem to be solved, *fixed* and *free* animals are distinguished. Fixed animals are considered distinct if they have different shapes or orientations. Free animals, on the other hand, are distinguished only by shape, not by orientation. In the mathematical literature, fixed polycubes are most discussed in the context of simple combinatorial problem — enumeration. Enumeration deals with determining the number of polycubes corresponding to a certain parameter, usually their size or perimeter [1]. It is very interesting that to this day there is no known analytic formula for calculation of the number of fixed d -dimensional polycubes of size n , $A_d(n)$, $d > 1$. The only known methods for computing $A_d(n)$ are based on explicitly or implicitly enumerating all the polyominoes or polycubes using various numerical algorithms [1–4]. Furthermore, the enumeration of lattice animals has traditionally served as a benchmark for computer performance and algorithm design [5–7].

* Corresponding author.

E-mail address: danica@ipb.ac.rs (D. Stojiljković).<https://doi.org/10.1016/j.cjph.2024.06.015>

Received 19 April 2024; Received in revised form 5 June 2024; Accepted 14 June 2024

Available online 18 June 2024

0577-9073/© 2024 The Physical Society of the Republic of China (Taiwan). Published by Elsevier B.V. All rights are reserved, including those for text and data mining, AI training, and similar technologies.

Extensive studies of lattice animals can also be found in statistical-physics literature, where fixed polycubes are usually referred to as strongly embedded lattice animals. Lattice animals play an important role in computing the mean cluster density in percolation processes [7,8]. Series expansions for the percolation probability or the average cluster size can be obtained as weighted sums over the number of lattice animals $g_{n,p}$, enumerated according to their size n and perimeter p [9]. Lattice animals have also been suggested as a model of branched polymers with excluded volume [10,11].

Recently, we have carried out extensive numerical simulations of random deposition of large collections of lattice animals and their binary mixtures on three-dimensional (3D) cubic lattices [12,13]. Random sequential adsorption (RSA) is a process in which particles of different shapes and sizes are constantly trying to attach themselves to randomly chosen places on the n -dimensional substrate [14]. If the incoming particle does not overlap any previously attached particles, it binds irreversibly. A quantity of central interest is the fraction of the substrate occupied by the deposited objects, $\theta(t)$, at time t . Because of the blocking effect by the already deposited particles, the limiting value θ_J is less than the close packing [15–17]. Due to the absence of relaxation, the formation of the limiting jammed state is governed by the infinite memory correlation effects.

In Refs. [12,13], we have found that the number of different orientations that lattice animals can take when placed on a cubic lattice exerts a decisive influence on the adsorption kinetics near the jamming limit θ_J . The results also suggested absence of correlation between the number of possible orientations of the object and the corresponding values of the jamming density θ_J . Depending on the local geometry of the objects making the mixture, the jamming coverage of a mixture θ_J^{mix} can be either greater than both single-component jamming coverages or can be in between these values. The first case is the most common, while in the second case, the jamming density of the mixture is very close to the higher jamming density for the pure component shapes.

During the RSA process, the number of deposited objects on the substrate increases so that they form clusters. A cluster is a group of occupied sites, so each site has at least one occupied nearest-neighbor site. Percolation assumes the existence of a large cluster that extends from one side to the opposite one of the system. In other words, percolation theory is based on finding the minimum coverage fraction for which a complete path of adjacent sites crossing the entire system becomes possible. This value of the fraction of the total area is named the effective percolation threshold θ_p . This transition is a geometrical phase transition where the critical concentration θ_p separates a phase of finite clusters from a phase where an infinite cluster is present. Forming long-range connectivity in disordered systems is important in many physical, chemical, and even sociological systems [18–20]. The percolation problem attracts considerable interest due to its applications in numerous practical issues, such as conductivity in composite materials, flow through porous media, polymerization, and behavior of scale-free random networks [21–26,26–33].

Numerous research papers have been published on percolations in three dimensions, which include some findings for more complex systems [34–38]. The study of irreversible deposition and percolation properties on 3D cubic lattices has mostly been focused on k -mers [39–41] and $k \times k \times l$ ($l = 1, k$) cubic objects [42,43]. Tarasevich and Cherkasova [39] have examined the percolation and jamming properties of dimers on simple 3D cubic lattices. In [41], the research of Tarasevich and Cherkasova has been extended to larger k -mers ($2 \leq k \leq 64$) to determine the relation between the jamming coverage and the size of the deposited k -mers for simple cubic lattices. The study has revealed that the ratio between the percolation threshold and the jamming coverage exhibits a nonuniversal behavior, decreasing to zero with an increase in k . These findings suggest that the percolation phase transition occurs for all values of k .

In the present study the percolation properties are analyzed for various shapes formed by connected sites on a 3D lattice. All lattice animals of size $n = 1 - 5$ (41 different shapes) are studied. Object size is the number n of nodes that a lattice animal covers on the grid. The number of examined lattice animals represents a good basis for studying the impact of the geometrical properties of the shapes on the jamming coverage θ_J and on the values of percolation threshold θ_p^* . Here, the relationship between the values of the percolation threshold θ_p^* of objects and the number of first neighbors N_1 and the gyration radius R_g of objects has been thoroughly analyzed. Random deposition of lattice animals on 3D lattices is a complex problem and it is difficult to develop even a qualitative understanding of the effects of shape on the packing density and percolation properties.

The paper is organized as follows. Section 2 describes the model and the details of the simulations. The percolation properties of lattice animals are analyzed in Section 3. Finally, Section 4 contains some additional comments.

2. Definition of the model and the simulation method

We are focusing solely on the free lattice animals on a simple cubic lattice (the term “free” is omitted in the following text). Table 1 shows all polycubes of size $n = 1, 2, 3$, and 4. Polycubes of size $n = 1, 2, 3$ are planar with a maximum of twelve different orientations (object V3). There are eight tetracubes (fourth-order polycubes), of which five are planar [44]. Polycubes are usually counted with mirror pairs (so-called chiral twins) distinguished, as would be natural for the cubical case in ordinary space. For example, a tetracube A4 and its mirror image B4 are considered distinct because there is no rigid motion that transforms one onto the other.

All polycubes of size $n = 5$ (pentacubes) are shown in Table 2. There are 29 distinct three-dimensional pentacubes [44]. As it can be seen, twelve pentacubes are flat and correspond to solid *pentominoes*. Among the nonplanar pentacubes, there are five that have at least one plane of symmetry (A5, L35, Q5, T15, T25) and each of them is its own mirror image. The remaining twelve nonplanar pentacubes form six chiral pairs: {J15, L15}, {J25, L25}, {J45, L45}, {N15, S15}, {N25, S25}, {V15, V25}. For two flats (I5, X5) of the 29 pentacubes, there are only three possible orientations. Ten pentacubes have twelve orientations and each of the remaining 17 pentacubes has 24 orientations.

As stated in Section 1, the structure of a polycube can be represented by means of a lattice animal that has a vertex for each cube and an edge for each two cubes that share a square. Several examples of lattice animals that are equivalent to corresponding

Table 1
All polycubes (x) of size $n = 1, 2, 3, 4$ and their number of orientations m .




























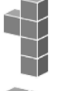













(x)	m	Shape	(x)	m	Shape
(M)	1		(I4)	3	
(D)	3		(L4)	24	
(I3)	3		(O4)	3	
(V3)	12		(P4)	8	
(A4)	12		(S4)	12	
(B4)	12		(T4)	12	

Table 2
All polycubes (x) of size $n = 5$ and their number of orientations m .

(x)	m	Shape	(x)	m	Shape	(x)	m	Shape	(x)	m	Shape
(A5)	24		(L25)	24		(S15)	24		(V25)	12	
(F5)	24		(L35)	24		(S25)	24		(W5)	12	
(I5)	3		(L45)	24		(T5)	12		(X5)	3	
(J15)	12		(N5)	24		(T15)	12		(Y5)	24	
(J25)	24		(N15)	24		(T25)	24		(Z5)	12	
(J45)	24		(N25)	24		(U5)	12				
(L5)	24		(P5)	24		(V5)	12				
(L15)	12		(Q5)	24		(V15)	12				

polycubes presented in Tables 1 and 2 are shown in Table 3. An overview of all lattice animals of size $n \leq 5$ is given in our previous works [12,13] (see, e.g. large Tables 1 and 2 in [13]). Table 4 shows the number of possible orientations m for polycubes of size $n \leq 6$ and the number of objects $A_3^m(n)$ with the specified number of orientations. Polycubes of size $n \leq 5$ can have 1, 3, 8, 12 or 24 different orientations.

The numerical algorithm used to deposit a lattice animal at randomly chosen places on the 3D substrate was already described in details in the previous papers [12,13]. Therefore, we shall present it briefly, giving the algorithm additions necessary for determining the percolation threshold.

The primary lattice animal is a group of connected sites in the cubic lattice that contains the origin $(0, 0, 0)$. We call that point the head of an object. At each Monte Carlo step, a lattice site is selected randomly. If the chosen site is unoccupied, deposition of the object is tried in one of the 24 orientations, which is chosen randomly. Then, we fix the head of the object at the selected site and search whether all necessary sites are unoccupied. If so, we occupy these sites and place the object. If the attempt fails, a new

Table 3

Several lattice animals (x) of size $n = 5$ and their number of orientations m . All lattice animals of size $n \leq 5$ are displayed in our previous works [12,13].

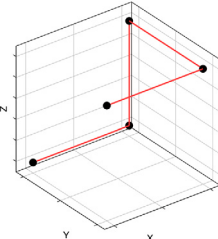
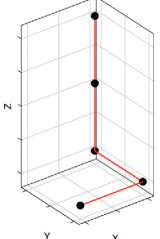
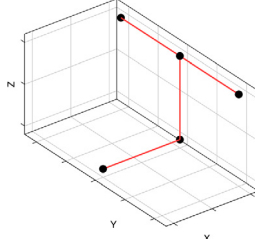
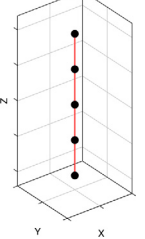
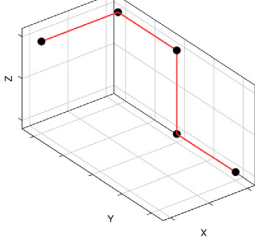
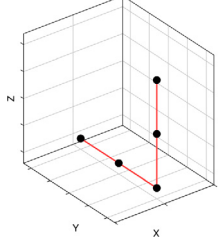
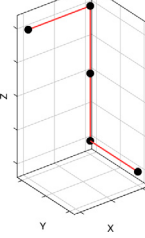
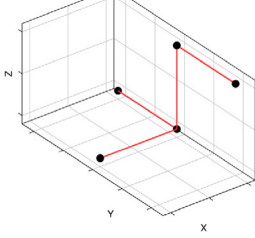
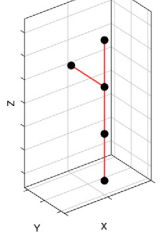
(x), m	Shape	(x), m	Shape	(x), m	Shape
(A5),24		(L45),24		(T25),24	
(I5),3		(N15),24		(V5),12	
(L15),12		(S25),24		(Y5),24	

Table 4

Shown here is the number of polycubes $A_3^m(n)$ of size n with the specified number of possible orientations $m = 1, 3, 4, 6, 8, 12, 24$. The results are shown for all polycubes of size $n \leq 6$.

	A_3^1	A_3^3	A_3^4	A_3^6	A_3^8	A_3^{12}	A_3^{24}	$N = \sum_m A_3^m$
$n = 1$	1							1
$n = 2$		1						1
$n = 3$		1				1		2
$n = 4$		2			1	4	1	8
$n = 5$		2				10	17	29
$n = 6$		1	1	3		34	127	166

site and orientation are selected randomly, and so on. The numerical algorithm that searches all possible object orientations and selects the random orientation of a lattice animal is given in the previous paper [12]. We have verified that using different heads for all examined objects gives quantitatively the same results for the temporal evolution of density $\theta(t)$ and the jamming limit θ_j .

The coverage of the surface is increased in the RSA process up to the percolation threshold, when the opposite edges of the system are connected via some path of nearest neighbor sites occupied by the particles. The tree-based union/find algorithm was used to determine the percolation threshold [45,46]. This is the most challenging and time-consuming step of the procedure. Each cluster of connected sites is stored as a separate tree, having a single “root” site. All cluster sites possess pointers to the root site, so it is simple to ascertain whether two sites are members of the same cluster. When a deposited object connects two separate clusters, they are amalgamated by adding a pointer from the root of the smaller cluster to the root of the larger one. This procedure is repeated until the percolation threshold is reached, i.e., until a single cluster connects the opposite sides of the lattice.

The Monte Carlo simulations are performed on a 3D cubic lattice of linear size up to $L_{\max} = 512$. Periodic boundary conditions are used in all directions. The data are averaged over 1024 independent runs for each investigated lattice animal. The time is counted by the number of attempts to select a lattice site and scaled by the total number of lattice sites $L^3 \approx 10\text{--}100$ million.

3. Results

Values of the percolation thresholds for the infinitely large lattice θ_p^* are obtained using the usual finite-size scaling analysis of the percolation behavior on three-dimensional lattices [47]. In such systems one assumes that the effective percolation threshold

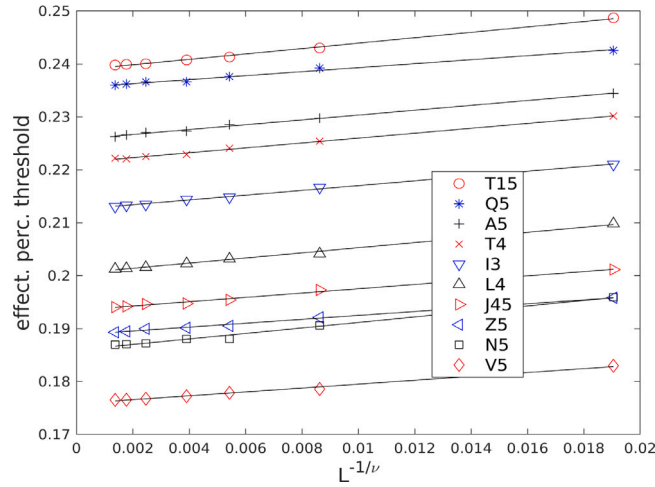


Fig. 1. Finite-size scaling of the percolation threshold θ_p against $L^{-1/\nu}$, with $\nu = 7/8$. The results are given for various lattice animals, as indicated in the legend (see, Tables 1 and 2).

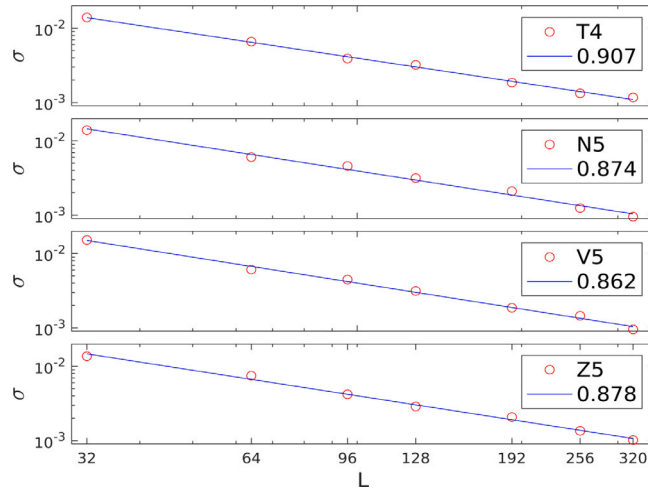


Fig. 2. Standard deviations σ of the percolation threshold on double logarithmic scale for four arbitrarily chosen lattice animals, as indicated in the legend (see, Tables 1 and 2). Straight lines correspond to the best fit according to the power law of Eq. (2) with the values of the exponent ν given on each plot.

$\theta_p(L)$ (the mean value of threshold measured for a finite lattice of linear size L) approaches the asymptotic value $\theta_p(L) \rightarrow \theta_p^*$ for $L \rightarrow \infty$ via the power law:

$$\theta_p(L) - \theta_p^* \propto L^{-1/\nu} . \tag{1}$$

Here the constant ν is the critical exponent that governs the divergence of the correlation length as $\xi \propto |\theta_p - \theta_p^*|^{-\nu}$. It should be noted that the universality class of random percolation in 3D is very well identified and the critical exponents are known, namely, $\nu = 0.8774(13) \approx 7/8$ [48,49]. The latter relationship allows us to extrapolate the threshold for an infinite system, $L \rightarrow \infty$. This kind of behavior, which is expected for systems without long-range correlations, has been observed in previous studies of percolation of extended objects on 3D lattices [40–43,49].

The effective percolation threshold $\theta_p(L)$ for each object was calculated for seven values of the linear lattice size $L = 32, 64, 96, 128, 192, 256, 320$. We plotted the mean value $\theta_p(L)$ of the threshold for various lattice sizes against $L^{-1/\nu}$ which confirmed the validity of the finite-size scaling in the system and enabled us to determine the asymptotic value of the percolation threshold θ_p^* . Finite-size scaling of the lattice threshold $\theta_p(L)$ against $L^{-1/\nu}$ for $\nu = 0.8774(13) \approx 7/8$ [48,49] is illustrated in Fig. 1 for ten arbitrarily chosen lattice animals. Values of the obtained percolation thresholds θ_p^* for all examined objects are given in Tables 5 and 6 together with the corresponding jamming coverages θ_j .

Table 5

For each lattice animal (x) of size $n = 1, 2, 3, 4$ with m possible orientations, $\theta_j^{(x)}$ and $\theta_p^*(x)$ are the jamming coverage and percolation threshold, respectively. Error estimates concerning the last digits are indicated between parentheses. Here, N_1 is the number of first neighbors and R_g is radius of gyration.

Shape (x), size n	m	N_1	R_g	$\theta_j^{(x)}$	$\theta_p^*(x)$
(M), $n = 1$	1	6	0.0000	1.0000(0)	0.3122(9)
(D), $n = 2$	3	10	0.5000	0.9184(1)	0.2566(9)
(I3), $n = 3$	3	14	0.8165	0.8390(2)	0.2125(11)
(V3), $n = 3$	12	13	0.6667	0.8788(2)	0.2396(10)
(A4), $n = 4$	12	16	0.7906	0.8178(2)	0.2260(11)
(B4), $n = 4$	12	16	0.7906	0.8178(2)	0.2260(11)
(I4), $n = 4$	3	18	1.1180	0.7808(3)	0.1801(11)
(L4), $n = 4$	24	17	0.9354	0.8339(2)	0.2004(11)
(O4), $n = 4$	3	16	0.7071	0.8079(3)	0.2419(12)
(P4), $n = 4$	8	15	0.7500	0.7941(3)	0.2414(12)
(S4), $n = 4$	12	16	0.8660	0.8149(2)	0.2206(11)
(T4), $n = 4$	12	16	0.8292	0.8114(3)	0.2214(12)

Table 6

For each lattice animal (x) of size $n = 5$ with m possible orientations, $\theta_j^{(x)}$ and $\theta_p^*(x)$ are the jamming coverage and percolation threshold, respectively. Error estimates concerning the last digits are indicated between parentheses. Here, N_1 is the number of first neighbors and R_g is the radius of gyration.

Shape (x)	m	N_1	R_g	$\theta_j^{(x)}$	$\theta_p^*(x)$
(A5)	24	18	0.8485	0.7716(2)	0.2258(11)
(F5)	24	19	0.9798	0.7860(3)	0.2069(10)
(I5)	3	22	1.4142	0.7369(4)	0.1555(10)
(J15)	12	20	1.0583	0.7635(2)	0.1899(11)
(J25)	24	19	0.9381	0.7839(2)	0.2092(11)
(J45)	24	20	1.0198	0.7958(3)	0.1934(11)
(L5)	24	21	1.2329	0.7695(3)	0.1715(11)
(L15)	12	20	1.0583	0.7635(3)	0.1899(11)
(L25)	24	19	0.9381	0.7839(2)	0.2092(11)
(L35)	24	19	0.9798	0.7774(3)	0.2026(11)
(L45)	24	20	1.0198	0.7957(2)	0.1934(11)
(N5)	24	20	1.1314	0.7866(3)	0.1860(9)
(N15)	24	19	0.9798	0.7842(2)	0.2079(13)
(N25)	24	18	0.8944	0.7790(3)	0.2243(11)
(P5)	24	19	0.8944	0.8017(3)	0.2201(13)
(Q5)	24	18	0.8000	0.7826(3)	0.2355(11)
(S15)	24	19	0.9798	0.7841(2)	0.2079(13)
(S25)	24	18	0.8944	0.7790(3)	0.2243(11)
(T5)	12	20	1.0198	0.7500(3)	0.1899(11)
(T15)	12	17	0.8485	0.7582(3)	0.2388(11)
(T25)	24	19	0.8944	0.7863(2)	0.2136(12)
(U5)	12	20	1.0198	0.7611(3)	0.1939(10)
(V5)	12	21	1.1314	0.7628(3)	0.1758(9)
(V15)	12	19	0.9381	0.7647(3)	0.2130(11)
(V25)	12	19	0.9381	0.7647(3)	0.2130(11)
(W5)	12	19	1.0583	0.7615(3)	0.2033(12)
(X5)	3	18	0.8944	0.7007(3)	0.2273(12)
(Y5)	24	20	1.0954	0.7595(3)	0.1877(13)
(Z5)	12	20	1.0954	0.7643(2)	0.1888(10)

According to the scaling theory, the standard deviation σ of the percolation threshold measured for a finite lattice L satisfies the power law:

$$\sigma \propto L^{-1/\nu} \tag{2}$$

In Fig. 2 the standard deviation σ vs. L is shown on a double logarithmic scale for several arbitrarily chosen lattice animals. For all lattice animals we confirmed the power law of Eq. (2) with the mean value of the exponent $\nu = 0.882 \pm 0.022$. Therefore, these results are in good agreement with the universal value $\nu \approx 7/8$ [48,49].

Upon examining the percolation threshold values θ_p^* for all objects of size $n \leq 5$ (see, Tables 5 and 6), we concluded that the number of object orientations m is not correlated with the values of θ_p^* . The coverage kinetics is known to be slowed down with the increase in the number of possible placements m of the shape [12]. However, it is not difficult to notice some other geometric properties of the deposited shapes that affect their percolation properties. Each lattice shape is surrounded by the first neighboring sites on the lattice. The obtained results show that the number of an object’s nearest neighbor sites N_1 significantly influences its percolation characteristics. For instance, when considering objects of size $n = 4$, object I4 has the highest number of first neighbors

($N_1 = 18$) and the lowest percolation threshold value ($\theta_p^* = 0.1801(11)$). Object I5, which is a shape of size $n = 5$, has the highest number of first neighbors ($N_1 = 22$) and hence corresponds to the smallest value of the percolation threshold ($\theta_p^* = 0.1555(10)$). Objects L5 and V5 have slightly higher percolation thresholds because they have one less first neighbor than object I5. All other objects of size 5 have fewer first neighbors ($N_1 \leq 20$) and, hence, higher percolation threshold values. Qualitatively, we can say that the value of θ_p^* depends on the object's capability to make connections with other depositing objects. The number of nearest neighbors N_1 seems to be a quantity closely related to the connectivity. Indeed, we observe that the object T15, with the largest threshold ($\theta_p^* = 0.2388(11)$), has the smallest number N_1 of the first neighboring sites on the lattice, i.e. $N_1 = 17$.

From Tables 5 and 6, it can be seen that there are objects of the same size n , with the same number of first neighbors N_1 , whose percolation thresholds θ_p^* differ significantly. The geometric characteristic of the objects that can be related to these changes in the percolation properties of the objects is the radius of gyration R_g . The radius of gyration is defined as the root-mean-square average of the distance of all lattice nodes occupied by the object from the center of mass of the object. Actually, the radius of gyration R_g of a lattice animal of size n that fills the nodes of the grid with coordinates $\{\vec{r}_i\} = \{(x_i, y_i, z_i)\}, i = 1, \dots, n$ is given by the expression

$$R_g = \left[\frac{1}{n} \sum_{i=1}^n s_i^2 \right]^{1/2}, \tag{3}$$

where

$$s_i^2 = (x_i - x_c)^2 + (y_i - y_c)^2 + (z_i - z_c)^2, \tag{4}$$

and

$$x_c = \frac{1}{n} \sum_{i=1}^n x_i, \quad y_c = \frac{1}{n} \sum_{i=1}^n y_i, \quad z_c = \frac{1}{n} \sum_{i=1}^n z_i. \tag{5}$$

For two lattice animals having the same size, the one with the larger radius of gyration is the more extended or less spherical one. If the value of R_g is small, then we can say the object is relatively compact.

In Figs. 3(a) and 4(a), the dependence of the percolation threshold θ_p^* on the radius of gyration R_g is shown for all lattice animals with a size of $n \leq 5$. Figs. 3(b) and 4(b) are included for a simpler insight into the number of nearest neighbors N_1 for each studied object. Due to the greater diversity of lattice animals of size of $n = 5$, let us first analyze the results shown in Fig. 4. It is clear that for lattice animals of the same size, the percolation threshold decreases with an increase in the number of the object's nearest neighbors. Indeed, the values of the percolation threshold θ_p^* for objects with $N_1 = 18$ first neighbors are in the range of $0.223 \lesssim \theta_p^* \lesssim 0.236$. For objects with a greater number of neighbors, the range of the percolation threshold values shifts towards lower values. Thus, for $N_1 = 19$, the percolation threshold is in the range of $0.201 \lesssim \theta_p^* \lesssim 0.221$, for $N_1 = 20$, it is $0.186 \lesssim \theta_p^* \lesssim 0.194$, and for $N_1 = 21$, the range is of $0.170 \lesssim \theta_p^* \lesssim 0.175$. Objects with $N_1 = 17$ and $N_1 = 22$ first neighbors have the highest and lowest percolation threshold values, respectively. Qualitatively the same correlation between the percolation threshold values and the number of first neighbors of objects of size $n < 5$ can be seen in Fig. 3.

If objects of the same size n have the same number of nearest neighbors N_1 , their percolation threshold θ_p^* decreases with an increase in the radius of gyration R_g (see, Figs. 3 and 4). The radius of gyration R_g can be considered as a measure of the compactness of an object. More compact objects have smaller linear dimensions along the lattice directions. For example, objects A5 and I5 are of the same size $n = 5$ (see, Table 3), while their radii of gyration differ significantly. Object I5 is elongated and has a large radius of gyration ($R_g = 1.4142$). Object A5 is compact and rounded, so its radius of gyration is considerably smaller ($R_g = 0.8485$). Compact objects cover space more efficiently and have a lower connecting probability. Compact objects tend to form dense, isolated islands on the lattice. Then, the connectivity in the system is poor at low densities, and percolation sets in at larger density values. This suggests that, for various objects of the same size, the percolation threshold θ_p^* of more compact and rounded shapes (smaller R_g) exceeds the θ_p^* of the elongated ones (larger R_g).

4. Concluding remarks

Our previous work [32] investigated percolation and jamming phenomena for random sequential deposition of objects of various shapes and sizes on a two dimensional (2D) triangular lattice. Self-avoiding lattice steps made the shapes. It has been shown that for various planar objects of the same length, the percolation threshold θ_p^* of more compact shapes (hexagons, triangles) exceeds the θ_p^* of elongated ones (line segments, angled objects). The present study reached similar conclusions by examining a significantly broader class of objects, lattice animals in three dimensions. A systematic approach is made by examining a wide variety of object shapes.

Our results suggest that for lattice animals of the same size:

- (i) the percolation threshold θ_p^* decreases with an increase in the number of the object's nearest neighbors N_1 ;
- (ii) The percolation threshold θ_p^* for compact and rounded objects is higher than for elongated ones. This behavior of the percolation threshold value is consistent with the size of the radius of gyration R_g of the lattice animal. If two objects are of the same size and have the same number of nearest neighbors N_1 , the object with the larger radius of gyration R_g is less compact or more extended. Therefore, as the object's radius of gyration R_g increases, the percolation threshold value θ_p^* decreases.

It is important to emphasize that there are lattice animals of the same size $n = 5$, which have an equal number of nearest neighbors N_1 and the same R_g value, but their percolation thresholds differ slightly (see, Fig. 4). Examples of such shapes are objects P5 and T25, or F5 and L35. We have not been able to identify any other geometric characteristic of the shape that would

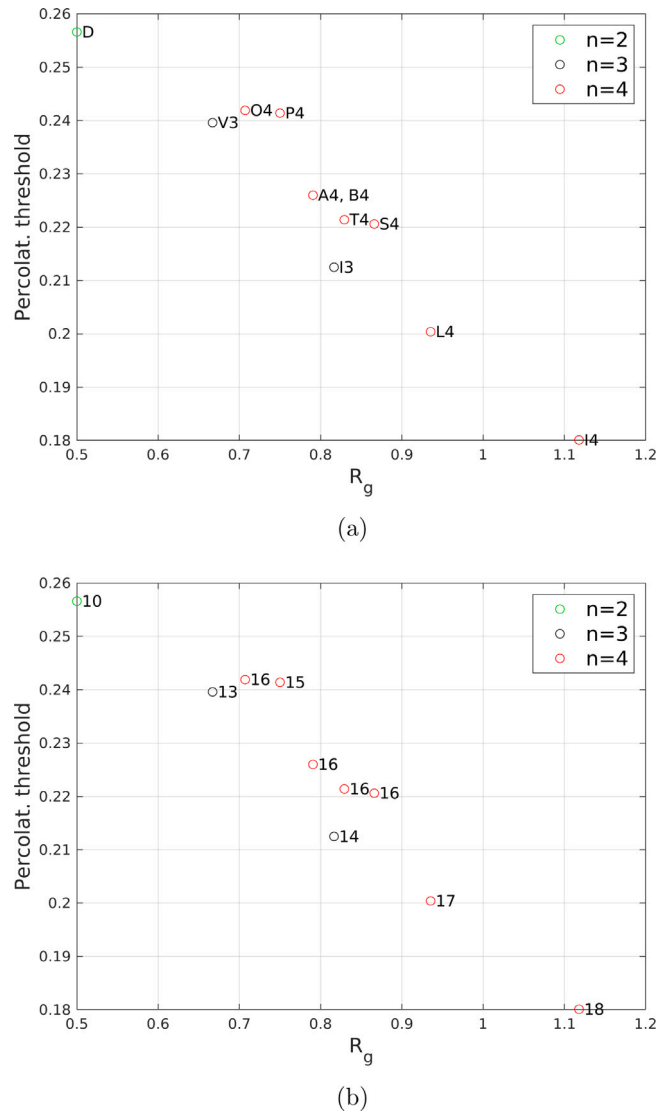
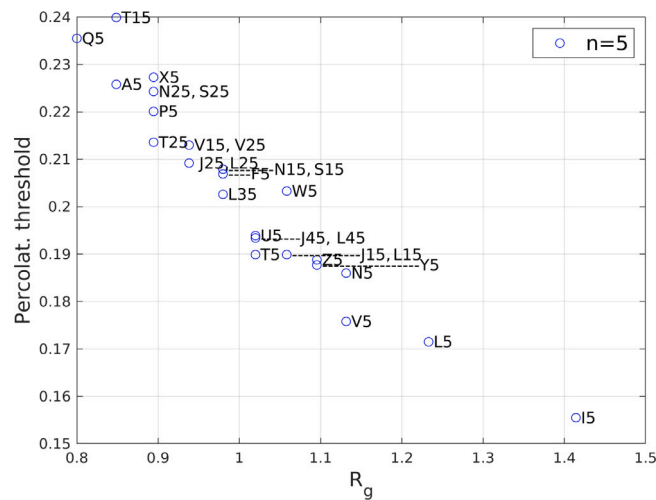


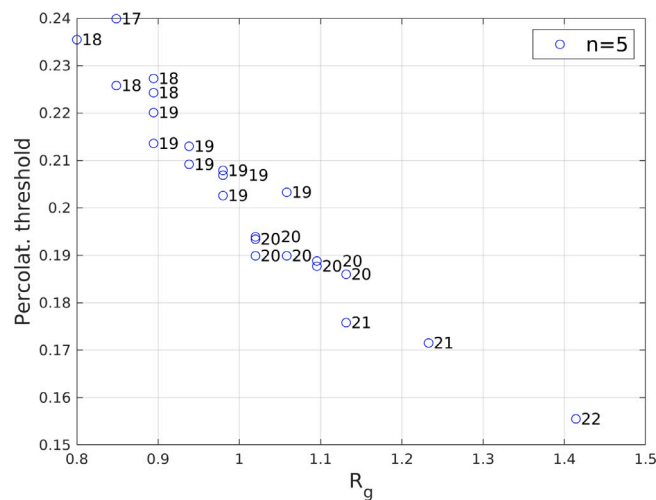
Fig. 3. Dependence of the percolation threshold θ_p^* on the radius of gyration R_g (Eq. (3)) for all lattice animals of size $n = 2, 3, 4$, as indicated in the legend. Both panels display the same results. On the right side of each symbol (circle), the name of the corresponding object (panel (a)) and the number of its first neighbors N_1 (panel (b)) are listed. Next to the symbols corresponding to chiral pairs, the names of both objects are listed. For θ_p^* the error bars do not exceed the size of the symbols.

correlate with this variation in the percolation threshold. In most cases, objects with greater anisotropy have a lower percolation threshold. A more detailed analysis of additional geometric characteristics of the shapes will be the subject of future work.

The model considered here is highly idealized and is not intended to reproduce a particular experimentally studied system. However, this work aims to encourage the development of more advanced models that can reproduce concrete experimental systems. Specifically, percolation theory has been successfully used to study the well-known sol–gel transition [50], in which the percolation threshold determines the point at which a system shifts from a liquid to a gel state. This transition is governed by the ability of molecules to form a network that traps solvent molecules, creating a semi-solid structure. It is well known that the shape of a molecule affects the gelation process by influencing how molecules interact, the number and strength of contact points, their conformational flexibility, and the nature of their self-assembly [51–55]. These factors collectively determine the efficiency and stability of the gel network formed. Examining these points requires a systematic approach using a wide variety of extended objects on a 3D lattice. Accordingly, the percolation of various shapes on 3D lattice could be an interesting topic for further research that will provide a better description of the gelation process.



(a)



(b)

Fig. 4. Dependence of the percolation threshold θ_p^* on the radius of gyration R_g (Eq. (3)) for all lattice animals of size $n = 5$. Both panels display the same results. On the right side of each symbol (circle), the name of the corresponding object (panel (a)) and the number of its first neighbors N_1 (panel (b)) are listed. Next to the symbols corresponding to chiral pairs, the names of both objects are listed. For θ_p^* the error bars do not exceed the size of the symbols.

CRedit authorship contribution statement

D. Stojiljković: Writing – review & editing, Validation, Software, Data curation. **J.R. Šćepanović:** Visualization, Formal analysis. **Z.M. Jakšić:** Writing – review & editing, Validation, Resources, Formal analysis, Data curation. **Lj. Budinski-Petković:** Writing – review & editing, Validation. **S.B. Vrhovac:** Writing – review & editing, Writing – original draft, Visualization, Supervision, Software, Project administration, Methodology, Funding acquisition, Formal analysis, Data curation, Conceptualization.

Declaration of competing interest

The authors declare that they have no known competing financial interests or personal relationships that could have appeared to influence the work reported in this paper.

Acknowledgments

This work was supported by the Ministry of Science, Technological Development and Innovation of the Republic of Serbia. Numerical computations were performed on the PARADOX-IV supercomputing facility at the Scientific Computing Laboratory, National Center of Excellence for the Study of Complex Systems, Institute of Physics Belgrade.

References

- [1] W.F. Lunnon, Counting polyominoes, in: A.O.L. Atkin, B.J. Birch (Eds.), *Computers in Number Theory*, Academic Press, 1971, pp. 347–372.
- [2] D.S. Gaunt, M.F. Sykes, H. Ruskin, Percolation processes in D-dimensions, *J. Phys. A: Math. Gen.* 9 (1976) 1899, <http://dx.doi.org/10.1088/0305-4470/9/11/015>.
- [3] G. Aleksandrowicz, G. Barequet, Counting polycubes without the dimensionality curse, *Discrete Math.* 309 (2009) 4576, <http://dx.doi.org/10.1016/j.disc.2009.02.023>.
- [4] I. Jensen, Enumerations of lattice animals and trees, *J. Stat. Phys.* 102 (2001) 865, <http://dx.doi.org/10.1023/A:1004855020556>.
- [5] D.H. Redelmeier, Counting polyominoes: Yet another attack, *Discrete Math.* 36 (1981) 191, [http://dx.doi.org/10.1016/0012-365X\(81\)90237-5](http://dx.doi.org/10.1016/0012-365X(81)90237-5).
- [6] S. Mertens, M.E. Lautenbacher, Counting lattice animals: A parallel attack, *J. Stat. Phys.* 66 (1992) 669–678, <http://dx.doi.org/10.1007/bf01060088>.
- [7] A.R. Conway, A.J. Guttmann, On two-dimensional percolation, *J. Phys. A: Math. Gen.* 28 (1995) 891, <http://dx.doi.org/10.1088/0305-4470/28/4/015>.
- [8] A.B. Harris, T.C. Lubensky, Connection between percolation and lattice animals, *Phys. Rev. B* 23 (1981) 3591, <http://dx.doi.org/10.1103/PhysRevB.23.3591>.
- [9] M.F. Sykes, M. Glen, Percolation processes in two dimensions. I. Low-density series expansions, *J. Phys. A: Math. Gen.* 9 (1976) 87, <http://dx.doi.org/10.1088/0305-4470/9/1/014>.
- [10] T.C. Lubensky, J. Isaacson, Statistics of lattice animals and dilute branched polymers, *Phys. Rev. A* 20 (1979) 2130, <http://dx.doi.org/10.1103/PhysRevA.20.2130>.
- [11] S. Flesia, D.S. Gaunt, C.E. Soteros, S.G. Whittington, Statistics of collapsing lattice animals, *J. Phys. A: Math. Gen.* 27 (1994) 5831, <http://dx.doi.org/10.1088/0305-4470/27/17/016>.
- [12] I. Lončarević, L. Budinski-Petković, J.R. Šćepanović, Z.M. Jakšić, S.B. Vrhovac, Random sequential adsorption of lattice animals on a three-dimensional cubic lattice, *Phys. Rev. E* 101 (2020) 012119, <http://dx.doi.org/10.1103/PhysRevE.101.012119>.
- [13] M. Beljin-Čavić, I. Lončarević, L. Budinski-Petković, Z.M. Jakšić, S.B. Vrhovac, Simulation study of random sequential deposition of binary mixtures of lattice animals on a three-dimensional cubic lattice, *J. Stat. Mech. Theory Exp.* 2022 (2022) 053206, <http://dx.doi.org/10.1088/1742-5468/ac68dd>.
- [14] J.W. Evans, Random and cooperative sequential adsorption, *Rev. Modern Phys.* 65 (1993) 1281, <http://dx.doi.org/10.1103/RevModPhys.65.1281>.
- [15] S.S. Manna, N.M. Švrakić, Random sequential adsorption: line segments on the square lattice, *J. Phys. A: Math. Gen.* 24 (1991) L671, <http://dx.doi.org/10.1088/0305-4470/24/12/003>.
- [16] J. Talbot, G. Tarjus, P. Van Tassel, P. Viot, From car parking to protein adsorption: an overview of sequential adsorption processes, *Colloids Surf. A* 165 (2000) 287, [http://dx.doi.org/10.1016/S0927-7757\(99\)00409-4](http://dx.doi.org/10.1016/S0927-7757(99)00409-4).
- [17] L. Budinski-Petković, I. Lončarević, D. Dujak, A. Karač, J.R. Šćepanović, Z.M. Jakšić, S.B. Vrhovac, Particle morphology effects in random sequential adsorption, *Phys. Rev. E* 95 (2017) 022114, <http://dx.doi.org/10.1103/PhysRevE.95.022114>.
- [18] M. Sahimi, G. Hunt (Eds.), *Complex media and percolation theory*, in: *Encyclopedia of Complexity and Systems Science Series*, Springer New York, NY, 2021, <http://dx.doi.org/10.1007/978-1-0716-1457-0>.
- [19] M. Sahimi, *Applications of percolation theory*, in: *Applied Mathematical Sciences*, second ed., Springer International Publishing, 2023.
- [20] M.E.J. Newman, D.J. Watts, Scaling and percolation in the small-world network model, *Phys. Rev. E* 60 (1999) 7332, <http://dx.doi.org/10.1103/PhysRevE.60.7332>.
- [21] G. Kondrat, A. Pękalski, Percolation and jamming in random sequential adsorption of linear segments on a square lattice, *Phys. Rev. E* 63 (2001) 051108, <http://dx.doi.org/10.1103/PhysRevE.63.051108>.
- [22] F. Rampf, E.V. Albano, Interplay between jamming and percolation upon random sequential adsorption of competing dimers and monomers, *Phys. Rev. E* 66 (2002) 061106, <http://dx.doi.org/10.1103/PhysRevE.66.061106>.
- [23] G. Kondrat, Influence of temperature on percolation in a simple model of flexible chains adsorption, *J. Chem. Phys.* 117 (2002) 6662, <http://dx.doi.org/10.1063/1.1505866>.
- [24] G. Kondrat, Impact of composition of extended objects on percolation on a lattice, *Phys. Rev. E* 78 (2008) 011101, <http://dx.doi.org/10.1103/PhysRevE.78.011101>.
- [25] J.G. Restrepo, E. Ott, B.R. Hunt, Weighted percolation on directed networks, *Phys. Rev. Lett.* 100 (2008) 058701, <http://dx.doi.org/10.1103/PhysRevLett.100.058701>.
- [26] R.M. Ziff, Explosive growth in biased dynamic percolation on two-dimensional regular lattice networks, *Phys. Rev. Lett.* 103 (2009) 045701, <http://dx.doi.org/10.1103/PhysRevLett.103.045701>.
- [27] N. Tsakiris, M. Maragakis, K. Kosmidis, P. Argyrakis, Percolation of randomly distributed growing clusters: Finite-size scaling and critical exponents for the square lattice, *Phys. Rev. E* 82 (2010) 041108, <http://dx.doi.org/10.1103/PhysRevE.82.041108>.
- [28] A.S. Ioselevich, A.A. Kornyshev, Approximate symmetry laws for percolation in complex systems: Percolation in polydisperse composites, *Phys. Rev. E* 65 (2002) 021301, <http://dx.doi.org/10.1103/PhysRevE.65.021301>.
- [29] N.A.M. Araújo, H.J. Herrmann, Explosive percolation via control of the largest cluster, *Phys. Rev. Lett.* 105 (2010) 035701, <http://dx.doi.org/10.1103/PhysRevLett.105.035701>.
- [30] N.I. Lebovka, N.N. Karmazina, Y.Y. Tarasevich, V.V. Laptev, Random sequential adsorption of partially oriented linear k -mers on a square lattice, *Phys. Rev. E* 84 (2011) 061603, <http://dx.doi.org/10.1103/PhysRevE.84.061603>.
- [31] Y.Y. Tarasevich, N.I. Lebovka, V.V. Laptev, Percolation of linear k -mers on a square lattice: From isotropic through partially ordered to completely aligned states, *Phys. Rev. E* 86 (2012) 061116, <http://dx.doi.org/10.1103/PhysRevE.86.061116>.
- [32] L. Budinski-Petković, I. Lončarević, M. Petković, Z.M. Jakšić, S.B. Vrhovac, Percolation in random sequential adsorption of extended objects on a triangular lattice, *Phys. Rev. E* 85 (2012) 061117, <http://dx.doi.org/10.1103/PhysRevE.85.061117>.
- [33] R. Cohen, K. Erez, D. ben Avraham, S. Havlin, Breakdown of the internet under intentional attack, *Phys. Rev. Lett.* 86 (2001) 3682, <http://dx.doi.org/10.1103/PhysRevLett.86.3682>.
- [34] J. Wang, Z. Zhou, W. Zhang, T.M. Garoni, Y. Deng, Bond and site percolation in three dimensions, *Phys. Rev. E* 87 (2013) 052107, <http://dx.doi.org/10.1103/PhysRevE.87.052107>.
- [35] M.I. González, P.M. Centres, W. Lebrecht, A.J. Ramirez-Pastor, Site-bond percolation on simple cubic lattices: Numerical simulation and analytical approach, *J. Stat. Mech. Theory Exp.* 2016 (2016) 093210, <http://dx.doi.org/10.1088/1742-5468/2016/09/093210>.
- [36] K. Malarz, Simple cubic random-site percolation thresholds for neighborhoods containing fourth-nearest neighbors, *Phys. Rev. E* 91 (2015) 043301, <http://dx.doi.org/10.1103/PhysRevE.91.043301>.
- [37] R.M. Ziff, S. Torquato, Percolation of disordered jammed sphere packings, *J. Phys. A* 50 (2017) 085001, <http://dx.doi.org/10.1088/1751-8121/aa5664>.

- [38] J.-F. Thovert, V.V. Mourzenko, P.M. Adler, Percolation in three-dimensional fracture networks for arbitrary size and shape distributions, *Phys. Rev. E* 95 (2017) 042112, <http://dx.doi.org/10.1103/PhysRevE.95.042112>.
- [39] Y. Tarasevich, V. Cherkasova, Dimer percolation and jamming on simple cubic lattice, *Eur. Phys. J. B* 60 (2007) 97, <http://dx.doi.org/10.1140/epjb/e2007-00321-2>.
- [40] G.D. Garcia, F.O. Sanchez-Varretti, P.M. Centres, A.J. Ramirez-Pastor, Percolation of polyatomic species on a simple cubic lattice, *Eur. Phys. J. B* 86 (2013) 403, <http://dx.doi.org/10.1140/epjb/e2013-40509-1>.
- [41] G. García, F. Sanchez-Varretti, P. Centres, A. Ramirez-Pastor, Random sequential adsorption of straight rigid rods on a simple cubic lattice, *Phys. A* 436 (2015) 558, <http://dx.doi.org/10.1016/j.physa.2015.05.073>.
- [42] P.M. Pasinetti, P.M. Centres, A.J. Ramirez-Pastor, Jamming and percolation of k^2 -mers on simple cubic lattices, *J. Stat. Mech. Theory Exp.* 2019 (2019) 103204, <http://dx.doi.org/10.1088/1742-5468/ab409c>.
- [43] A.C. Buchini Labayen, P.M. Centres, P.M. Pasinetti, A.J. Ramirez-Pastor, Jamming and percolation of k^3 -mers on simple cubic lattices, *Phys. Rev. E* 100 (2019) 022136, <http://dx.doi.org/10.1103/PhysRevE.100.022136>.
- [44] O.F. Inc, Sequence A000162, in: N.J.A. Sloane (Ed.), *The on-Line Encyclopedia of Integer Sequences*, 2019, published electronically.
- [45] M.E.J. Newman, R.M. Ziff, Efficient Monte Carlo algorithm and high-precision results for percolation, *Phys. Rev. Lett.* 85 (2000) 4104, <http://dx.doi.org/10.1103/PhysRevLett.85.4104>.
- [46] M.E.J. Newman, R.M. Ziff, Fast Monte Carlo algorithm for site or bond percolation, *Phys. Rev. E* 64 (2001) 016706, <http://dx.doi.org/10.1103/PhysRevE.64.016706>.
- [47] D. Stauffer, A. Aharony, *Introduction To Percolation Theory*, Taylor & Francis, London, 1994.
- [48] P.H.L. Martins, J.A. Plascak, Percolation on two-and three-dimensional lattices, *Phys. Rev. E* 67 (2003) 046119, <http://dx.doi.org/10.1103/PhysRevE.67.046119>.
- [49] Z. Koza, J. Poła, From discrete to continuous percolation in dimensions 3 to 7, *J. Stat. Mech. Theory Exp.* 2016 (2016) 103206, <http://dx.doi.org/10.1088/1742-5468/2016/10/103206>.
- [50] A. Coniglio, H.E. Stanley, W. Klein, Site-bond correlated-percolation problem: A statistical mechanical model of polymer gelation, *Phys. Rev. Lett.* 42 (1979) 518, <http://dx.doi.org/10.1103/PhysRevLett.42.518>.
- [51] R.B. Jadrich, D.J. Milliron, T.M. Truskett, Colloidal gels, *J. Chem. Phys.* 159 (2023) 090401, <http://dx.doi.org/10.1063/5.0170798>.
- [52] E.J. Garboczi, K.A. Snyder, J.F. Douglas, M.F. Thorpe, Geometrical percolation threshold of overlapping ellipsoids, *Phys. Rev. E* 52 (1995) 819, <http://dx.doi.org/10.1103/PhysRevE.52.819>.
- [53] O. Ursini, R. Angelini, S. Franco, B. Cortese, Understanding the metal free alginate gelation process, *RSC Adv.* 11 (2021) 34449, <http://dx.doi.org/10.1039/D1RA06599H>.
- [54] A. Karoyo, L. Wilson, Physicochemical properties and the gelation process of supramolecular hydrogels: A review, *Gels* 3 (2017) 1, <http://dx.doi.org/10.3390/gels3010001>.
- [55] P. Smrdel, The influence of selected parameters on the size and shape of alginate beads prepared by ionotropic gelation, *Scientia Pharmaceutica* 76 (2008) 77–89, <http://dx.doi.org/10.3797/scipharm.0611-07>.

Long-term effects of abrupt environmental perturbations in model of group chase and escape with the presence of non-conservative processes

J. R. Šćepanović¹, Z.M.Jakšić¹ Lj.Budinski-Petković² and S.B.Vrhovac¹

¹*Institute of Physics Belgrade, Pregrevica 118, Zemun 11080, Belgrade, Serbia*

²*Faculty of Engineering, Trg D. Obradovića 6, Novi Sad 21000, Serbia*

Abstract. This paper examines the influences of environmental perturbations on dynamical regimes of model ecosystems. We study a stochastic lattice model describing the dynamics of a group chasing and escaping between predators and preys. The model include smart pursuit (predator to preys) and evasion (preys from predators). Both species can affect their movement by visual perception within their finite sighting range. Non-conservative processes that change the number of individuals within the population, such as breeding and physiological dying, are implemented in the model. The model contains five parameters that control the breeding and physiological dying of predators and preys the birth and two death rates of predators and two parameters characterizing the birth and death of preys. We study the response of our model of group chase and escape to sudden perturbations in values of parameters that characterize the non-conservative processes. Temporal dependencies of the number of predators and preys are compared for various perturbation events with different abrupt changes of probabilities affecting the non-conservative processes.

REFERENCES

1. Alfred J. Lotka, "Elements of physical biology," Science Progress in the Twentieth Century (1919-1933) 21, 341-343 (1926).
2. A. Pekalski, "A short guide to predator-prey lattice models," Computing in Science Engineering 6, 62-66 (2004).
3. Wibor Antal, Michel Droz, Adam Lipowski, and Géza Ódor, "Critical behavior of a lattice prey-predator model," Phys. Rev. E 64, 036118 (2001).
4. Tongfeng Weng, Huijie Yang, Changgui Gu, Jie Zhang, Pan Hui, and Michael Small, "Predator-prey games on complex networks," Communications in Nonlinear Science and Numerical Simulation 79, 104911 (2019).